NASA TECHNICAL NOTE

NASA TN D-3505

NASA TN D-3505

THE METEOROID SATELLITE PROJECT PEGASUS FIRST SUMMARY REPORT

George C. Marshall Space Flight Center
Huntsville, Ala.

NATIONAL AERONAUTICS AND SPACE ADMINISTRATION • WASHINGTON, D. C. • NOVEMBER 1966

NASA TN D-3505

THE METEOROID SATELLITE PROJECT PEGASUS

FIRST SUMMARY REPORT

George C. Marshall Space Flight Center
Huntsville, Ala.

NATIONAL AERONAUTICS AND SPACE ADMINISTRATION

For sale by the Clearinghouse for Federal Scientific and Technical Information
Springfield, Virginia 22151 – Price $3.00

TABLE OF CONTENTS

		Page
	SUMMARY	1
	INTRODUCTION	1
I.	STRUCTURAL DESIGN AND DATA SYSTEMS OF SPACECRAFT - William G. Johnson	4
II.	THERMAL DESIGN CONSIDERATIONS - Gerhard B. Heller	18
III.	METEOROID DETECTOR DEVELOPMENT AND TESTING - Mary J. Smith	29
IV.	OPERATIONAL ASPECTS OF PROJECT PEGASUS - William G. Johnson	55
V.	METEOROID DATA RECORDED ON PEGASUS FLIGHTS - James B. Dozier	65
VI.	SECONDARY MEASUREMENTS BY PEGASUS - Gerhard B. Heller, Russell D. Shelton, and James B. Dozier	77
	CONCLUSIONS	109
	REFERENCES	110

LIST OF ILLUSTRATIONS

Figure	Title	Page
1.	Pegasus Spacecraft	5
2.	Electronic System	7
3.	Power Distribution System	7
4.	Communications Subsystem	8
5.	Temperature Subsystem	9
6.	Attitude Subsystem	12
7.	Detector Subsystem	15
8.	Data Subsystem	16
9.	A Schematic of Word Formats	17
10.	The Electronics Canister	22
11.	Flight Configuration Detector Panel	36
12.	Damage to 0.2-mm Aluminum Face Sheets without the Fiberglass Center Barrier	37
13.	Damage to 0.4-mm Aluminum Face Sheets with 0.4-mm Fiberglass Center Barrier	38
14.	Damage to Final Foam Configuration by Particle at Meteoric Velocity	39
15.	Pegasus Meteoroid Detector Impact Test Program Test Data Sheet	43
16.	Data Recorded From Shot No. 1813	44

LIST OF ILLUSTRATIONS (Continued)

Figure	Title	Page
17.	Pulses Emanating from Detector Exposed to Electron Radiation Environment (15 V Bias)	46
18.	Leakage Current from Detector Exposed to Gamma Radiation Environment	47
19.	Sample Leading Edges of Radiation-Induced Pulses	48
20.	Typical Radiation-Induced Pulses at Low Temperature	50
21.	Dependency of Counting Rate on Electron Energy for 0.2-mm Target Sheet Capacitors	51
22.	Dependency of Counting Rate on Electron Energy for 0.4-mm Target Sheet Capacitors	51
23.	Results from Irradiation Tests of Two Similar Capacitors Manufactured Under Identical Conditions	52
24.	Pulse Height Distribution of Negative Pulses Obtained During Electron Irradiation of 0.2-mm Aluminum Front Plate	53
25.	Pulse Height Distribution of Negative Pulses Obtained During Energy Surveys of 0.4-mm Aluminum Front Plate	53
26.	Relationship of SATCON to Other Functional Elements in the SATCON Operation	56
27.	Pegasus Telemetry Data Links	57
28.	Internal SATCON Data Analysis Operation During Prelaunch Period	59
29.	Time History of Cumulative Hits on 0.04-mm Panels (Pegasus I)	70
30.	Time History of Cumulative Hits on 0.04-mm Panels (Pegasus II)	72

LIST OF ILLUSTRATIONS (Continued)

Figure	Title	Page
31.	Time History of Cumulative Hits for 0.2-mm Panels (Pegasus II)	74
32.	Time History of Cumulative Hits for 0.4-mm Panels (Pegasus II)	75
33.	Time History of Cumulative Hits for all Three Panel Thicknesses (Pegasus III)	76
34.	Composite Temperature Graph--Forward Solar Cell Panels (Feb. 18, 1965)	79
35.	Battery B Internal Average Temperature	79
36.	Temperature Data from Detector Panels in Flight (Feb. 17, 1965)	80
37.	Temperature Data from Detector Panels in Flight (Mar. 16, 1965)	80
38.	Reference Temperature Sensor	82
39.	Absorptance-Infrared Emittance Ratio of Pegasus I Reference Sensors Vs Equivalent Sun Time	83
40.	Electron Spectrometer	85
41.	Peak Radiation Pass For Feb. 24, 1965 (Pegasus I)	87
42.	Data Coverage and Channel A Maximum Flux History for Pegasus I (Feb. 16 through Mar. 15, 1965)	88
43.	Data Coverage and Channel A Maximum Flux History for Pegasus I (Mar. 16 through Apr. 12, 1965)	89
44.	Data Coverage and Channel A Maximum Flux History for Pegasus I (Apr. 13, 1965 through June 4, 1965)	90

LIST OF ILLUSTRATIONS (Concluded)

Figure	Title	Page
45.	Orbit and Flux History for Single Pass Through Anomaly, Pegasus I	92
46.	Flux History for 24-Hour Period, Pegasus I	92
47.	Isoflux Curves in B, L (Pegasus I)	93
48.	Integrated Flux History (Pegasus I)	93
49.	Schematic of Pegasus Showing Coordinate System	94
50.	One Slit of Solar Aspect Sensor	95
51.	Solar Aspect Sensors	96
52.	Sun Vector Resolved on Sensor Axes	96
53.	Pegasus Earth Sensor	97
54.	Build-Up in Spin Rate for Pegasus III	99
55.	Sun Azimuth Angle in Satellite Coordinates (Pegasus III)	100
56.	Sun Elevation Angle in Satellite Coordinates (Pegasus III)	101
57.	Pegasus I Spin Rate	102
58.	Pegasus II Spin Rate About Longitudinal Axis	103
59.	Pegasus III Spin Rate	103
60.	Time History of Precession Cone Angle About Angular Momentum Vector (Opening Angle - Pegasus I)	105
61.	Motion of Pegasus I Angular Momentum Vector	108

LIST OF TABLES

Table	Title	Page
I.	Results of Hypervelocity Test Series at Hayes International Corp.	45
II.	Shorting History of Detectors in Hypervelocity Test Series at Hayes International Corp.	45
III.	Pegasus Penetration Data	71
IV.	Temperature Sensors on Pegasus	78
V.	Range of Pegasus Temperatures	81

ACKNOWLEDGMENTS

The meteoroid satellite project Pegasus was initiated in 1962 under the Headquarters Program Management of the Space Vehicles Division, Office of Advanced Research and Technology, and the Project Management of Dr. W. G. Johnson, first at Research Projects Laboratory, Research and Development Operations, and later at the Saturn I/IB Program Office, Industrial Operations George C. Marshall Space Flight Center. The evaluation of Pegasus data has been under Dr. J. Dozier, Research Projects Laboratory.

Valuable help in the areas of sensor design and sensor testing, provided by members of the Langley Research Center, and in the area of data acquisition and transmission by Goddard Space Flight Center, is gratefully acknowledged.

The following Marshall Space Flight Center personnel contributed to the First Summary Report on Project Pegasus: W. G. Johnson, J. B. Dozier, R. Shelton, G. Heller, W. Snoddy, F. Rodrigue, M. J. Smith, B. Naumann, G. Urban, R. Potter, R. Holland, T. C. Bannister, and E. R. Miller.

THE METEOROID SATELLITE PROJECT PEGASUS
FIRST SUMMARY REPORT

SUMMARY

The objective of the Pegasus Meteoroid Project is the collection of meteoroid penetration data in aluminum panels of three different thicknesses in near-earth orbits. This document provides a detailed description of the project. History and development of the Pegasus spacecraft are briefly discussed. Satellite instrumentation and data retrieval procedure are described. An evaluation of the results of Project Pegasus will be presented later when more data have been accumulated and analyzed. Three Pegasus spacecraft were launched with Saturn I carriers. At present, the 0.04-mm-thick sensors accumulate penetrations at the rate of 65 per m^2 per year; 0.2-mm sensors at the rate of 4 per m^2 per year; and 0.4-mm sensors at the rate of 1.3 per m^2 per year.

Results available to date indicate that the penetrating meteoroid flux near the earth is lower than expected in the lower meteoroid mass range, and about as expected in the upper mass range. Measured data do not allow a reliable extrapolation to great thicknesses.

INTRODUCTION

Measurements of meteoroid abundance in the vicinity of the earth were made during past years in two ways: with meteoroid impact sensors on space-borne vehicles, and with optical and radar systems from the ground. By 1962, the first method had provided a number of data points for meteoroids of the mass range 10^{-11} to 10^{-7} g; the second method had provided data on meteoroids of the mass range 10^{-4} g to several grams. These measurements gave only a rough idea of the number-mass distribution of meteoroids in near-earth space. Interpolation of the measured distribution functions over the mass range 10^{-7} to 10^{-4} g was afflicted by an uncertainty factor of almost 10^3. This mass range, however, is of utmost importance for the design of spacecraft. In fact, the abundance of meteoroids in the mass range 10^{-5} to 10^{-3} g will be decisive with respect to the necessary meteoroid protection for future long-duration manned missions.

The first statistically significant penetration measurements were made with Explorer satellites which were equipped with pressurized cans of 0.025 and 0.050-mm wall thickness. Explorer 13, launched on August 25, 1961, with a Scout vehicle, remained only three days in orbit [1]. Explorer 16, launched on December 16, 1962, with a Scout vehicle, had a useful lifetime of eight months [2]. Explorer 23, launched on November 6, 1964, with a Scout vehicle, is still in orbit [3]. It confirmed in essence the penetration data provided by Explorer 16.

Penetration measurements on Explorer satellites were restricted to relatively thin target materials and small target areas. In response to the need for extension of penetration measurements to greater thicknesses and larger areas approaching those of spacecraft walls, consideration was given to large meteoroid measuring satellites. These studies culminated in the Pegasus project.

Possibilities of meteoroid measurements in the mass range 10^{-9} to 10^{-5}g with large satellites have been studied at various places for several years. The Office of Advanced Research and Technology (OART) of NASA and some of the NASA Field Centers investigated the feasibility of large-scale meteoroid projects based on Atlas and Saturn carrier rockets. Several possible systems were compared, and in 1962 OART gave preliminary approval to a proposal from the Marshall Space Flight Center to fly on a Saturn I-boosted satellite a meteoroid impact sensor which was under development at the Langley Research Center. Rough calculations showed that a total sensitive area on the order of 200 m^2 could be carried on a Saturn I-launched satellite. During a useful lifetime of one year, approximately 100 meteoroid punctures through an aluminum sheet of about 0.4-mm thickness could be expected according to interpolated abundance data.

A work statement for competitive bidding by industrial contractors was distributed in the fall of 1962, and in February 1963, the Fairchild-Stratos Corp., later re-named the Fairchild-Hiller Corp., was awarded a NASA contract to develop a large-area meteoroid-sensing satellite. Program management was exercised by the NASA Office of Advanced Research and Technology in Washington; project management was assigned to the Marshall Space Flight Center. The NASA Langley Research Center provided substantial support throughout the duration of the project.

Shortly after initiation of the project, it became apparent that large-scale manufacturing of the capacitor-type sensors required considerably more

development effort than previously expected. Also, testing of the sensors under high-velocity particle impact proved to be more difficult and far more time consuming and costly than anticipated. Finally, the study of potential effects of Van Allen electron radiation upon the dielectric layers of the capacitor sensors turned out to be very complex and tedious, a fact that was not anticipated or known at the time of contract award.

Originally, only two flights were planned. This number was later increased to three, and as a consequence of modifications in the Apollo Program, the meteoroid satellite was elevated from the status of "passenger payload" to that of "prime objective payload." The three satellites, Pegasus I, II, and III, were successfully launched on February 16, May 25, and July 30, 1965, respectively. To date, all three are generating useful meteoroid data (as of Mar. 4, 1966).

Results of these flights obtained to date are mentioned only briefly since detailed discussions of the measurements are the subjects of separate publications [4. 5].

I. STRUCTURAL DESIGN AND DATA SYSTEMS OF SPACECRAFT

William G. Johnson*

Introduction

The primary mission of the Pegasus Project is to obtain data on the flux of meteoroids in near-earth space (between the altitudes of 500 and 750 km) capable of penetrating selected thicknesses of aluminum. This is basically an engineering mission. The experiment is designed to obtain data immediately applicable to the determination of the hazard presented to structures by meteoroids. As a result, 2024 aluminum, a material of engineering interest for structural use, has been chosen as the target material of the sensors. The thickest sensor, 0.4 mm, was selected as a compromise between the requirements that it be as close as possible to thicknesses normally of interest for space structures, and that the rate of penetrations experienced during the flight be sufficiently great to be statistically meaningful. The thinnest material, 0.04 mm of type 1100 aluminum foil, was selected to provide a convenient tie point with the Explorer XVI and XXIII 0.025 and 0.050-mm data.

Mechanical Structure

The Pegasus Spacecraft, Figure 1, is designed to fit within the space available in the boilerplate model Apollo Service Module and Service Module Adapter. During launch, the wings are clamped in a folded position against the spacecraft center structure. The Service Module, the Service Module Adapter, and the Command Module form the shroud over the spacecraft during launch. After injection, explosive nuts, which secure a tie at the top of the Service Module to the top of the spacecraft and secure the Service Module to the Service Module Adapter, are activated and the Service Module and Command Module are ejected forward by a spring-powered separation system. The Pegasus remains attached to the Service Module Adapter, Instrument Unit, and depleted S-IV stage.

---

* Manager, Pegasus Project Office, Saturn I/IB Program Office, MSFC, now Technical and Scientific Assistant to Director, Research and Development Operations, MSFC.

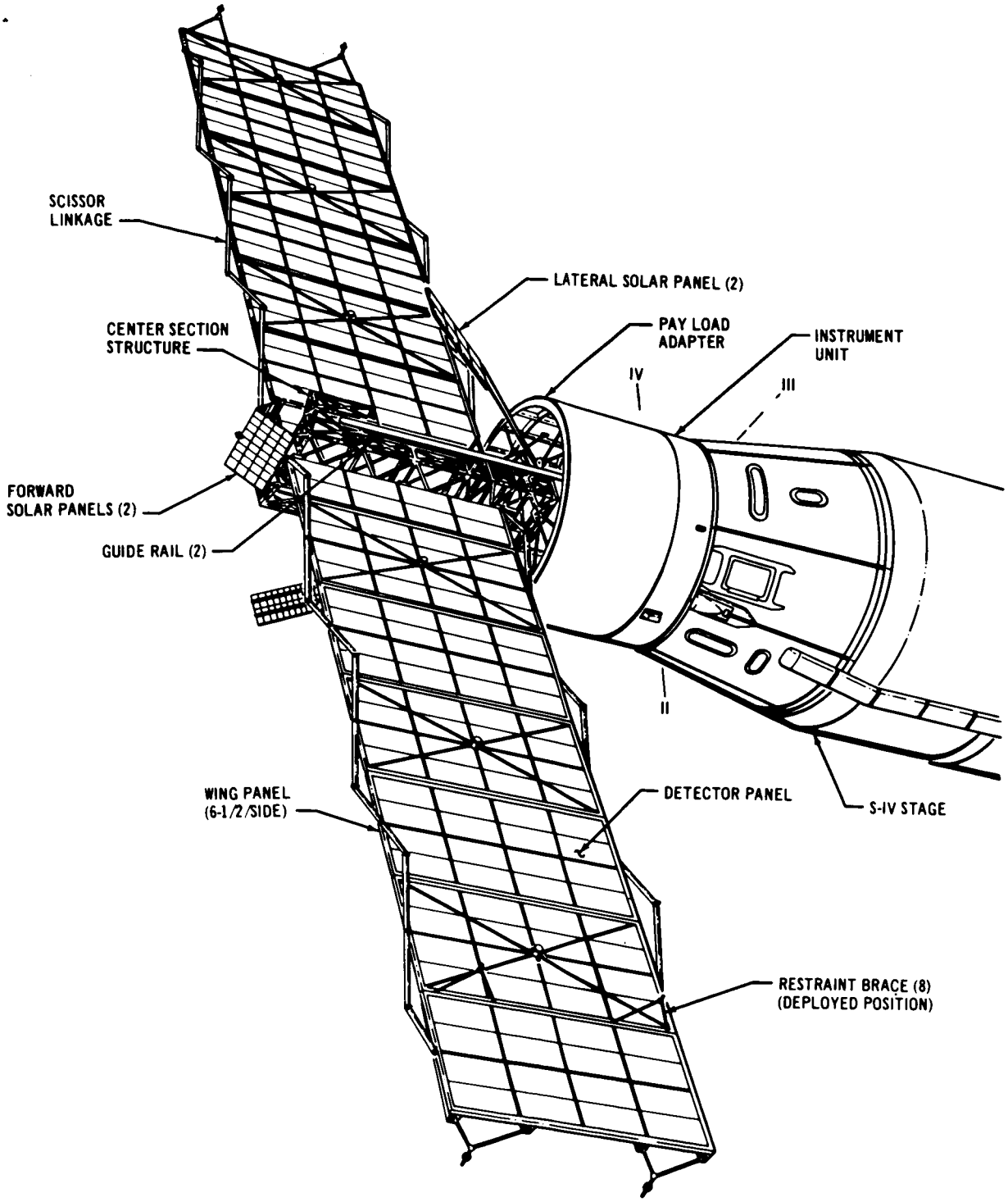

FIGURE 1. PEGASUS SPACECRAFT

Sixty seconds after initiation of ejection of the shroud, explosive nuts securing the wing cinching arms are activated. The wings are forced outward by means of springs placed in the hinges between wing sections. An electric motor-gearbox system connected to the wings by means of a torque tube and scissor linkage serves to control the rate of deployment of the wings and as a backup deployment system to assure positive locking of the wings in the extended configuration.

In the deployed configuration, the wings span a distance of approximately 29.3 m from tip to tip. The wing width is 4.1 m. The total meteoroid detector area, both sides of the wings combined, is about 200 m^2. Of this area, 8 m^2 are composed of the 0.04-mm-thick detectors; 17 m^2 of 0.2-mm-thick detectors; and 175 m^2 of the 0.4-mm-thick detectors.

The center structure of the spacecraft is an open framework of square drawn aluminum tubing. In addition to providing the supporting structure for the wing frame members, it also supports the deployable solar cell array. It is attached to the Service Module Adapter at the separation plane between the Adapter and the Service Module by a six-point mounting pad support system. The upper section of the spacecraft, carrying the wings and solar cell arrays, is cantilevered above the mounting plane. The center structure extends about 0.5 m below the mounting plane; the major electronic systems are housed in a thermally controlled canister located in this area.

Electronic Systems

The Pegasus electronic system may be readily divided into six major subsystems (Fig. 2).

The power system (Fig. 3) is a conventional solar-cell-battery system designed to provide and control the power for all other on-board systems. However, it does not provide power to actuate the deployment mechanisms. This power is obtained from batteries located in the Saturn Instrument Unit. The solar cells, connected in a series-parallel configuration to yield a peak voltage of about 45 V at 2.85 A, are mounted on metal substrate sheets to form easily handled modules. These modules are mounted, in turn, on four deployable panels in such numbers that each panel is capable of providing the full power required by the spacecraft. In the deployed configuration the panels form a tetrahedron (Fig. 1).

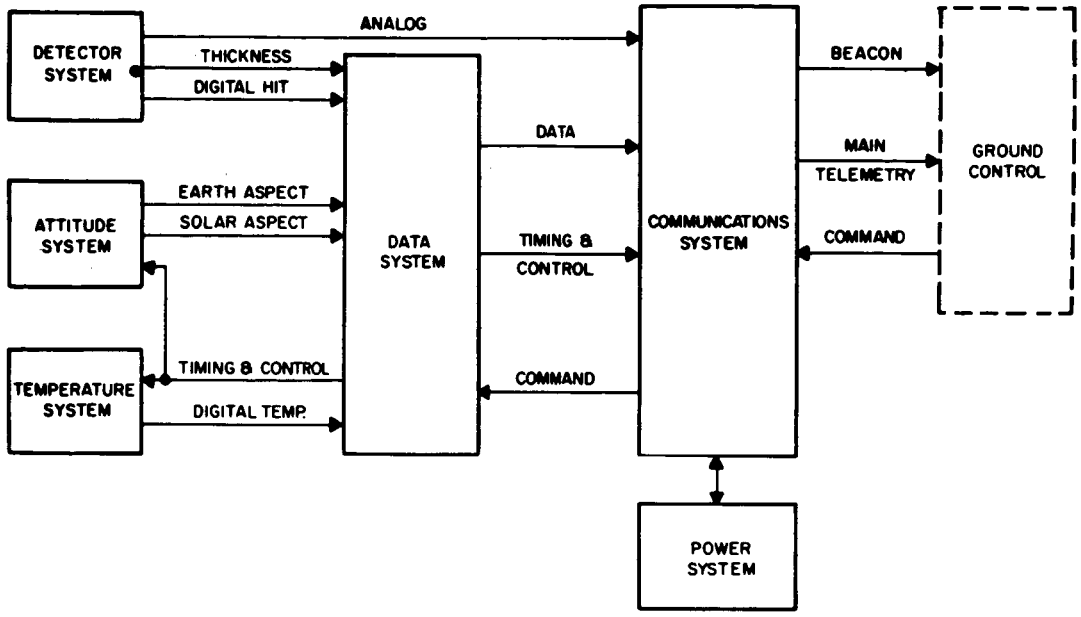

FIGURE 2. ELECTRONIC SYSTEM

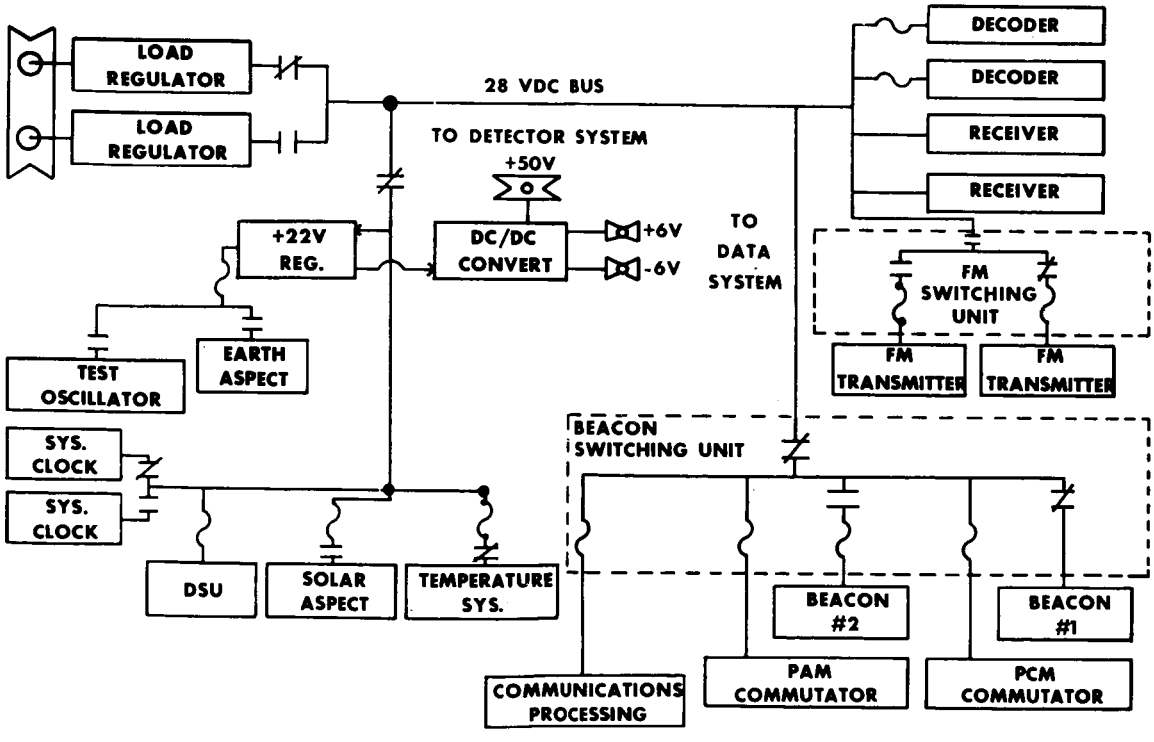

FIGURE 3. POWER DISTRIBUTION SYSTEM

The data system employs low-speed logic circuitry to control data flow and to effect digitization, processing and storage of all primary data, and of selected housekeeping; i.e., system performance data. Additionally, all of the housekeeping data are collected, processed, and transmitted in real-time in analog format. Timing and control of the data flow is effected in the data subsystem.

The communication subsystem (Fig. 4) provides for real-time transmission of data and for commanded transmission of data stored in the on-board memory. The subsystem is designed to afford redundant communication channels both for the collected data and for command control of the on-board systems.

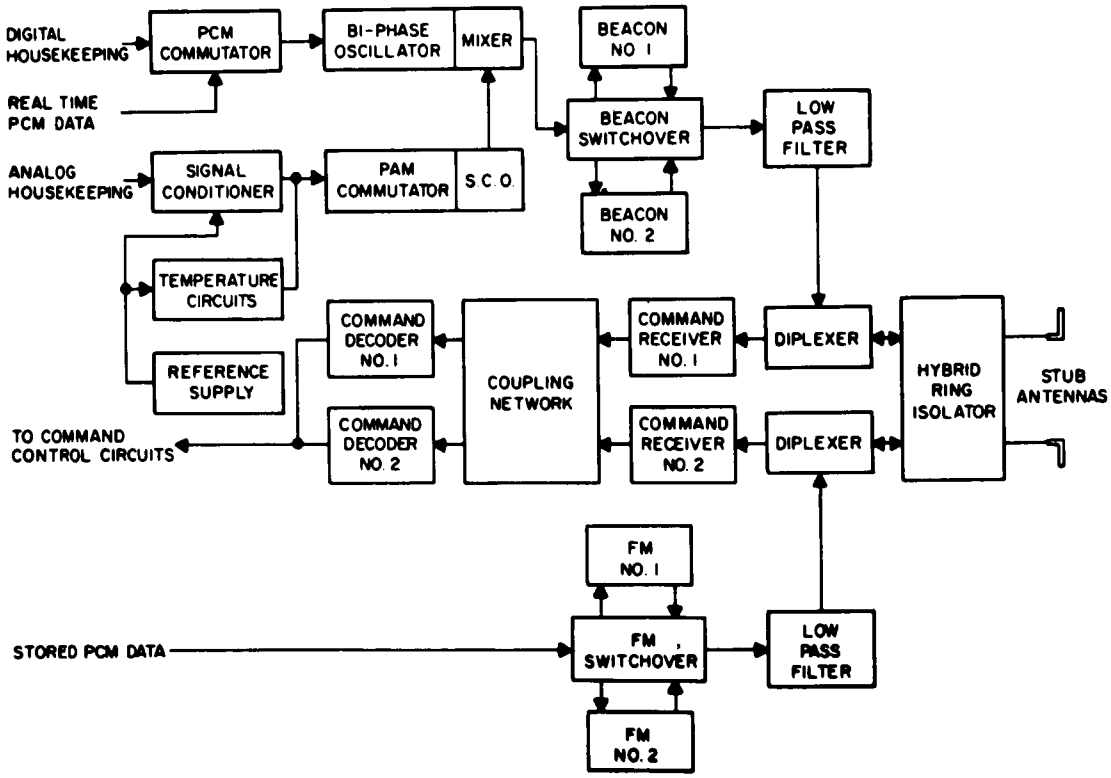

FIGURE 4. COMMUNICATIONS SUBSYSTEM

The data collection subsystems are the temperature system, the attitude system, and the meteoroid detection system. Since these are the subsystems of primary interest, they will be discussed in detail below.

Temperature Subsystem

While temperature measurements are not considered to be primary data in the sense of the primary mission of Pegasus, such data are essential to the evaluation of the performance of the spacecraft. They provide information necessary to the validation of the meteoroid data. Three classes of temperature measurements are obtained (Fig. 5). The first class contains those collected on the thermal behavior of the electronic packages; the second, on the thermal behavior of the meteoroid detectors; and the third, on a set of standard thermally isolated surfaces. These last data are used to evaluate the behavior of the several passive thermal control surfaces used in the spacecraft. *

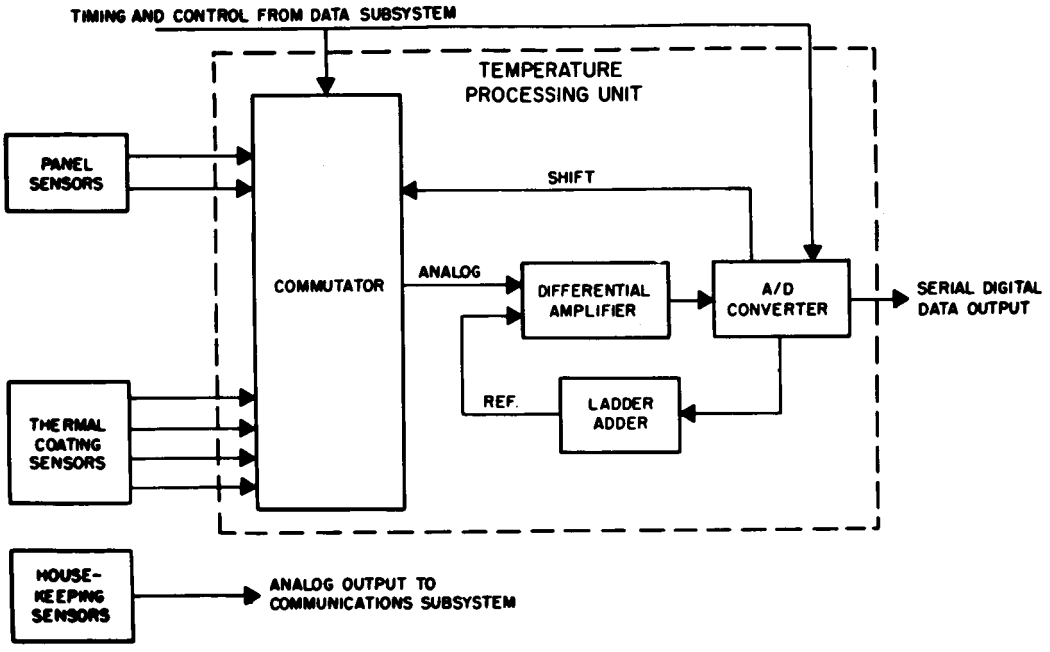

FIGURE 5. TEMPERATURE SUBSYSTEM

Control of the thermal environment which the major electronic subsystems experience is maintained by a combination of passive elements (coatings, blankets, and finishes) and an active louver system. ** The entire electronic package is assembled into a canister which is covered with a multilayer "super-insulation" and is located in the lower center structure. The bottom of the

---

* See Chapter VI.

** See Chapter II.

canister is fitted with a thermally controlled louver system so arranged that as the temperature within the canister rises the louvers open and the electronic components "look out at" the top of the depleted S-IV stage. The temperature of the S-IV stage is controlled by a specially developed, highly reflective paint. Because the stage is massive, its temperature stays essentially constant (near 265°K). The stage thus serves as a constant temperature sink to which the electronic packages can radiate energy as required. The louvers control the rate of heat flow out of the canister, permitting the establishment of an operating temperature in the range 290° to 320°K in which the electronic subsystems can readily survive. Temperatures of power subsystem components, data subsystem boxes, and structure are taken with resistance thermometers bonded to the cases and structures. Measurements from these sensors are processed and fed directly to the communication subsystem for real-time transmission to earth. None of the housekeeping temperature measurements are stored in memory. These temperature data are periodically recorded and analyzed to establish trends for selected electronic boxes.

The meteoroid detector is a capacitor with a mylar layer as dielectric. * So that the temperature of the detectors does not exceed the acceptable characteristics of mylar, a specially developed chemical conversion coating is used on the outer aluminum surface to obtain a ratio of absorptance to emittance (α/ϵ) of about 1.0. With a properly applied thermal coat, detector temperatures are maintained at values below about 370°K when exposed to the sun. During passage through the earth's shadow, and on the "dark" side of the wing, the detector temperature is appreciably lower (about 220°K). Since the electric behavior of the dielectric is dependent upon its temperature, measurements of temperatures are essential to the final determination of the operating characteristics of the detectors. In practice, a pair of detector samples, not used for meteoroid detection, are instrumented with resistance-thermometers affixed to the detector surface and are mounted near the outer edge of the wing frame. Data from these panels are collected at five-minute intervals, converted to digital form, and stored in the memory.

Early in the development of the spacecraft, it became apparent that if the temperature data obtained in flight were to be used to evaluate the effectiveness of the several coatings used for passive thermal control, a set of "standard" sensors would be required. As a consequence, four such standard sensors have been flown on each Pegasus. The sensor consists of a small, carefully constructed thermally isolated disc, the front surface of which is coated with a

---

* See Chapter III.

thermal control material (S-13 paint, Alodine/MTL3, Rutile, Lowe Brothers' Black, or other). The S-13 coating was used on all of the three Pegasus satellites. The other coatings used have varied; on Pegasus II and III, however, one of the coatings used was an Apollo candidate thermal balance coating. To each disc is attached a low-mass, carefully calibrated thermometer. The temperature of the disc is read, converted to digital form, and stored in memory once each minute for the first 120 minutes following memory readout. The sensors have low thermal inertia, the sensitivity of the attached thermometer systems is quite good (± 1 percent full scale), and care is exercised in the assembly and housing of the sensors to assure good thermal isolation of the sensor from the spacecraft. The sensors are mounted in such a manner that a 2 π steradian field of view is provided which is unobstructed by the vehicle. Since the on-board system can be duplicated in the laboratory, measurements made in flight, when compared with those made on sensors not exposed to the space environment, yield meaningful information on the long-term effectiveness of the particular coating material being tested. Also, since the coatings selected have generally stable long-term characteristics, measurement of short-term fluctuations in temperature detected in a single orbit yield valuable information on the thermal environment of space. The standard temperature sensors thus constitute a secondary experiment of interest to the space scientist evaluating the thermal environment.

Radiation Sensors

Subsequent to initiation of spacecraft development, studies at Langley Research Center on the entrapment and subsequent release of electrons in a dielectric indicated the possible existence of a potentially serious problem. * Early data seemed to indicate that upon release the electrons stored in the dielectric of the capacitor-type detector produced discharge pulses with characteristics similar to those of the pulses produced by impact discharge. Further investigation revealed that sufficient differences existed between the pulse heights and shapes to permit acceptable discrimination and control of the spurious radiation-induced charges; however, to provide a source of information which would permit an additional test of validity of the meteoroid data, a radiation sensor system was installed which was designed to measure the omnidirectional flux of electrons encountered by the spacecraft as a function of position in orbit. Since the spacecraft electronics configuration was well established at the time of installation of the radiation sensor, decisions were

* See Chapter III.

made to relinquish a set of detector panel thermal measurements, to condition the output signals from the radiation sensor to make them compatible with input signal characteristics required for the temperature subsystem, and to utilize the temperature subsystem to process the electron flux data. These data, the flux of electrons in the energy ranges 500 keV (100 keV on Pegasus III) to about 11 MeV, and 2 MeV to about 11 MeV, are sampled once every five minutes and stored in digital form in the memory. The data are subsequently processed to yield electron flux as a function of position in space. To date there is no evidence of correlation between measured electron flux and recorded pulse rates of the meteoroid detectors. *

Attitude Subsystem

The Pegasus in orbit is a freely tumbling body. Knowledge of its orientation in a space-fixed coordinate system is essential to the evaluation of each of the other data sets derived. The necessary attitude information consists of position and orientation of the spacecraft with respect to the earth, orientation of the spacecraft with respect to the sun, and relative earth-sun position. A combination of solar sensors and earth sensors is required to gather the necessary on-board data. The attitude subsystem is shown in Figure 6.

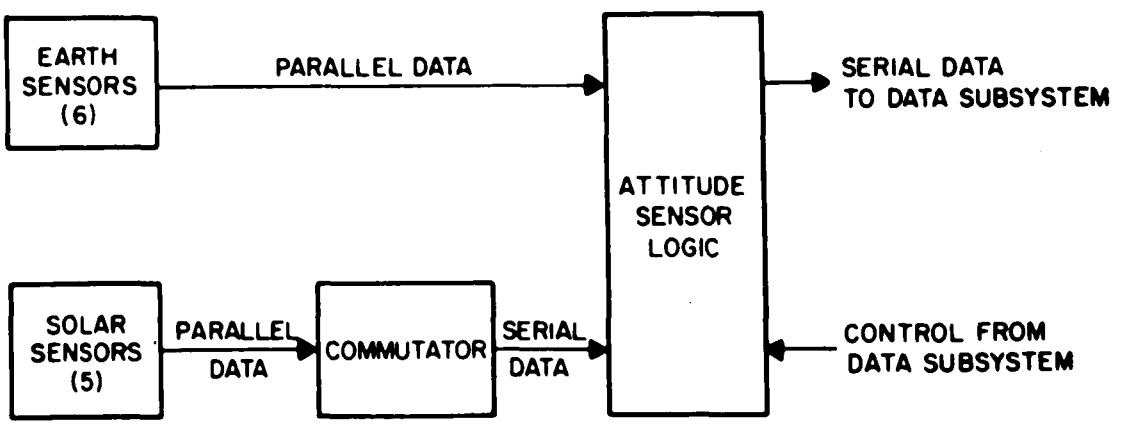

FIGURE 6. ATTITUDE SUBSYSTEM

Early tumbling rate calculations indicated that the rate would be so low as to make impractical the use of infrared sensors of the type customarily employed to determine orientation in the earth-fixed coordination system using the time of passage of the sensor line of sight across the horizon of the earth.

---

* See Chapter VI.

Consequently, an earth sensor system proposed by the Barnes Engineering Co. was developed and used. The sensor consists of a pair of thermopiles affixed to opposite sides of a thin, low thermal mass substrate and centered in a thermally isolated collimator tube such that each receives its energy primarily from single opposing ends of the tube. As long as both ends of the sensor are exposed to space, the two thermopile output levels are the same. When a sensor is so oriented that one of its elements receives energy from the earth (the other being exposed to space), a difference in output levels of the thermopiles occurs. This difference signal is processed to identify the "on" sensor and fixes its pointing direction within the cone subtended by the earth at the spacecraft. Six such sensor pairs are employed in an array forming a dodecahedron. Orientation of the spacecraft with respect to the center of the earth can be determined with an accuracy of 3° to 5° through a knowledge of the sensor states.

The solar sensors are somewhat more conventional. The sensor consists of two arrays of solar cells arranged orthogonally to each other and mounted on a planar substrate. A quartz lens and a slit collimator are fixed above each solar cell array. The position of the plane containing the sun and the long axis of the slit is determined by arranging the solar cell array to provide a G ray angular displacement code output which varies for each degree that the sun-slit plane varies from the plane perpendicular to the substrate plane and containing the long axis of the slit. The line of intersection of the two orthogonal sun-slit planes for each sensor uniquely defines the position of the sun with respect to the sensor plane. Good definition of the angular position is obtained so long as the sun is not below a position of about 60° from the perpendicular to the sensor plane. Five of these sensors are arrayed such that all directions from the spacecraft are "within view" of one or more sensors. Since it is possible for more than one sensor to be illuminated simultaneously, sensor outputs are first processed to determine the one most nearly perpendicular to the sun (highest output level). Once the sensor has been identified, the states of its solar cells are sensed and recorded.

Normally, attitude data are sensed and recorded in the memory once every five minutes; however, provisions are made to command the system into a continuously recording mode (rapid attitude) in which complete sets of attitude data are recorded every 1.25 seconds. The loss of solar sensor data during passage through the earth's shadow is compensated by extrapolating the satellite motion and smoothing through that portion of the orbit. *

---

* See Chapter VI.

Detector Subsystem

The source of primary data is the detector subsystem. * The meteoroid penetration detector will be discussed separately below. A penetrating impact of a detector which produces a momentary short of the capacitor resulting in a rapid drop in impressed voltage is described briefly. Subsequent to the passage of the impacting particle the short "heals" and the impressed voltage rises along a curve determined by the resistance of the recharge circuit and the capacitance of the detector.

The detector subsystem is shown in Figure 7. Opposite wings of the spacecraft are wired separately through functionally identical signal processing circuits. There are 30 information channels on the -Y wing, while the detector panels of the +Y wing form 32 information channels. Since there are 200 detectors on each wing, each information channel is connected to a group of detectors (groups of two, each, of the 0.04-mm thickness, and groups ranging from three to eight detectors, each of the 0.2 and 0.4-mm thickness on each wing). The detectors in a group are electrically isolated from each other by a resistor-diode circuit between the detector and signal lead. Also, on Pegasus II, a 0.0100, and on Pegasus III a 0.050-A fuse was placed in the circuit between each detector and the signal lead. The signal is passed through a low-pass filter consisting of a series resistor and a zener diode and series capacitor to ground, connected to clip the level of high-frequency negative signals. In each information channel is a disconnect relay which permits the removal of noisy and shorted detector groups from the system.

Recharge current is supplied to each of the detector groups from three of fourteen identical power sources. No two detector groups are connected to the same three power sources. Therefore, by sensing the state of current flow from all power sources (current recharge amplifiers) immediately after impact, the identity of the panel group impacted may be uniquely established (panel identification). The length of time that recharge current is drawn above a threshold level is also measured. This time is directly related to the depth of discharge of the capacitor.

Information channels from each of the three thicknesses of material on one wing are grouped and serve as the input to one of three identical hit amplifiers. The hit amplifier contains the major discrimination circuitry for

---

* See Chapter III.

separating high-frequency disturbances (and "radiation pulses") from the desired meteoroid impact data. Discrimination is effected by accepting only negative pulses at the input of the amplifier, and by integration of signal level with respect to time to assure that the energy in the pulse is above a threshold level. This threshold level is set at a value such that an instantaneous drop of 4 V* in impressed voltage at a detector panel, followed by normal recharge, is just sufficient to activate the follow-on circuitry. Pulses meeting the "hit" criteria with respect to level and duration trigger a "hit" signal output pulse. All "hit" output pulses are of a single size and duration. The other wing functions in an identical manner.

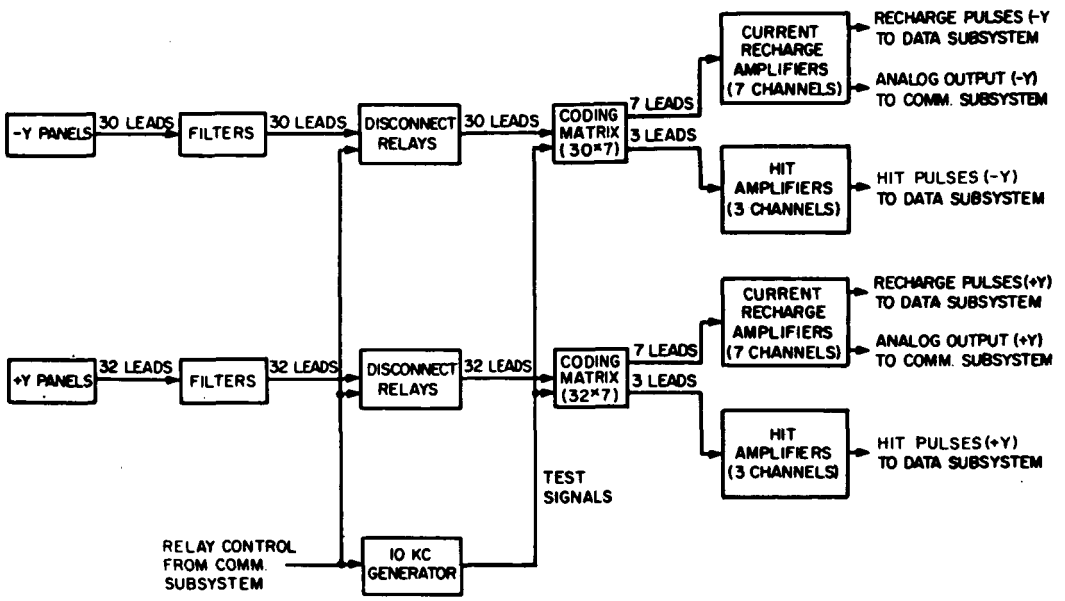

FIGURE 7. DETECTOR SUBSYSTEM

The Data System

The most complex of the Pegasus subsystems is that through which the data are assembled and processed (Fig. 8). The processing of such information

---

* The thresholds on Pegasus I were approximately 5 V for the 0.4 and 0.2-mm capacitors and 3 V for the 0.04-mm capacitors. (See Chapter IV.)

as attitude data and temperature data is periodic and is controlled by an on-board clock. The meteoroid data are primary and aperiodic. Therefore, they are processed upon occurrence and take precedence over all other data.

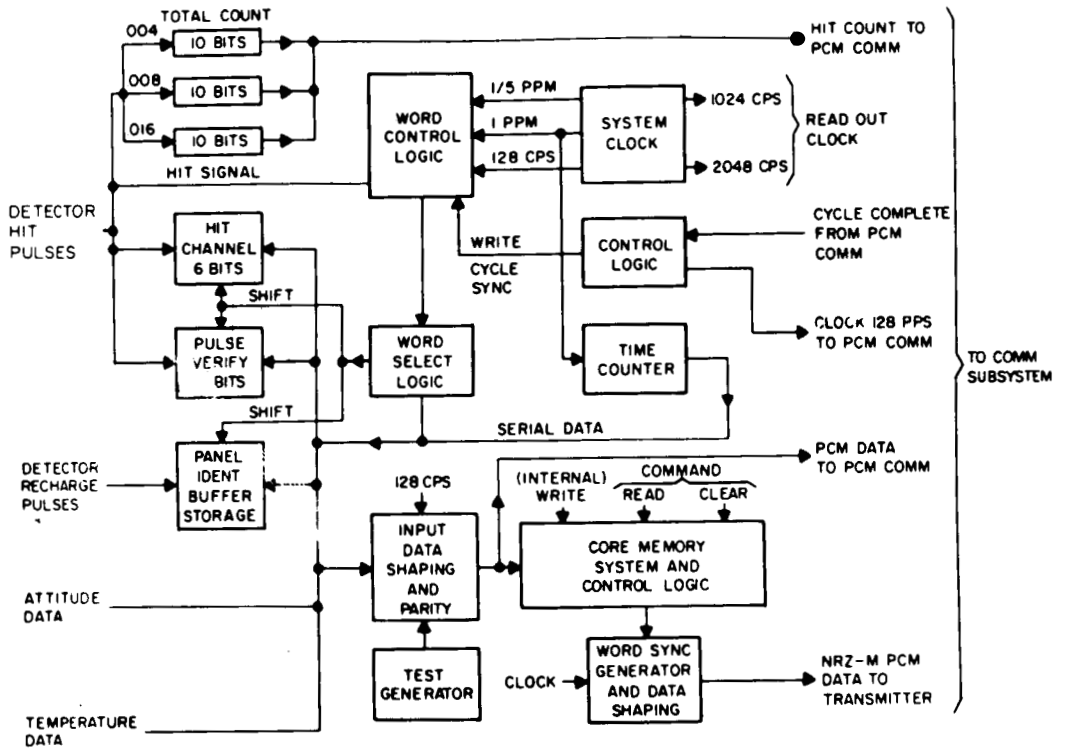

FIGURE 8. DATA SUBSYSTEM

The hit pulse generated by the hit amplifier described above serves to key a number of functions. It activates the word control logic circuitry. The word control logic, in turn, gates the word select which establishes the word identification code and initiates the flow of data to the input data shaper and parity generator. The hit pulse is gated to and increments a total hit counter, selected on the basis of thickness of material penetrated.

Simultaneously, it gates the output of the current recharge amplifiers to permit flow of panel identification information and pulse lengths information into the respective storage buffers. It activates a hit channel register encoded to identify the wing (+Y or -Y) and the thickness of material penetrated. The

hit word, fed in parallel to memory for storage and to the PCM transmitter for real-time transmission, is highly redundant in information. It contains identification of the panel impacted, thickness identification, wing identification, verification of pulse (duration), and time of occurrence of impact to one-minute accuracy. A schematic of the various word formats is shown in Figure 9.

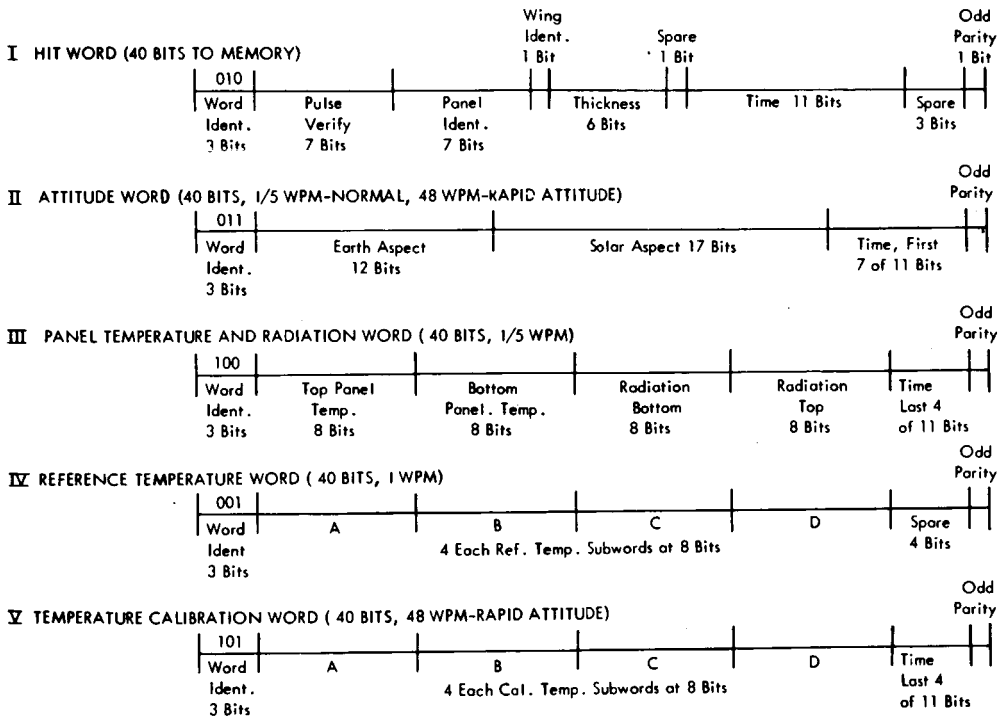

FIGURE 9. A SCHEMATIC OF WORD FORMATS

N67 11383

II. THERMAL DESIGN CONSIDERATIONS

Gerhard B. Heller*

Definition of Parameters

Symbol	Parameter	Unit
σ	Stefan-Boltzmann constant	$W/m^2 \circ K^4$
α_s	Solar absorptance	--
ϵ_T	Infrared emittance	--
MAS	Angle between sun vector and satellite momentum vector	--
RAS	Angle between solar vector and radius vector	--
S	Solar constant	W/m^2
E	Earth's IR constant	"
F_r	Earth radiation geometry factor	--
T_x	Percent time in sunlight	--
$\dot{Q}_i$	i^{th} heat flux	W

Introduction

The micrometeoroid detector panels and the electronics were the critical areas for thermal design. The problem associated with the detector panels was

---

* Deputy Director, Research Projects Laboratory, MSFC

the possibility of severe thermal variations which could conceivably cause panel delamination. * A detailed study of this problem revealed that the only readily controllable parameters were the optical properties of the panel exterior surfaces. The orbital temperatures were defined for all sets of possible optical properties. A search was made to find the coating with suitable optical properties; the chemical conversion coating, Alodine, was finally selected. This coating was subjected to ultraviolet radiation in the laboratory to verify the space stability of its properties. Also, a detector panel was studied in a thermal space chamber at hard vacuum. T. C. Bannister and R. J. Eby have elaborated further on the Pegasus thermal design in "Pegasus Thermal Design," a NASA TN publication.

The thermal problem associated with the electronics insures that they do not go beyond the prescribed "upper" and "lower" limits. ** The temperatures of most electronic components is a strong function of internal heating rates, thermal linkage to the supporting structures, structure temperature, and radiation heat transfer to other parts of the spacecraft and to space. Usually, several of these can be controlled to a degree by design. Where possible, the electronic components were placed in a thermally insulated canister with a "sized window" to radiate the internally generated heat to a cold sink. This window was faced toward the S-IV bulkhead to eliminate direct solar radiation from entering the canister. With random orientation, such a variable input as the direct solar radiation would greatly increase the design requirements.

Throughout this report the terms "SMA" and "sink" are used interchangeably when speaking of the canister radiation heat sink. This SMA is an adaptor to the Service Module. The window sees the internal areas of the SMA, IU (Instrument Unit), and S-IV stage bulkhead.

Since most of the factors affecting the canister thermal design are variable, it is useful to consider a thermodynamic "hot" and a thermodynamic "cold" case. If the varying factors are not too severe, the window could be sized to keep both the hot and cold cases within specified limits.

With moderate parameter variations, the steady-state "hot" and "cold" extreme temperatures can each be kept within the design range. In the case of Pegasus, it became apparent that this was an inadequate method of control. After several alternatives were evaluated, an active louver system which prohibits radiant heat flow through the window in the cold case without much hindrance to the heat flow in the hot case was employed.

---

* See Chapter III.

** See Chapter I.

A list of thermal specifications for the components of Pegasus was prepared by the contractor. A summary outline of the thermal requirements is as follows:

A. Electrical Components

1. Inside the Canister

a. Batteries	272° to 322°K
b. Others	262° to 332°K

2. Outside the Canister

a. Zener diodes	218° to 358°K
b. Solar cells	194° to 339°K

B. Other Components

1. Micrometeoroid Detector Panels	167° to 394°K and $\dot{T}$ less than 100°K/min
2. Infrared Detector	222° to 388°K

Thermal Design of Components not in the Electronics Canister

In addition to the detector panels, the IR sensors, Zener diodes, solar cells, and other components outside the thermally controlled electronics canister were analyzed in great detail. To present a more comprehensive discussion of the vitally important electronic canister which contains the components very sensitive to temperature, such as the batteries, these thermal analyses and the computer analyses are not covered herein.

Electronic Canister Thermal Design

The thermal design of the electronics canister must insure that the component temperatures do not exceed the prescribed "upper" and "lower" limits. The temperature of most electronic components is a strong function of internal heating rates, thermal linkage to the supporting structures, structure temperature, and radiative heat transfer to other parts of the spacecraft and to space.

Several of these can be controlled to some degree by design. On Pegasus, the first attempt was to place the electronic components in a thermally insulated canister (Fig. 10) with a "sized window" to radiate the internally generated heat to a cold sink. This window was faced toward the bulkhead of the S-IV stage to eliminate direct solar radiation entering the canister.

However, it became apparent that an open window did not allow a sufficient margin for variations of input parameters. After several alternatives were evaluated, an active louver system was employed which prohibits radiant heat flow through the window in the cold case, but allows an outflow of heat in the hot case.

Among the reasons for adopting an active thermal control system were:

1. Uncertainty about the internal canister heat generation levels.

2. Uncertainty about the orbit parameters like eccentricity which affect solar heat balance.

3. Uncertainty about the temperature of the heat sink, i.e., the SMA, IU, and S-IV stage.

4. Uncertainty about the environmental effects on Pegasus thermal control coatings.

As it turned out, all of these factors changed considerably; Factors (1) and (2) changed because of several adjustments of power consumption and injection parameters during the project design and implementation. Factors (3) and (4) changed as unpredicted degradation caused orbit temperatures to be some 40°K above predicted levels. The louver system has maintained the electronic temperatures within acceptable ranges on all three Pegasus vehicles since the beginning of their flights.

Thermal Analysis of Canister

The analysis of the electronic canister consisted of (1) desk calculations of representative average heat balance equations, and (2) detailed studies utilizing a complex computer program. The computer studies were used to validate the desk calculations.

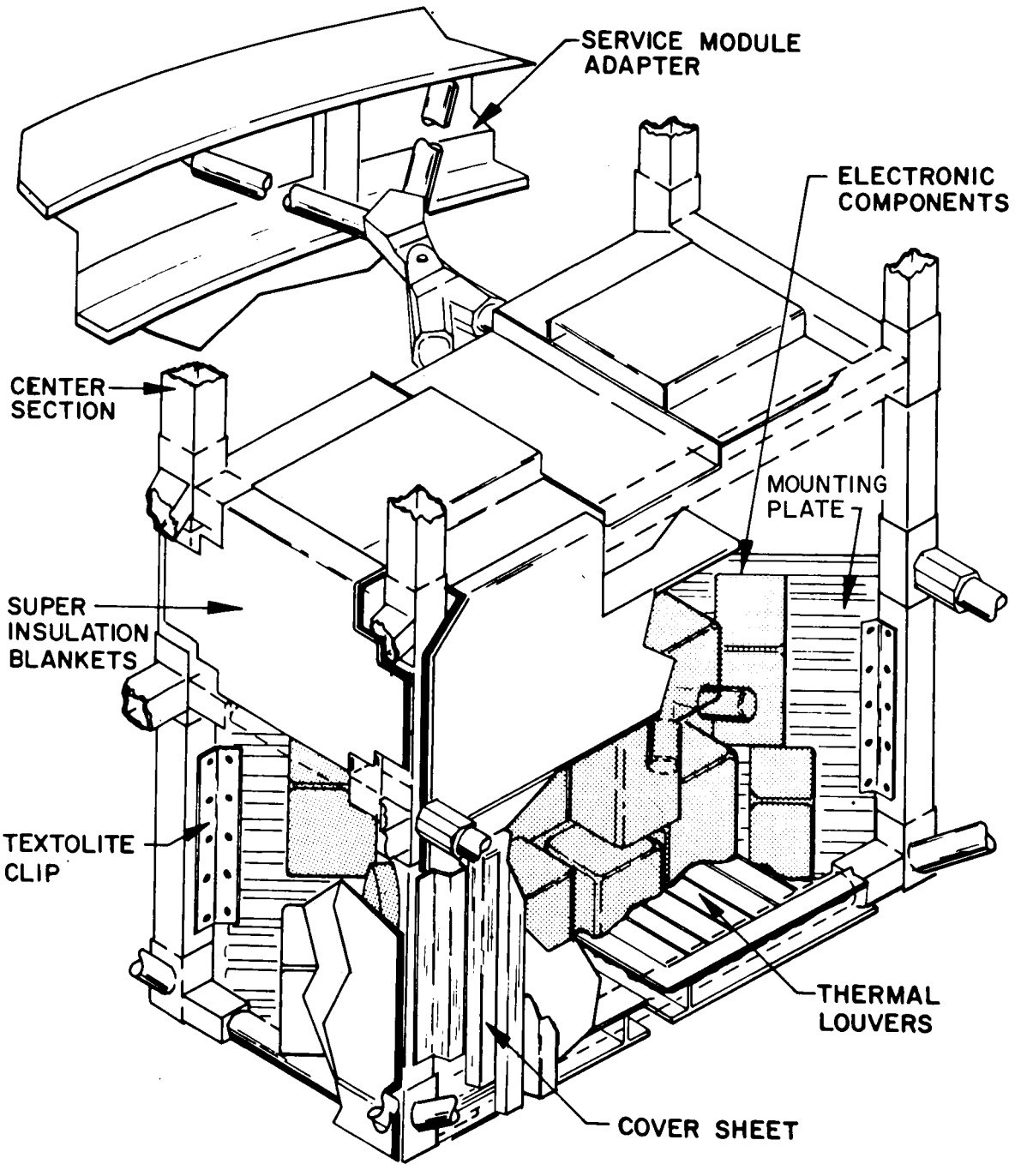

FIGURE 10. THE ELECTRONICS CANISTER

The canister (Fig. 10) was designed to be thermally isolated for the following reasons: (1) to prevent the components from being thermally linked to heat sources of difficult-to-determine temperatures, such as the Pegasus center structure; (2) to insure that the components will not be affected by varying radiant sources of heat, such as direct solar radiation; and (3) to maximize the controllable heat transfer by minimizing extraneous heat transfer. Therefore, the difference in controllable heat transfer between the hot and cold cases is minimized. This is most important because it is basically this difference that determines the amount of active thermal control required.

Primarily three techniques were employed to obtain this thermal isolation: (1) the canister side walls were equipped with ten layers of superinsulation,* consisting of highly reflective sheets of aluminized mylar, which greatly restrict radiant heat transfer through the side walls; (2) the internal mounting bracket for the components was fashioned as a double "y" and attached to the supporting structure with special fiberglass clips to restrict heat conduction to the center structure; and (3) the connecting cables and possible radiant heat leakage areas were covered with a low-emittance aluminized mylar tape, which minimized the radiant linkage between the canister components and the supporting cold structure.

In systems with large thermal time constants, the average heat balance analysis can generally be used without difficulty. Care must be taken to insure that erroneous results are not obtained in an over-simplified model. The analysis employed in the thermal design of the Pegasus electronics canister was carefully worked out, and later verified by more detailed computer studies and thermal vacuum tests.

Two of the dominant heat inputs vary primarily because of the eclipse of the sun by the earth. It is useful, therefore, to define T_x as the percentage of time-in-sunlight per orbit. For the Pegasus orbit, the range of T_x is 63 to 78 percent [6]. The internal heat generation of the electronic canister depends upon T_x primarily because the solar cell output of electric power depends on the amount of incident sunlight. Also, the solar radiation absorbed by the external satellite surfaces depends strongly on T_x.

---

* Mr. Jack Light at National Research Corp. was employed as advisor in the use of superinsulation.

The internal heat generation, the second dominant factor, was determined to be 45 to 63 W, when averaged over one orbital period.* It should be noted that the maximum heat generation occurs at maximum time in sunlight.

The T_x is used, along with the following attitude considerations, to determine the sink temperature as a function of the radiometric or optical properties of the SMA, IU, and S-IV external surfaces. The angle between sun vector and a vehicle-fixed vector along the S-IV axis is an important consideration in the thermal design of the Pegasus canister. Obviously, if the long cylindrical SMA, IU, and S-IV become oriented with the rear of the S-IV toward the sun, the sink temperature (T_s) will become very low. Besides this "cold case," the attitude can produce two "hot cases": the sun vector lined up with the axis but 180° from the cold case, and the sun perpendicular to the vehicle axis. The problem is, therefore, to predict on a statistical basis the probabilities of attitude angles with respect to the sun vector. For a freely tumbling body like Pegasus, the angular rates of tumbling in the three axes have to be considered and compared to the thermal time constant of the electronics canister. The time constant is defined as the time required to reduce a suddenly applied temperature differential to 1/e of its initial value after a sudden change in heating has occurred. This time is 15 hours for the Pegasus electronics container. The analysis had to take various tumbling modes into account. It could be expected that the final rotational mode of Pegasus would be a "flat spin" about the axis of the maximum moment of inertia.** Unlike the early Explorers, the spin around the longitudinal axis would cease and the total momentum would be around an axis perpendicular to the S-IV axis and perpendicular to the wing areas. The rate of angular motion could be expected to exceed 1 radian in 15 hours. The dangerous "cold case" due to solar attitude was, therefore, not likely to occur.

An average value for the thermal radiation geometry factor Υ can be derived from

$$\Upsilon = \frac{1}{t} \int_0^t \sin \Theta \, dt,$$

wherein t = time

---

* Mr. Mott, Fairchild-Hiller Corp.

** See Chapter VI.

Θ = angle between sun vector and forward vehicle axis.

In the limiting case for rapid spin, this becomes $2/\pi$ if the sun vector is perpendicular to the spin axis. An evaluation of the integral over a wide range of spin rate showed that the form factor will always exceed 60 percent. The maximum case of 100 percent occurs if the sun vector is parallel to the tumble axis.

The "cold case" of a form factor of zero cannot occur for this flat spin mode. However, the thermal control analysis had to consider other spin modes also. The analysis included the mode of a precession cone around the momentum vector. This did not prove to be a limiting case for large angles of the precession cone ($\geq 30°$).

The "cold case" could occur during the early period of orbital flight if all of the rotational momentum were in the plane of the minimum moment of inertia (around the longitudinal axis). The possibility of this case led to a recommendation of a launching window which would place the sun vector in the forward hemisphere at injection, and it also contributed to the decision to use an active control system.

The actual rotational behavior of Pegasus is described in the section, "The Rigid Body Motion of Pegasus" of Chapter VI. It started out with rotation about the longitudinal axis, then the rotational momentum transferred to the other two axes in a transitional precession cone. Eventually, the motion will end up in a "flat spin." In the analysis of thermal measuring results, all of these cases have to be considered.

To evaluate the temperatures analytically, the heat-balance equation for the sink is used:

$$\frac{1}{\tau} \int_0^{\tau} \sum_{i=1}^{n-1} Q_i \, dt = 0,$$

where $\dot{Q}_i$ = heat flow rates into the sink in W

dt = differential time in sec

τ = orbital period in sec

Expanding and separating, the following form can be obtained for the SMA temperature T_s

$$\left(\frac{T_s}{100}\right) = \frac{S}{\sigma\pi}\left\{\alpha_s/\epsilon_T\left[\cos(\text{MAS})\,T_x + \frac{F_{\gamma r}\,\overline{\cos(\text{RAS})}}{2}\,B\right] + F_{\gamma r}\,E\right\} + \frac{\dot{Q}_0}{\sigma A_T},$$

where $\dot{Q}_0$ = flux through the top of the SMA in W

A_T = external area of the SMA, IU, and S-IV in m^2

Other parameters have been defined in the first section of this chapter.

The canister temperature (T_c) is now expressed in terms of T_s with its heat-balance relation:

$$A\,F\,\sigma\left[\left(\frac{T_s}{100}\right)^4 - \left(\frac{T_c}{100}\right)^4\right] + \dot{Q}_1 + \dot{Q}_g = 0,$$

where $\dot{Q}_g$ = average orbital internal heat generation of the canister in W

$\dot{Q}_1$ = extraneous heat loss through insulation, etc., in W

A = area of radiating window in m^2

F = radiation factor (window geometry)

As expected, parametric studies revealed that the mean value of T_s, range of T_s, and value of $\dot{Q}_1$ were of prime importance. $\dot{Q}_1$ has to be minimized; and T_s must be cold to obtain the greatest effect of the window for control. Thus a low α_s/ϵ_T space-stable coating was desirable. After an exhaustive search, S-13* (ZnO in Methyl Silicone) was recommended by Mr. Edgar R. Miller of

---

* The S-13 is a highly reflective white paint developed at the Illinois Institute of Technology (IIT) under sponsorship of MSFC. This coating was shown to be space stable ($\Delta\alpha_s \cong 0.04$) after 200 hours of 10 sun-intensity ultraviolet irradiation.

MSFC. After due consideration of the laboratory data available, a range of 0.2 to 0.3 of α_s / ϵ_T was established to be used in the thermal design calculations of T_s. The $\dot{Q}_1$ range was calculated to be approximately 10 to 40 W. An "A" could not be selected which would maintain T_c within its limits. This means that the compensation obtained by $(T_s^4 - T_c^4)$ was not sufficient between the hot and cold cases. After a comprehensive study, thermal control louvers similar to those used on Mariner II were added to the canister window to make F controllable $(0.15 < F < 0.60)$ [7]. [It is noted that with louvers, one must replace $(T_s^4 - T_c^4)$ with $(T_e^4 - T_c^4)$, where $T_e^4 = \frac{T_s^4 + T_c^4}{2}$ when the louvers are closed.] The range of the canister temperature is then 275° to 305° K.

A computer analysis of the electronic canister was performed which evaluated the calorimetric heat-balance equations without resorting to the use of averaging; the thermodynamic model was broken down into 45 nodes with 45 simultaneous first-order differential equations. These equations were solved on the IBM 7090 Mod. II, utilizing the "General Space Thermal Program" developed at MSFC. The sink temperature range obtained was 209° to 240° K. Several runs were made using various values of the parameters directly affecting the canister temperatures.

A series of thermal vacuum tests was made at Fairchild-Hiller Corp. (FHC), Bladensburg, Maryland, under close monitoring by MSFC. In these tests, the thermal design was verified and further developed. The tests were designed to thermally simulate the SMA, S-IV, and Pegasus center structure temperatures, and to evaluate the resultant canister temperatures for both the hot and cold cases.

Approximately 200 thermocouples were utilized in monitoring the canister, sink, and structure temperatures. They were placed on each electrical component, across various heat paths, etc. The sink and exterior structure temperatures, programmed at orbital extremes, were obtained by the use of heater blankets with an adjustable heating current system.

The thermal vacuum development and design verification tests were made without simulation of the solar spectrum. The solar energy balance was calculated and duplicated in the tests with the heater blankets. This approach

was felt to be as reliable as the solar spectrum simulator systems with a substantial savings in time and equipment; duplicating the solar spectrum over a minimum area of 25.0 m^2 would have been extremely demanding.

In the first series of runs, the battery temperatures were running at 266°K. These low temperatures were found to result from excessive extraneous heat leaks. Several methods were employed to eliminate excessive heat leakage, one of which was wrapping the electronic harness with aluminized mylar. In a later run, a minimum battery temperature of 281°K was obtained in the cold case. The time constant was verified at 15 hours.

All other specifications were met during these tests. A summary of the Pegasus-A thermal vacuum data follows.

Canister Prototype Thermal Vacuum Test

Test 1	Heat Dissipation (W)	Average Internal Temperature (°K)	Battery Temperature (°K)
Hot Case	74	294	296
Cold Case	44	264	266
Test 2			
Hot Case	64.1	300	300
Cold Case	44.9	279	281

III. METEOROID DETECTOR DEVELOPMENT AND TESTING

Mary J. Smith*

Introduction

The major pacing development item of the Pegasus Project was the meteoroid detector. At the time of initiation of the project, the capacitor detector was under development by the Langley Research Center, and effectiveness of the system as a detector had been established in principle. However, at that time no production technology had been developed, nor had sufficient tests been run on conceptionally equivalent systems to adequately establish effects of the space environment. The final detector panel which evolved is designed to permit relatively easy manufacture with reasonable yield rates of acceptable units, to limit the effects of temperature extremes on the structures, and to be self-shadowing from back impacts (which would probably result in shorting of the detector).

An extensive investigation was made of the effects of electron radiation on the detectors and associated circuitry. In addition to the tests conducted by MSFC specifically as a part of the Pegasus development project, Mr. H. Heyson and co-workers at the Langley Research Center conducted very extensive experimental studies of radiation effects on Pegasus type meteoroid detectors, cables, and associated electronic subsystems. Due primarily to the inherent inability to completely simulate the space environment in a laboratory facility, the experimental research did not conclusively establish an expected rate of radiation-induced impulses; however, the available data tended toward support of the conclusion that the "false count" rate would be sufficiently low as to not distort seriously the meteoroid penetration rate data. Actual flight experience has shown no evidence that the meteoroid data are being falsified by unrecognized radiation discharge pulses. In fact, to date, only three events explicable as a radiation discharge have been recorded.

Several test series were conducted to determine the response of the detectors to hypervelocity impact. The first series of tests was used to further

---

* Saturn I/IB Program Office (Pegasus Project Office), now in Research Projects Laboratory, MSFC

the development of the capacitor and were conducted by MSFC. The final test series was to determine the efficiency of the flight system and was conducted by the Fairchild-Hiller Corp. In this final test series, each of the three types of capacitor was shown to be approximately 80 percent efficient in detecting penetrating impacts and to reject almost 100 percent of all nonpenetrating impacts.

Selection of Sensor Type

Several factors influenced the choice of the detector to be used on the Pegasus satellites. The purpose of Pegasus is to provide a direct measurement of the frequency of penetrations through known thicknesses of known materials.* So that statistically significant data be obtained, it is necessary that relatively large areas of the material be exposed for appreciable periods of time. Based on the best data available at the time of initiation of the project, it was estimated that an area of not less than 100 m^2 exposed for a period of one year would be required if a significant number of penetrations were to be experienced through a thickness approaching that of interest to the structural designer (i.e., in the range 0.8 to 2.5 mm).

At least four general types of detection devices appeared to be available and applicable at the initiation of the project. Each of these was considered. The first two types were the pressure cell detector and the wire grid detector which were being developed by the Langley Research Center and were subsequently successfully flown on the Explorer 16 and 23 satellites. The major problems associated with the use of these detectors include the large area to be instrumented and the fact that the sensor is destroyed by the first penetration. To instrument a large area in a manner which would have prevented high percentage losses on each detected penetration would have required a large number of independently constructed sensors (particularly on the thinner materials) and very complex data processing circuitry. Also, large area pressure cells were not available at the time.

At the time of project initiation, the Marshall Space Flight Center had under development an infrared sensor designed to detect the flash produced by penetrating impact. After a very thorough review, it was concluded that the state of development of this system precluded its selection as the sensor type to be flown in the Pegasus project.

---

* See Chapter I.

Two sensor systems, both utilizing the effect of a momentary discharge of a capacitor created by the penetrating passage of hypervelocity particles, were available and were undergoing laboratory tests. Lewis Research Center had developed and was testing a coincidence capacitor-type detector [8]. The sensor was made by bonding a thin, metallized dielectric sheet (aluminized mylar) to opposite sides of a "target plate." A pair of charged capacitors was formed by impressing on the two outside electrodes a voltage (about 300 V) with respect to the center target plate. Penetration of the system was assumed when both capacitors were discharged simultaneously. Laboratory tests then in progress indicated that the problem of isolating the detectors in such a way that "cross-talk" between the two, leading to the generation of false coincidences, had not yet been solved. Therefore, it was concluded that perfection of the system to flight status most probably could not be accomplished within the planned project time of 13 months.

Langley Research Center had developed and was testing a capacitor-type sensor appreciably less complex than the Lewis model [3]. It consisted of a single capacitor formed by bonding thin aluminized mylar to the back of the target plate. Reports from early tests indicated excellent detection characteristics at an impressed voltage as low as 10 V. The associated detector electronic circuits were relatively simple and easily constructed.* Based on the early test reports, major problems to be anticipated were primarily in the area of establishing techniques for the production of quantity runs of flight quality units.

Conceptual Design of Sensor System

Early conceptual studies of a meteoroid measuring satellite revealed that the total area of meteoroid sensor surface which could be exposed would be limited, for a simple structural design, to about 200 m^2. Further, structural considerations resulted in the selection of a "paned window frame" type of mounting for the detectors such that the optimum size of an individual sensor was about 100 by 50 cm. In the final design, the Pegasus spacecraft contained 416 individual detectors or sensors, each with a sensitive area of approximately 100 by 50 cm. Because it was anticipated that failures of the capacitors could result in types of malperformance necessitating the removal of a sensor from the data processing electronics, the system specifications required the capability of "commanded" disconnection of sensors in flight. The largest capacity command decoder available (then in development) permitted the control

---

* A modified version of this capacitor was later flown on Explorer 23.

of 70 functions. Analysis of the system led to the identification of seven necessarily controlled functions; therefore, 62 channels were reserved for the control of the sensors leaving one spare. Thus the 416 individual sensors were grouped into 62 logic groups or information circuits, each of which can be switched on and off the data processing electronics by command from the ground.

Sensor Design Studies

To initiate production technology studies, fabrication of scale-sized units was undertaken utilizing specifications developed at the Langley Research Center. The early models consisted of 20 by 20-cm flat aluminum plates to which was bonded a 6.4-μ-thick mylar film, one side of which was covered with vapor-deposited aluminum. To control charge leakage at the edge, and to provide a vapor seal, a 2-cm-wide plain mylar strip was bonded along all four edges of the target plate extending beyond the edge of the plate. Electrical leads were attached to the capacitor by soldering to the target sheet and by pressure and conductive adhesive to the vapor-deposited aluminum. Contact resistance less than one ohm was required at each surface. Immediately after fabrication samples met this specification; however, it was found that after a few weeks of storage the contact resistance at the deposited electrode-electrical lead interface had increased to excessive values. Some of the samples even had become open. Additionally, thermal-vacuum tests performed on the samples resulted in delamination of the mylar film from the target sheet, beginning along the lines at which the aluminum coated mylar was deflected to pass over the inserted strip at the edge of the plate. After several months of effort, attempts to establish production techniques utilizing the originally suggested structures and specifications were discontinued, and two parallel research and development programs were begun to establish basic requirements and specifications for a capacitor sensor more amenable to manufacture.

Fairchild-Hiller (FHC) developed a technique for first laminating the mylar dielectric to the target sheet, and then applying a second coating of adhesive to the mylar. Small sheets of 4-μ gold foil were then rolled onto the mylar to create the second plate of the capacitor. Electrical contact to the gold foil could be obtained using a low temperature indium solder. Rolling the gold foil into place was a hand operation, and hence quite difficult to control effectively. The foil had a tendency to crack during the rolling process and produce electrically isolated areas. These cracks could be repaired with a second layer of gold; however, since no additional adhesive was used, the foil would later separate in doubled areas. The bond between gold and mylar was

not very strong, and during subsequent testing the gold foil was occasionally pulled from the mylar, isolating large areas of the capacitor. It would not be possible to detect these isolated areas if such separations occurred during flight. Also, in the very early hypervelocity impact tests, it was found that the thin foil would burn away from the area of impact before the capacitor had sufficient time to complete its discharge. A thicker foil was not desirable since this would probably lead to permanent shorting problems under impact.

The G. T. Schjeldahl Co. developed a technique for laminating the mylar dielectric to the target sheet and then vapor depositing a copper layer onto the mylar. The deposition process could be easily controlled to yield the desired copper thickness (approximately .07μ), and the copper was tightly adherent to the mylar. The copper surface was also quite easy to inspect for defects. After the vapor deposition process the resultant capacitor was "burned out" by application of increasing voltages with limited current to remove low resistance points created in the manufacturing process, and then electrical contact was made using brass tabs and standard 60/40 solder. Use of a template during the deposition process eased the problem of acquiring the desired outline of copper. The copper was recessed slightly from the edge of the target sheet to provide a bare mylar border, and around the areas of the Lord mount attachment clips (fiberglass clips used in the attachment of the capacitor to the spacecraft) to reduce the possibility of permanent shorting at the stress concentration points.

Because of the ease of manufacture and the greater ability to control and inspect the sensors during fabrication, in addition to the better behavior under test, the Schjeldahl sensor was chosen for use on the satellite.

A fiberglass terminal block with standard electrical pins was designed and installed on the capacitors to simplify the connection from the spacecraft wiring to the capacitors. This allowed easy connections and made it possible to resolder connections without large risk of damage to the capacitor.

The in-flight temperature of the detector panels had to be controlled within the range suitable for the mylar dielectric. To allow a safety margin, the highest permissible temperature was specified to be 394°K. This necessitated a coating having an absorptance to emittance ratio, α/ϵ, of 1.0, and this, in turn, set the lower temperature limit at 167°K. The thermal control coating on the sensors had to be as thin as possible to avoid any influence on the meteoroid penetration data. The only coatings which met these requirements were vapor deposited silicon monoxide and Alodine, the product of a

chemical conversion process.* The silicon monoxide was prohibitively expensive for the large areas needed; therefore, development started on the Alodine process. The Alodines then available showed a tendency to degrade under prolonged ultraviolet exposure. FHC developed a modified Alodine, MTL-3, which was capable of withstanding prolonged ultraviolet and vacuum exposure without degradation. During the testing of this coating, it was found that readings of the thermal properties of the coating had to be made without breaking the vacuum as the Alodine had a strong tendency to reabsorb water upon short exposures to the atmosphere.

It was initially assumed that only tightly adherent coatings could successfully withstand handling damage and the space environment; therefore, a "rub test" was instituted, with all coatings which caused any visible discoloration of the white rubbing cloth being rejected. It was found, however, that the slightly loose coatings had better thermal properties, probably because they were thicker, and a test program was started to determine if some of these coatings could be used. Both vibration and acoustic testing, as well as handling tests, failed to cause any damage to the coatings. Ultraviolet exposure tests as long as 2000 equivalent sun hours produced no detectable degradation in any of the coatings. As a result, an arbitrary definition of acceptable looseness was made on the basis of discoloration of the rub cloth, and the slightly loose coatings were accepted for flight use.

At the start of manufacture the MTL-3 technology was transferred from FHC to Schjeldahl. In the larger tanks at Schjeldahl the Alodine bath was found to undergo a buffering action upon the addition of chemicals, so a technique was developed to allow the constant addition of small amounts of the chemicals with periodic checks to determine whether the bath was within the specified composition limits.

The Alodine could not be applied to the aluminum sheet at the start of the fabrication process since the subsequent exposure to a high temperature-vacuum environment during the vapor deposition process tended to degrade the coating. Consequently, a technique was developed for masking the copper surface and applying the alodine after the deposition process. The same adhesive used to bond the capacitor to the foam core was applied over the copper and cured to form the mask.

---

* See Chapter II.

In an accelerated life test performed just prior to the start of flight hardware production, the capacitors were exposed to 200 hours under vacuum at 394°K. Periodic checks were made on the electrical properties of the capacitors during these tests. After exposures ranging from 6 to 30 hours, the insulation resistance of the capacitors were found to decrease to unacceptable limits. After this degradation had occurred the temperature coefficient of resistance had disappeared and could not be recovered. No explanation of this phenomenon was found. The use of a thicker layer of mylar was not desirable since this would once again lead to comparable thicknesses of the target sheet and other materials, so a trilaminate of 3.8-μ mylar was tried. When the insulation resistance of the trilaminate did not show any tendency to degrade under the prolonged high-temperature and vacuum exposure, this design was adopted. The adhesive layers on the trilaminate were reduced in thickness to preserve the original 12.6-μ total dielectric thickness. No positive explanation for the better performance of the trilaminate has been found; however, it is known that the thinner mylar undergoes additional filtering for contaminants in its manufacturing process. Also, the use of three layers of mylar probably leads to a mismatching of defects. The trilaminate capacitors were found to yield better results in the functional tests than the single layer units.

At the time of the initial satellite design, it was planned to bond one capacitor to each side of a rigid, closed-cell foam core. This foam core would serve both as a structural backing for the capacitors and as a stopping agent for debris created in the meteoroid impact. The detector panel thus formed would be mounted to the satellite wing at six points with rubber Lord mounts.

The coefficient of thermal expansion of the foam was appreciably higher than that of the aluminum. During the temperature excursions expected in the space environment, this would result in an undersirable stress concentration in the mylar dielectric. In laboratory tests this shear stress most often resulted in cracks in the foam, but the point of failure could shift into the capacitor, as was the case with gold foil units. As a result, the foam core was modified to a 1.27-cm layer of the rigid, closed cell foam for structural stiffness with a 0.64-cm layer of flexible, open cell foam bonded to either side. This flexible foam absorbed the shear stress protecting the capacitor from damage. In the event of a failure in the flexible foam under prolonged thermal cycling, the capacitor would still be held in place by the fiberglass attachment clips, and no area loss would be incurred. No such failure occurred during the tests of the panel. Solid blocks of the rigid foam were retained under the attachment clips to prevent unnecessary flexing of the capacitor. The completely rigid core was retained for the 0.04-mm capacitors since they were flexible enough to follow the

excursions of the foam with no damage to the capacitor. The rigidity of the solid foam core was also needed on this unit to prevent damage to the thin capacitors during handling operations.

The final panel design is shown in Figure 11.

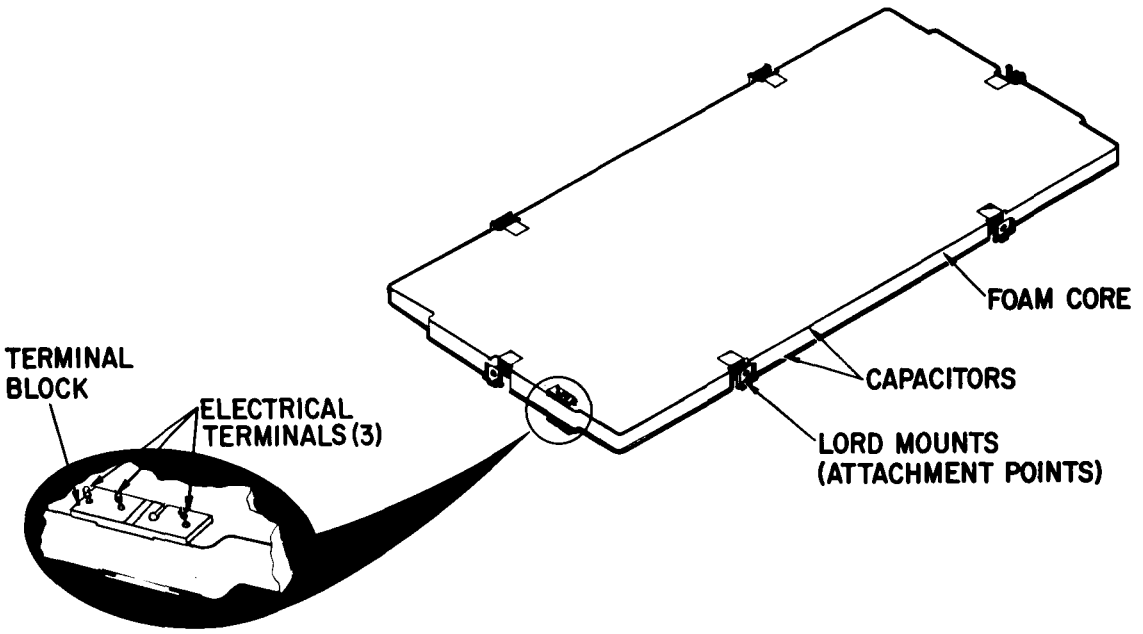

FIGURE 11. FLIGHT CONFIGURATION DETECTOR PANEL

Impact Testing with Hypervelocity Particles

The first hypervelocity impact tests on the detectors were performed at the Utah Research and Development Corp. (URDC) to determine the ability of the foam core to prevent impact debris from impinging on the rear capacitor of the detector panel. The capacitor is susceptible to permanent shorting when particles strike from the thin plate side. Particles larger than 10^{-4} g having velocities of approximately 5 km/sec were found to be capable of completely penetrating the foam and reaching the rear capacitor. Particles having this amount of energy were expected to be relatively rare in the space environment, but attempts to improve the foam core were made. A layer of fiberglass was inserted at the centerline of the foam core to serve as a barrier to the hypervelocity debris. This barrier was found to entrap gases produced by the hypervelocity impact and actually result in greater damage to the panel. Figures

12 and 13 show comparative damage to a sample panel with and without the fiberglass barrier. In both cases the particle is large and extremely slow with

0. 2-mm Aluminum Face Sheets (not capacitors)
2. 54-cm Rigid Foam
5. 66 · 10^{-3}-g Aluminum Particle at 4. 5 km/sec

FIGURE 12. DAMAGE TO 0. 2-mm ALUMINUM FACE SHEETS WITHOUT THE FIBERGLASS CENTER BARRIER (The particle entered at top of picture and debris completely penetrated the foam. A rear capacitor would probably have been permanently shorted in this impact.)

respect to those anticipated in space. Faster particles show a greater tendency to break up on the target sheet with less resultant penetration into the foam. When the change to the three layer core was made, a similar series of tests was run, and the new core was found to be superior to the completely rigid one. They layer of adhesive between the rigid and flexible foams acted as a barrier to the debris, but the open cell foam permitted the gases to escape and prevented the blowback phenomena created by the barrier in the solid core. Figure 14 shows damage in the final configuration foam produced by a particle more realistically simulating those expected in space. Particles as large as 5. 10^{-5} g moving at 6 km/sec could be stopped in the foam without damage to the rear capacitor when the 0. 2-mm target sheet was used.

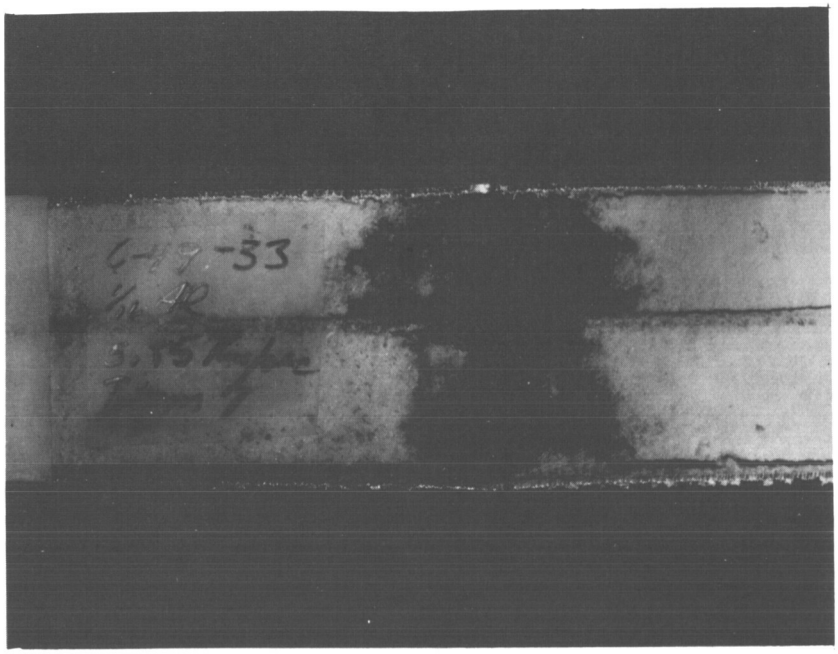

0. 4-mm Aluminum Face Sheets (not capacitors)
2. 54-cm Rigid Foam with 0. 4-mm Fiberglass Barrier in Center
5. 66 · 10^{-3}-g Aluminum Particle at 5. 85 km/sec

FIGURE 13. DAMAGE TO 0. 4-mm ALUMINUM FACE SHEETS WITH 0. 4-mm FIBERGLASS CENTER BARRIER
(Note blowback and resultant increased foam damage at fiberglass barrier. Both front and rear capacitors would probably have been permanently shorted in this impact.)

The last few shots under the foam testing effort at the URDC light gas gun facility were devoted to preliminary tests of the discharge characteristics of small sample capacitors with the gold foil inner plate. Several samples were tested with the associated electronics, and then tubular capacitors were connected in parallel with the samples to simulate the capacitance of the full-sized capacitor. Penetrations of both of these configurations resulted in acceptable depths of discharge. At the end of these tests impacts were made into full-sized capacitors with the gold foil back plate. No signals were obtained. It was postulated that the large, fast energy dump in the full-sized units was burning the gold foil away from the contact area before the discharge could be completed. In the simulated units the reactance in the tubular capacitors would have slowed

the discharge and prevented this from occurring. A full-sized capacitor with the copper inner plate showed acceptable discharges. From the results of these tests, it was decided that all future impact tests would be performed with the full-sized capacitor.

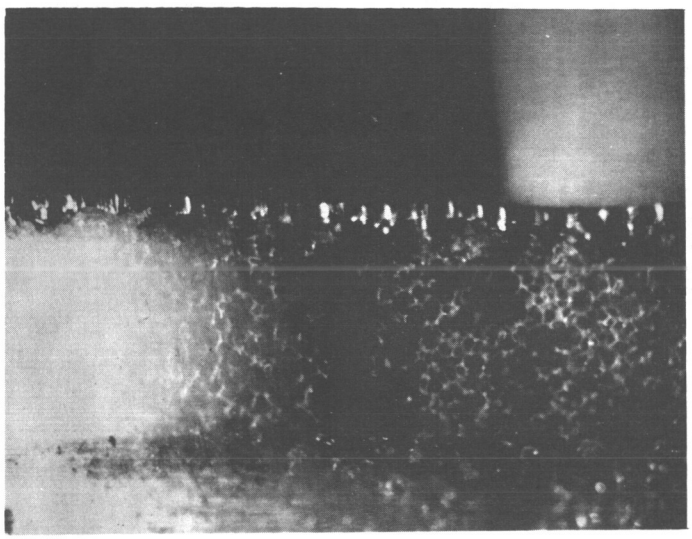

0. 2-mm Aluminum Target Sheet Capacitor
0. 64-cm Flexible Foam Bonded to 1. 27-cm Rigid Foam
$5.8 \cdot 10^{-4}$-g Glass Particle at Velocity in Excess of 30 km/sec

FIGURE 14. DAMAGE TO FINAL FOAM CONFIGURATION BY PARTICLE AT METEORIC VELOCITY
(Dark horizontal streak at bottom of picture is glue line between foam layers. Dark area in center extending from capacitor to glue line is crater. There was no damage in the rigid foam and no evidence of delamination.)

The test series at URDC was extended for development tests of the full-sized capacitor. All the capacitors had 0. 2-mm target sheets and were clamped against a foam core. The capacitor was connected to the flight-type electronics with a 40-V bias on the capacitor and a 10-V level for acceptance of a signal as a hit. Unfortunately, it was discovered late in the series that the sabot was tumbling in flight and impacting on the sabot catcher prior to the impact of the particles on the capacitor. Since the method of velocity measurement used the

time of flight from the initiation of the gun firing to the impact flash of the first event in the target chamber, all of the velocity measurements except those few where the first impact flash could be correlated with a capacitor discharge were invalidated.

At the time of initiation of the second URDC series, it was recognized that the relatively large and slow-moving particles produced by a light gas gun did not provide a realistic test of capacitor performance. In an attempt to produce particles which would just barely penetrate the capacitor, a contract was let to the Hayes International Corp. to demonstrate the ability of their powder gun facility to produce such particles at velocities in excess of 6 km/sec and then conduct a series of impact tests into the 0.2-mm capacitors, using a set-up similar to that at URDC.

These two test series yielded an average discharge of the capacitor in excess of 20 V. Although the overall average at URDC was higher than that at Hayes there did not seem to be any correlation between discharge voltage and particle size or velocity in the ranges covered. No capacitors became permanently shorted as the result of a first particle impact, although there were a few permanent shorts created by large debris and by multiple impacts during a single shot. These tests showed the ability of the detector system to operate properly with a relatively large percentage (greater than 75 percent) of discharges on perforation which would be accepted by the electronics as valid hit indications.

In an attempt to determine the response of the capacitor to extremely fast particles, a few shots were made at the Rhodes and Bloxsom facility. This gun was powered by a large capacitor bank, and valid electrical measurements were difficult to make in this environment. The facility appeared to be capable of producing particles at velocities in excess of 15 km/sec, and the capacitor seemed to be responding to the particles with approximately the same discharge levels which were observed with the slower particles. It was known, however, that the electric noise generated by the capacitor bank discharge was affecting the electrical measurements in the facility. The amount of time estimated to be required to shield the system and establish the validity of the measurements was prohibitive, so these tests were discontinued.

At the completion of development testing, proof tests of the capacitor system were conducted by Fairchild-Hiller at the Hayes facility. Each of the three types of capacitors were tested in a test set-up simulating the flight configuration as closely as possible. The capacitors were bonded to a 1.27-cm foam (one half of a detector panel was used) and were connected in parallel

groups to simulate the detector logic groups on the satellite. The 0.04-mm capacitors were tested two in parallel, the 0.2-mm six in parallel, and the 0.4-mm eight in parallel. In functional tests performed on the Pegasus prototype it had been found that the grouping of capacitors in the logic group would help the recharge current amplifiers in recharging the discharged capacitor of that group. This would prevent the proper identification of the logic group in which the discharge had occurred. As a result, diode-resistor parallel combinations were placed in series with the signal line at each capacitor to prevent the flow of current from an unpunctured capacitor to a punctured capacitor within one logic group. These diode-resistor modules were used during the tests at Hayes. In addition, a fuze was placed in the signal line to each capacitor to simulate a modification made to Pegasus II as a result of experience gained from Pegasus I. The detector electronic circuits of the spacecraft were reproduced in a test bus so that the spacecraft load on the capacitors would be correctly simulated and the behavior of the electronics verified. The capacitors were biased to 40 V, and the level for acceptance of a signal as a valid hit indication was set at 4 V.

In the early part of the tests the velocity of the particle was determined by a measurement of the time of flight between the firing of the gun and the discharge of the test capacitor. Unfortunately, two problems were present with this system. In the large majority of the shots more than one particle impacted the capacitor. Since the capacitor signal was taken for the time of flight measurement, it was impossible to determine if the capacitor had responded to the first penetration. On some shots the capacitor failed to respond although penetrations were found after removal of the capacitor from the target chamber. Thus it was necessary to develop an independent system for the measurement of the particle velocity and for the determination of the time of the first penetration. A photocell system was developed which looked at the back of the capacitor and detected the flash resulting from the first, and subsequent, penetrations. However, it was also capable of detecting nonpenetrating impacts after the formation of the first hole through the detector. As a result, only the time of the first penetration was used as a valid data point. While the photocell system was being installed, the baffle in the test chamber was modified to reduce the average number of impacts on the capacitor during any one shot, and the program was reoriented to require shots with single penetrations as primary sources of data. With only one penetration per shot it would be possible to relate the discharge to a given hole formed by a particle moving at a known velocity and hence allow a more complete analysis of the data. One hundred such single penetration events were desired in each of the three capacitor types, and 237 events of this type were actually obtained (104 in the 0.4-mm and 70 in each of the other two types). Particle velocities ranged upward to 10 km/sec.

A set of data taken for a typical shot is shown in Figures 15 and 16. The capacitance and resistance of the capacitor were measured before and after each shot. The impact time of the penetrating particle recorded by the capacitor had to agree with the impact time determined by the photocell or the capacitor was recorded as not responding to the first penetration. The recorded size of the hole is the diameter measured under a microscope after removal of the capacitor from the target chamber. T_0 in the trigger column refers to the time of the firing of the gun.

At the conclusion of the test series, a careful analysis was made of the results. Each of the three types of capacitors was capable of producing signals greater than 4 V on a large percentage of the single penetrations. The majority of the events on which signals less than 4 V were obtained showed no detectable signal at all, so a lower threshold would not have resulted in a significant increase in detected hits. Table I gives the number of shots with single penetrations into each of the three types of capacitors with the number detected and the actual percentage detected. The last column is the probability of detecting a single event calculated at the 0.95 confidence level. Table II gives the number of single penetration events which resulted in a permanent short of the capacitor and hence would have resulted in a loss of area on the satellite. The last column gives the maximum percentage of penetrating events which would be anticipated to result in a permanent shorting of the capacitor, calculated at the upper 0.95 confidence level.

There was no clearly recognizable indication of a trend of discharge voltage with either particle velocity, size of hole, or appearance of hole from the data gathered in these test series.

A series of tests was conducted by MSFC at the North American Aviation impact facility in a second attempt to check the behavior of the capacitors upon penetration by higher velocity projectiles. Approximately seventy shots were fired into the 0.04-mm capacitors with velocities up to 14 km/sec. The resultant discharges compared very well with the results from the Hayes facility.

Effects of Electron Radiation on Detectors

Shortly after the initiation of the Pegasus program, a series of tests at the Langley Research Center indicated that electrons stored in the capacitor dielectric when the detector was placed in a radiation environment were

PEGASUS METEOROID DETECTOR
IMPACT TEST PROGRAM
TEST DATA SHEET

1. DATE: 4/29/65

2. DATA SHOT NUMBER: 1813

3. CAPACITOR DETECTOR SERIAL NUMBER: C 42-456
DETECTOR THICKNESS: .0015 BONDED
CAPACITANCE PRE-TEST 1.02 μf
POST-TEST 1.02 μf
RESISTANCE PRE-TEST 17. MEG OHMS
POST-TEST 17. MEG OHMS

4. PHOTO MULTIPLIER OUTPUTS: 1
PHOTO MULTIPLIER VELOCITY: 20.4K FT/SEC _____ FT/SEC
_____ FT/SEC _____ FT/SEC
_____ FT/SEC _____ FT/SEC

5. CAPACITOR DISCHARGES: 1 COUNTER TIME: 1123 μs
VELOCITY 20.4K FT/SEC
_____ FT/SEC

6. CAPACITOR DEPTH OF DISCHARGE 16 VOLTS

7. NUMBER OF PERFORATIONS: 1
HOLE SIZE: 1 .005 4 _____
(INCHES) 2 _____ 5 _____
3 _____ 6 _____

8. DETECTOR SHORTED? NO ✓ YES _____
DUE TO FIRST PENETRATION _____
DUE TO MULTIPLE PENETRATIONS _____
DUE TO DEBRIS _____

9. DETECTOR CLEARED? NO _____ YES _____
SHORT RESISTANCE _____ OHMS
POWER SUPPLY VOLTAGE _____ VOLTS
POWER SUPPLY CURRENT _____ AMPS

10. COMMENTS: _____

11.

SCOPE NO.	TYPE	TRACE	SIGNAL	VERT. SETTING	HORIZ. SETTING	TRIGGER
1	555	TOP	HIT OUT	5V/CM	500μs/CM	T_o + 500μs
1	555	MIDDLE	CAPACITOR	20V/CM	500μs/CM	T_o + 500μs
1	555	BOTTOM	CAPACITOR	20V/CM	500μs/CM	T_o + 5000μs
2	555	TOP	CAPACITOR	10V/CM	100μs/CM	T_o + 500μs
2	555	BOTTOM	PM TUBE	5V/CM	100μs/CM	T_o + 500μs
3	555	TOP	PM TUBE	1V/CM	200μs/CM	T_o + 2400μs
3	555	BOTTOM	PM TUBE	1V/CM	200μs/CM	T_o + 4200μs
4	535A	RASTER	PM TUBE	1V/CM	200μs/CM	T_o + 500μs
					BLANKING PULSE EVERY 1900 50μs	
5	535A	TOP	CAPACITOR	10V/CM	5μs/CM	2V CAP. DISCH.

FIGURE 15. PEGASUS METEOROID DETECTOR IMPACT TEST PROGRAM TEST DATA SHEET

SCOPE 1

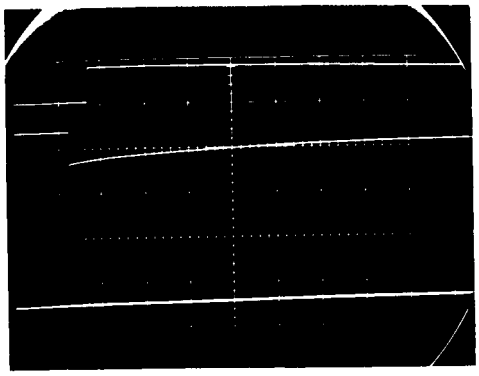

SCOPE 4

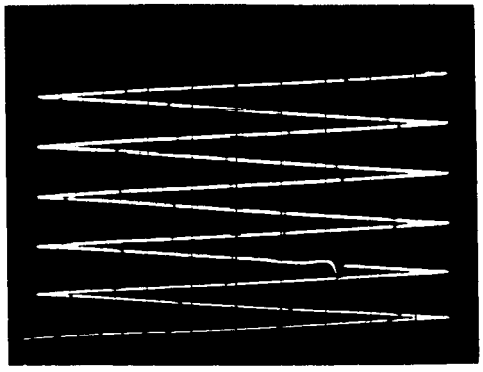

SCOPE 2

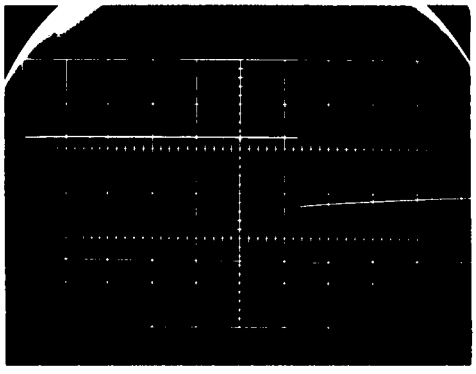

SCOPE 5

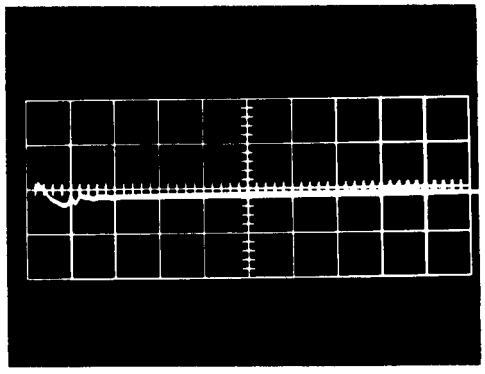

SCOPE 3

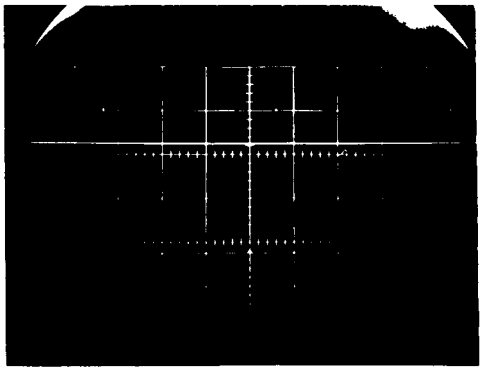

FIGURE 16. DATA RECORDED FROM SHOT NO. 1813

TABLE I. RESULTS OF HYPERVELOCITY TEST SERIES AT HAYES INTERNATIONAL CORP.

Type Detector (mm)	No. Shots with Single Penetration	No. Shots with Resultant Hit Indications	Actual Percentage Hit Indications	Percentage Hit Indications Anticipated (at 0.95 upper confidence level)
0.04	70	60	86	77
0.2	70	60	86	77
0.4	104	85	82	76

TABLE II. SHORTING HISTORY OF DETECTORS IN HYPERVELOCITY TEST SERIES AT HAYES INTERNATIONAL CORP.

Type Detector (mm)	No. Shots with Single Penetration	No. Shots with Resultant Permanent Short	Actual Percentage Permanent Shorts	Percentage Permanent Shorts Anticipated (at upper 0.95 confidence level)
0.04	70	0	0	4
0.2	70	6	8.6	17
0.4	104	8	7.7	13

subsequently released in spontaneous short noise bursts. Each of these discharges had a shape similar to the capacitor discharge pulse produced by a meteoroid penetration and frequently had an amplitude several times greater than the capacitor bias voltage. A picture of a few of these pulses is shown in Figure 17. It was feared that these pulses might occur at rates sufficiently high to render uncertain the meteoroid measurements obtained with the capacitor system.

0.2 MILLISEC/DIV 20 VOLTS/ DIV

20 MILLISEC/DIV 20 VOLTS/ DIV

FIGURE 17. PULSES EMANATING FROM DETECTOR EXPOSED TO ELECTRON RADIATION ENVIRONMENT (15 V BIAS)

An attempt was made to theoretically estimate the magnitude of the problem in the space environment. The number of electrons which would be stopped in the mylar dielectric was calculated on the basis of the energy spectrum and flux of the electrons in the Pegasus orbit, with the aluminum target sheets being considered as absorbers. The leakage of this stored charge was estimated from known data on the leakage current of mylar as a function of temperature, and increased leakage as a function of radiation intensity in a gamma environment was considered. Unfortunately, test results on capacitors in a radiation environment found in the literature reported only on the degradation of the dielectric and not on any intermittent discharges which might have occurred during the tests. Only a few papers were found which treated the

storage and discharge mechanisms, but the results did not permit ready treatment of the difficult problem in the mixed space environment. It was not possible to predict with any certainty the frequency with which discharges could be expected in space or the voltage level of these discharges. It was therefore impossible to determine whether the radiation-induced discharges would be comparable in number with the penetration discharges, greater in number, or low enough in number to create no problem.

In an attempt to gain data from which a better theoretical approach to the problem could be made, a contract was let to the Admiral Corp. to measure leakage currents in sample meteoroid detectors as a function of radiation intensity and temperature [9]. These measurements were to be performed under vacuum in a Co^{60} facility. A sample of these data is shown in Figure 18. The Langley Research Center started a parallel theoretical effort at the Research Triangle Institute [10]. An experimental program, using beta source, was planned to follow the theoretical analysis. Both of these attempts were expected to be very time consuming and difficult, so an experimental approach to the problem was instituted which, hopefully, would lead to a technique of discriminating against the radiation-induced pulses.

A contract was let to Ling-Temco-Vought, Inc., (LTV) for utilization of the Company's Van de Graaff facility in these tests. The initial purpose was primarily the production of a sufficient number of radiation-induced discharges to determine the characteristics of the pulses so that a discrimination circuit could be designed and tested. An early prototype circuit was tested in the facility and found to have inadequate discrimination capability. Subsequently, an engineering effort was started at Fairchild-Hiller to completely redesign the hit detection portions of the Pegasus data system.

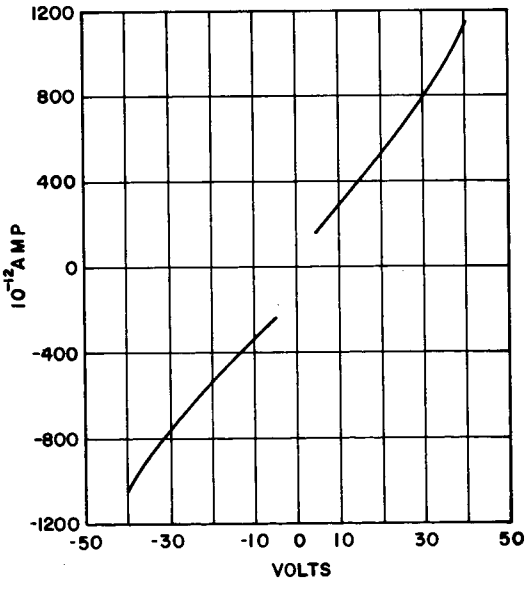

FIGURE 18. LEAKAGE CURRENT FROM DETECTOR EXPOSED TO GAMMA RADIATION ENVIRONMENT

The pulses were characterized by a fast-ringing leading edge occasionally followed by a base line shift. Samples of the leading edge of these pulses are shown in Figure 19. The middle picture shows the pulse shape

which accounted for approximately 80 percent of the total observed, i.e., a fast damped oscillatory pulse with no base line shift. Using faster oscilloscopes the leading edge of the high-frequency ring could be seen to go to a 45-V maximum excursion. In later tests at Ion Physics, careful impedance matching and shielding in the lines reduced the ringing and identified the source as a transmission line shock resulting from a low-amplitude signal at the capacitor with approximately a 10-MHz frequency. A low-pass filter was placed at the front end of the new circuit to reduce the effect of the high-frequency component of the pulse. The discharge resulting from a hypervelocity penetration had some oscillation about the maximum discharge level (Scope 5 trace of Fig. 16), but did not produce the ringing about the baseline characteristic of the radiation-induced discharge.

A characteristic of the remaining 20 percent of the radiation-induced discharges was a low-level dc shift followed by a proper capacitor recharge. The direction, magnitude, and frequency of occurrence of these dc shifts did not appear to depend on the direction or magnitude of the capacitor bias voltage. Since the direction of the discharge of the pulse resulting from a hypervelocity impact was determined by the direction of the capacitor bias (target plate ground and copper plate positive) the data processing circuit was designed to accept only negative pulses. Since average magnitude of the penetration pulses is a function of the magnitude of the bias voltage, the bias of the capacitor was increased from 15 V to 40 V to increase the difference in average magnitudes between the radiation and the penetration pulses. Further increase of the bias voltage above the 40-V level was not possible because of limitations of transistors then available.

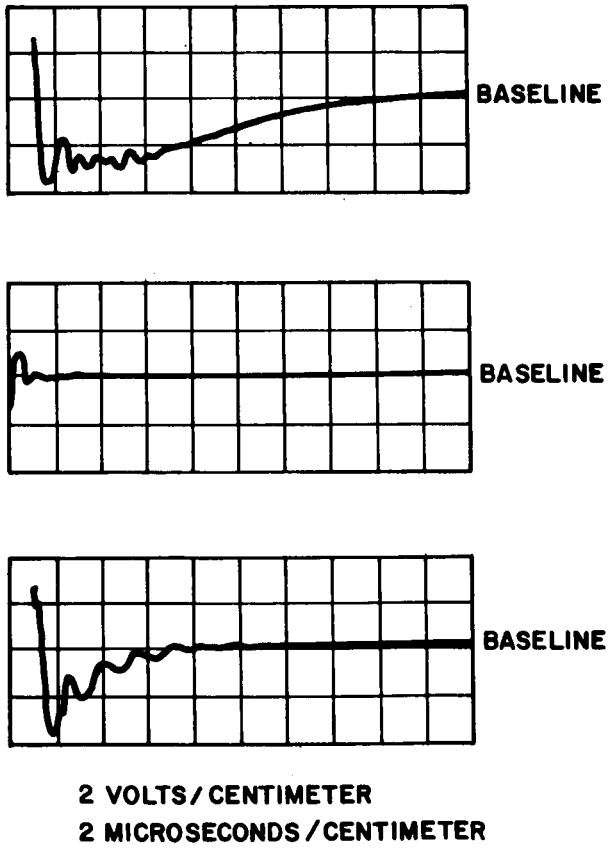

FIGURE 19. SAMPLE LEADING EDGES OF RADIATION-INDUCED PULSES

The magnitude of the large majority of the radiation-induced pulses

was less than 5 V, and only a very few were higher than 10 V, so the level for discrimination between the two types of pulses was set at 10 V in an attempt to reject all of the radiation-induced discharges. That some of the penetration discharges would be less than this level and hence rejected was recognized, but it was assumed that calibration of the system in this regard would be the simpler of the two problems. A straightforward pulse height discrimination was not acceptable, since many of the high-frequency ringing pulses would be passed through the filter section at levels sufficiently high to permit actuation of the data processing electronics. Accordingly, an integrator was designed which would function only on pulses greater than 2 V and perform a voltage-time integration during the first 250 μsec of the pulse. This would eliminate the high-frequency pulses since they have relatively small areas under the curve. At the end of the integration period, the level of the integrator was to be compared with a pre-set level and only those pulses with 2500-V/μsec area would be accepted. The threshold level at the comparator was set in the flight system such that a dc shift of 4 V, measured at the detector terminals, followed by a normal current recharge characteristic, was sufficient to activate the follow-on currents. * When this criterion was met, a hit output pulse would be generated for further processing by the data system.

The magnitude and frequency of the radiation-induced pulses increased with decreasing temperatures of the capacitor under test. For that reason, the majority of the following tests were made at the lowest operating temperature expected for the detectors in space. Figure 20 shows some typical pulses obtained during the low temperature tests.

After the design of the discrimination circuit, the circuit was tested in the LTV facility and found to be capable of discriminating against all of the radiation-induced pulses created. All of these tests were made on 20 by 20-cm samples with an 18-cm^2 area in the center of the sample being irradiated. It was highly desirable to irradiate the total area of a full-sized detector but there was no facility available which could accommodate a full-sized sample. It was possible with one of the Van de Graaff generators at the Ion Physics Corp. (IDC) to irradiate the entire area of a half-sized sample (50 by 50 cm). Tests at this facility were undertaken by FHC, and a second contract was let to LTV to perform further tests on the smaller samples to provide a firm basis for extrapolation to the full-sized units.

The number of pulses during a given period of time is a function of the energy of the incident electrons. Figures 21 and 22 show the dependency of counting rate on electron energy for the 0.2 and 0.4-mm target sheet capacitors.

---

* The thresholds on Pegasus I were approximately 5 V for the 0.4 and 0.2-mm capacitors and 3 V for the 0.04-mm capacitors.

Each point of the curve represents 1000 counts. The dotted curve on each graph shows the results obtained from previous tests made prior to the change from the single layer of 6.4-μ mylar to the trilaminate. The counting rate on the trilaminate decreased by approximately an order of magnitude. This is felt to be the result of a lowering of the average pulse height (the counting rate is for events larger than 0.1 V), but the actual reason for this effect is not known. Figure 23 shows the results from two similar sample capacitors and illustrates the difference in behavior found between units manufactured under identical conditions. Figures 24 and 25 show the pulse height distribution of the negative pulses obtained during these irradiation experiments. Since the pulse height distribution changes slightly with energy, this is perhaps not too meaningful; however, it should be noted that each graph is the result of approximately 17 000 pulses recorded above the 0.1-V level, less than 1000 of which reached the 0.4-V level required for processing by the multichannel analyzer after passing through the filter section of the discrimination circuit. Tests were also made at LTV with varying diameter beams and varying size samples. In all of the tests approximately 100 000 pulses were observed with none being recorded in the 6 to 10-V range of the multichannel analyzer. There were 11 pulses greater than 10 V recorded in an overflow detector; however, an extended background run with no sample under irradiation resulted in a similar overflow pulse count, so these pulses were most likely the result of outside interference. All of these tests were made at low temperatures (115°K) and at relatively high flux levels (10^{11} e/cm^2/sec). The total dose obtained in these tests was 10^{17} e/cm^2/sec, which is equivalent to approximately 100 years exposure in space.

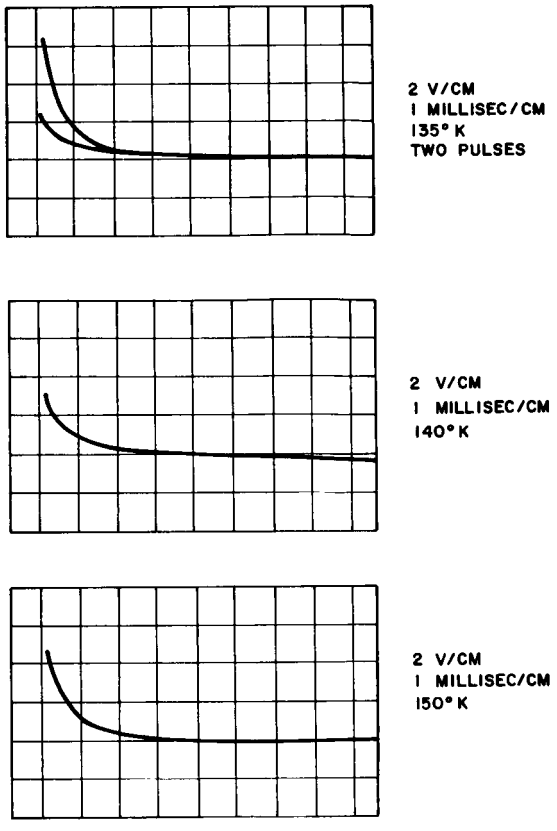

FIGURE 20. TYPICAL RADIATION-INDUCED PULSES AT LOW TEMPERATURE

The results of the tests at the IPC facility generally supported the LTV results. The tests were intended to show the ability of the detector electronics

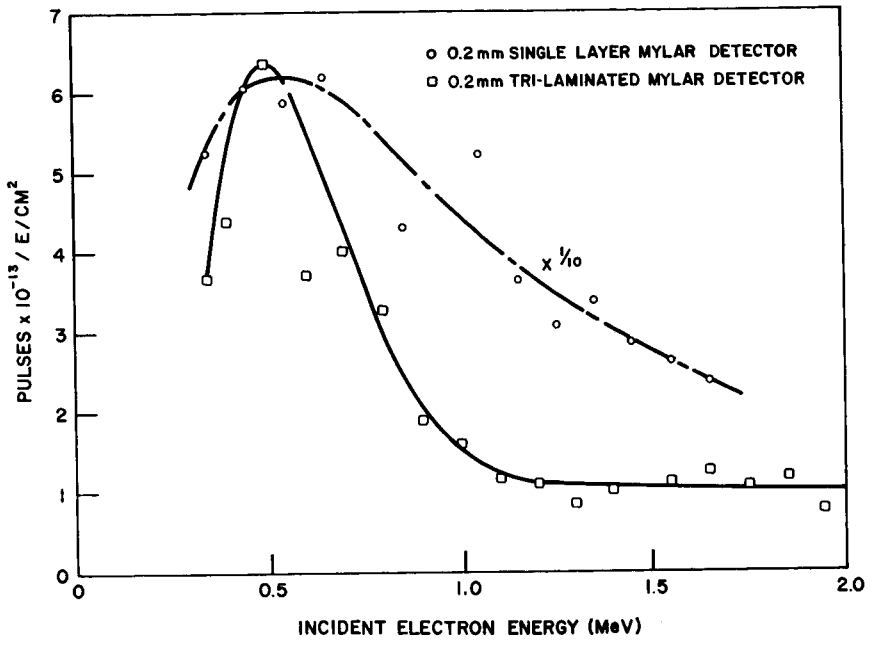

FIGURE 21. DEPENDENCY OF COUNTING RATE ON ELECTRON ENERGY FOR 0.2-mm TARGET SHEET CAPACITORS
(Note difference between single layer and trilaminated mylar.)

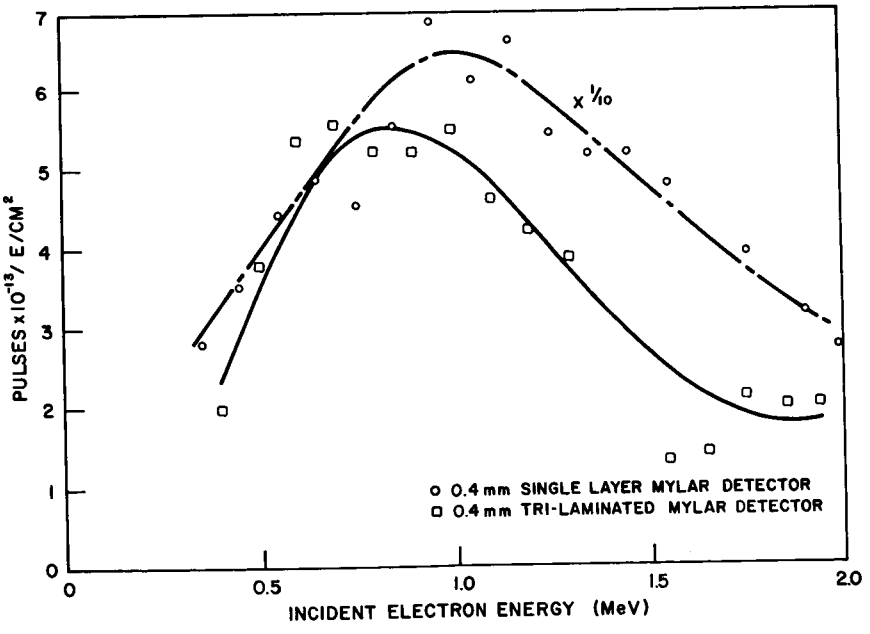

FIGURE 22. DEPENDENCY OF COUNTING RATE ON ELECTRON ENERGY FOR 0.4-mm TARGET SHEET CAPACITORS
(Note difference between single layer and trilaminated mylar.)

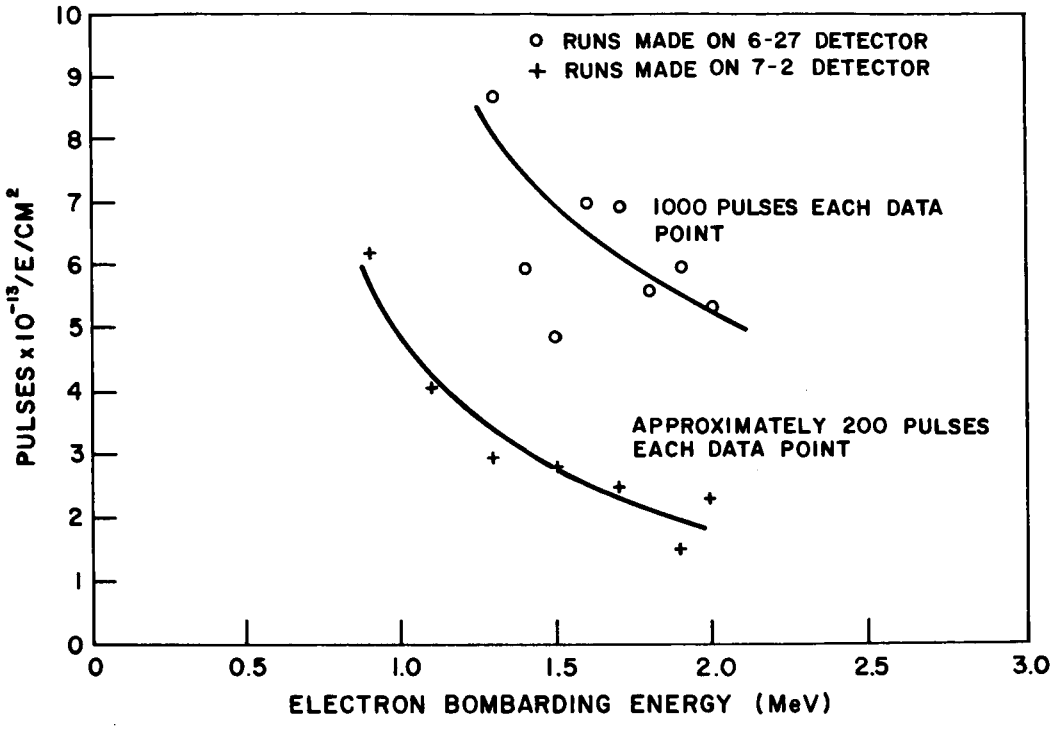

FIGURE 23. RESULTS FROM IRRADIATION TESTS OF TWO SIMILAR CAPACITORS MANUFACTURED UNDER IDENTICAL CONDITIONS

to reject radiation-induced pulses and, hence, were not as highly instrumented as the LTV tests. There were measurements of pulse heights only at three levels. The frequency of pulses on a bare capacitor in terms of incident electrons per square centimeter per second was almost identical to that measured at LTV. The pulse frequency on a panel was greater due to the presence of the foam core. The pulse frequency was measured as a function of electron energy, electron flux rate, and panel temperature. The variation with energy was different due to a second maximum created by the presence of the foam. There was a slight increase of pulse frequency with electron flux rate. The maximum frequency was found to occur near 190°K.

During one period, pulses with high amplitudes (10 to 20 V) were observed. Since there was some trouble with the accelerator at this time, the facility was repaired and completely checked out before tests were resumed. Although it could not be definitely proved that the high-amplitude pulses were created by the fluctuations in the accelerator, these pulses disappeared after the tests were resumed. With the exception of this period, the pulse amplitudes were approximately the same as was observed at LTV.

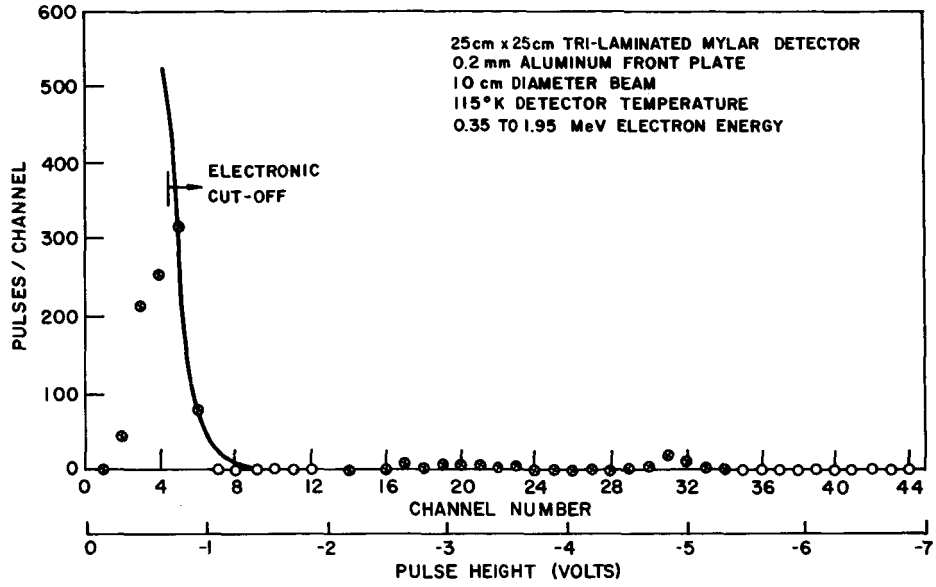

FIGURE 24. PULSE HEIGHT DISTRIBUTION OF NEGATIVE PULSES OBTAINED DURING ELECTRON IRRADIATION OF 0.2-mm ALUMINUM FRONT PLATE

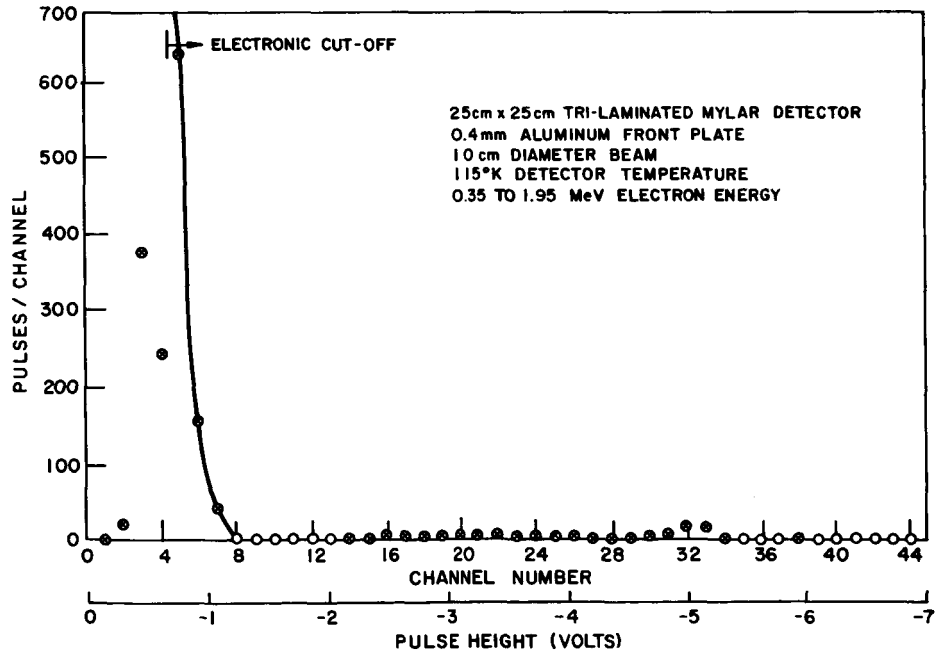

FIGURE 25. PULSE HEIGHT DISTRIBUTION OF NEGATIVE PULSES OBTAINED DURING ENERGY SURVEYS OF 0.4-mm ALUMINUM FRONT PLATE

Some tests were conducted at IPC to determine whether radiation-induced pulses originating in the mylar tape cabling leading to the detector panels might cause a problem. All of these pulses were of low amplitude and were successfully rejected by the detector electronics.

Radiation tests were conducted on full-sized detector panels and cabling at the Langley accelerator facility. In general, the results indicated that radiation-induced discharges would only infrequently be accepted as hit indications. The frequency of such false hits was not sufficiently high to invalidate the meteoroid measurements since they occurred at the rate of less than one for the radiation exposure of all panels of the spacecraft predicted during a flight time of one year.

Since all of these tests were conducted under extremely severe conditions, the results were not very representative of what would be anticipated in a space environment. All of the tests were conducted with monoenergetic, monodirectional electron beams and flux rates from one to four orders of magnitude higher than the maximum predicted for the Pegasus orbits. In addition, there was no cycling of temperature or radiation as would occur in space. A proposal was made to subject an entire wing frame containing 16 panels to low-level radiation and temperature cycling, but these tests would have been performed after the launch of Pegasus I and, hence, were rejected.

Some work is being performed on the behavior of a panel exposed to radiation at low levels and over an energy spectrum using an isotope source. The results are not yet available.

IV. OPERATIONAL ASPECTS OF PROJECT PEGASUS

William G. Johnson*

Introduction

The meteoroid measuring satellites Pegasus I, Pegasus II, and Pegasus III were launched on Saturn I vehicles SA-9, SA-8, and SA-10. Responsibility for preflight launch and inflight operations of the Pegasus spacecraft was vested in the Pegasus Project Office at MSFC, in conjunction with Fairchild-Hiller as prime contracter. The role of Pegasus Flight Director was assumed by the Pegasus Program Manager (OART). The Pegasus Project Office was supported before, during, and after launch operations by members of other MSFC Laboratories, and by KSC.

In addition to the launch team operations, major centers of activity during the launch phase of each Pegasus satellite were the Satellite Control Station at KSC under the Pegasus Project Office; the Pegasus Computation Group in the Computation Laboratory at MSFC; and the Pegasus Evaluation Group in the Research Projects Laboratory at MSFC. This chapter deals with methods and facilities used at the Satellite Control Station to evaluate Pegasus performance in flight, and to control on-board operations.

Satellite Control Station Requirements

The Satellite Control facility (SATCON) was established to provide a single point for the collection and analysis of engineering data sufficient for the evaluation of spacecraft systems performance. Within the framework of the overall mission of the Pegasus Project, the function of the SATCON is to "fly" the satellites in a manner to assure continuing optimum performance. In this role, SATCON personnel monitor and evaluate data from the spacecraft to determine operating condition, initiate routine operational commands to control spacecraft on-board functions, and, when necessary, initiate commands to the spacecraft for corrective action.

---

* Manager, Pegasus Project Office, Saturn I/IB Program Office, MSFC, now Technical and Scientific Assistant to Director, Research and Development Operations, MSFC.

Figure 26 illustrates the relationship of SATCON to other functional elements of the overall mission that are directly related to SATCON operation. There are three paths of communication with the spacecraft: one via the Satellite Tracking and Data Network (STADAN) under control of the Goddard Space Flight Center, and the other two via either the Eastern Test Range (ETR) stations or the Mandy station under control of the Kennedy Space Center. The STADAN network provides both data receiving and command capabilities; the ETR and Mandy paths provide only data receiving. ETR is capable of receiving and transmitting to SATCON the Pegasus MM2 data link. The STADAN and Mandy stations are capable of receiving and transmitting to SATCON the Pegasus MM1, the stored data, and MM2, the real-time data (Fig. 27).

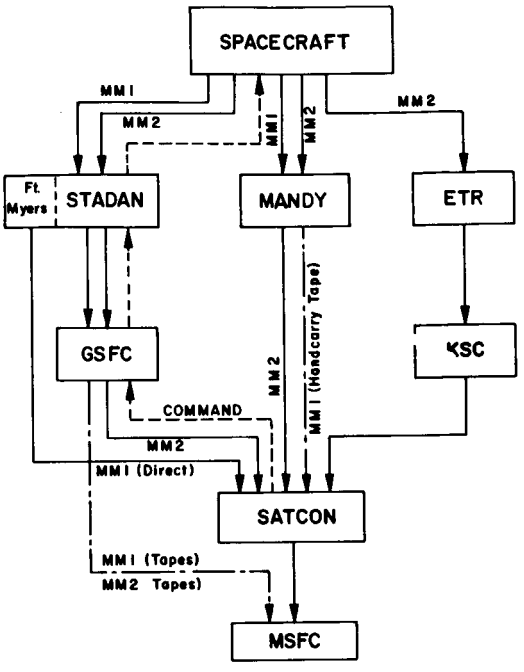

FIGURE 26. RELATIONSHIP OF SATCON TO OTHER FUNCTIONAL ELEMENTS IN THE SATCON OPERATION

The data (Chapter I) received by SATCON may be divided into two categories: (1) operational data, and (2) scientific data. The operational data, which provide information on the operating condition of the satellite and all of its component systems, are of prime importance to SATCON. The scientific data, which will be analyzed to assess the meteoroid hazard, are less important to SATCON and are monitored and analyzed only to the extent necessary for the determination of spacecraft operation.

Operational data are received in both analog (PAM) and digital (PCM) form. The PCM data are displayed in digital form for on-line monitoring and printed out on a line printer (in digital form) for "quick-look" analysis. The PAM data are printed out on strip chart recorders for monitoring and "quick-look" analysis.

Engineering and scientific data are included in the PCM information received by SATCON. The same data are received on magnetic tapes of memory

readout (MM1). These data are monitored and observed for deviations that indicate malfunctions or other conditions that may be corrected by command.

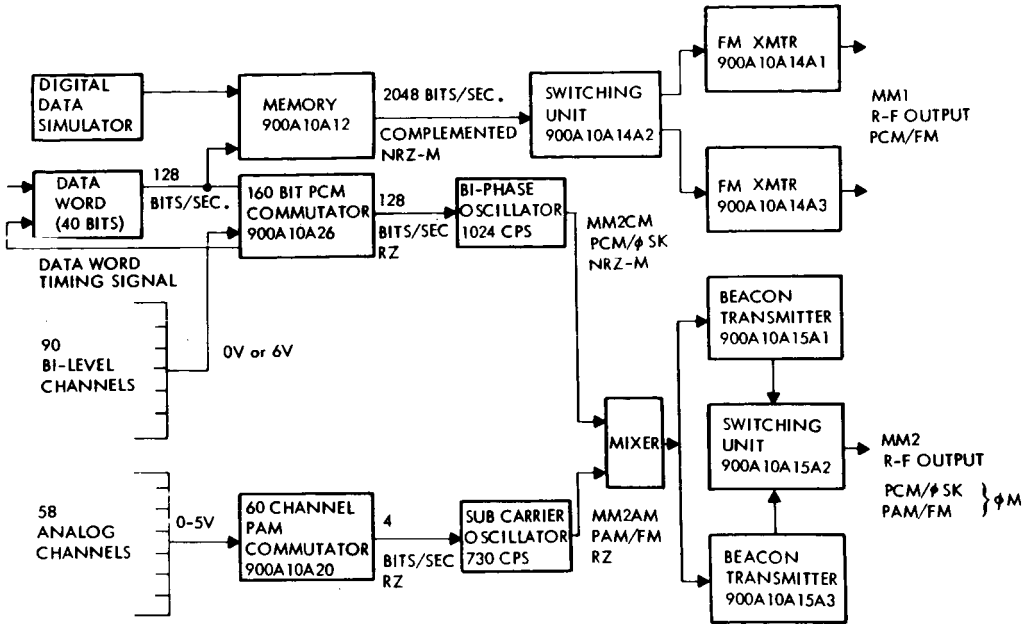

FIGURE 27. PEGASUS TELEMETRY DATA LINKS

Commands are initiated by SATCON to (1) select modes of spacecraft operation; (2) activate the required systems and subsystems for the selected mode; (3) take corrective action (changing modes of operation, turning systems on or off, switching power sources, etc.) in the event of malfunction, and (4) test spacecraft systems and subsystems.

The SATCON Facility

The concept underlying the establishment and selection of site of SATCON was to provide a facility physically isolated from pre-launch activities but located to permit continuous communication with the spacecraft during pre-launch operations, immediate and direct input of the data received by Eastern Test Range stations during the launch and deployment operations, and convenient access during the launch and deployment phase and during the first few orbits to engineering personnel responsible for system design. It was

apparent that the responsible system engineers would be located at the Kennedy Space Center during launch operations to be available to assist the checkout and launch crew should malfunctions occur; consequently, SATCON was located there. The facility is housed in two rooms of Hangar AF.

The SATCON equipment room contains all instrumentation necessary for the reception and display of the spacecraft data, communications with the launch crew, the Eastern Test Range and the STADAN network, and on-board systems status display. It is, in fact, the control center for post-launch operations. A second room is arranged to provide work areas and desks for personnel involved in data reduction and analysis. This arrangement permits ready control of access to the equipment room during launch and early post-launch operations, while providing a location, outside the active operational area, in which information can be made immediately available to the interested observer.

SATCON Operations

SATCON operations can be divided into three distinct phases. The first phase consisted of the launch operations. Responsibility for the check-out (countdown) of the spacecraft rested with the launch crew during this phase; however, SATCON played a very active supporting role. Signals from the spacecraft were received by the Mandy station and were transmitted by wire to SATCON. The PCM and PAM telemetry data were separated, processed, and displayed (Fig. 28). Since most of the pertinent "housekeeping" or performance data are carried on the PAM telemetry channel, three parallel strip chart recorders were used to record and display these data. During launch operations, the subsystem design engineers responsible for each of the major on-board subsystems formed the senior data evaluation team in SATCON. Thus, each engineer had real-time access to the performance data from his subsystem, and each, through the command center, could have immediate contact with the launch crew.

The second phase encompasses the flight from liftoff through the first two orbits. At liftoff, responsibility for the evaluation of spacecraft performance and for operational control of the spacecraft passed to SATCON. Through injection into orbit and deployment of the spacecraft the Mandy Station, Eastern Test Range telemetry stations at Antigua and Ascension Island, and the STADAN stations at Johannesburg and Pretoria, formed the data reception network. Signals from all of these stations were available to SATCON. Internal to SATCON, the best incoming signal was selected and the data displayed and evaluated. Had a potentially catastrophic subsystem failure occurred during this period,

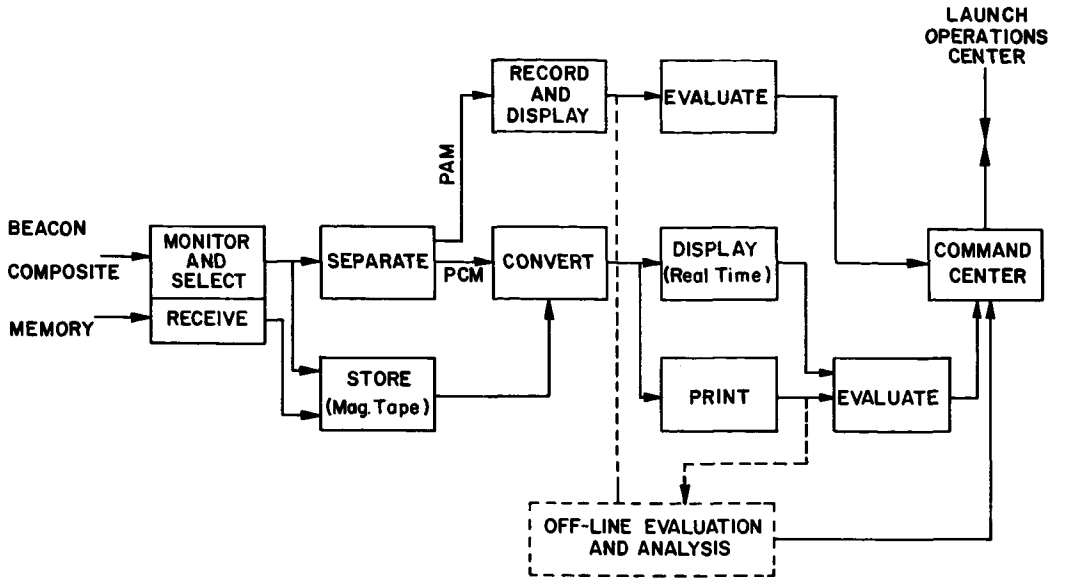

FIGURE 28. INTERNAL SATCON DATA ANALYSIS OPERATION DURING PRELAUNCH PERIOD

corrective command would have been transmitted to the spacecraft through the Johannesburg station. Senior design engineers, who were most familiar with the spacecraft, were a part of the SATCON team and therefore immediately available to the SATCON Director (Command Center) for consultation and assistance in determining the proper corrective action.

During the second orbit of the Pegasus spacecrafts, support of the mission by ETR telemetry stations was terminated and routine satellite control operations were begun. The command route from SATCON to the spacecraft is through the STADAN network. Advantage is taken of the location of a STADAN station at Fort Myers, Florida, to monitor, in real-time, on-board performance during commanded operations. Additionally, communications permitting data transmission (except stored memory data) are maintained routinely with the Woomera, Australia, and the Rosman, North Carolina, station. The reception capability of Mandy is available to SATCON, on call. The third, and routine phase of operations was initiated by SATCON at the end of the second orbit. During this phase, SATCON schedules the normal operational commands to the spacecraft; it receives, records, displays, and analyzes data from the spacecraft. It routinely evaluates spacecraft performance and provides a single center through which communications with the spacecraft flow and through which they are controlled and recorded.

The primary function of SATCON is to support the engineers responsible for maintaining the integrity of the Pegasus satellites as measuring systems. In performing this function, the SATCON personnel perform a preliminary and, frequently, cursory analysis of the "housekeeping" data from the spacecraft. On the basis of this preliminary analysis, the SATCON personnel determine what information is required to establish changes in spacecraft operational modes to improve performance and perform the more detailed analysis of operational data dictated by these preliminary findings. Selected data are periodically analyzed to establish performance trends.

Pegasus I Performance

Pegasus I was launched on February 16, 1965. On February 14, two changes were effected in the Meteoroid Detection Data Subsystem. One logic group of each of the three thicknesses of detector panels was electrically isolated from its voltage source by the insertion of a 10-μfarad capacitor in the voltage-signal line in order to serve as detectors for radiation-induced bits only, and the threshold voltage at which the detector electronics responded was reduced from 10 V to the "lowest possible value" (4 to 5 V). Only such tests as could be made with the spacecraft assembled on the launch pad were conducted. These tests were sufficient only to establish that the system remained operational. They could not establish sensitivity levels and response levels. The tests did reveal that as the loading of the detector electronics was decreased, i. e., as detectors were removed from the circuits, a condition was reached in which the system could become electrically unstable. Since the spacecraft was not readily accessible for performing the required tests, the threshold for this condition was not precisely established.

Countdown and launch of the spacecraft was accomplished without incident. Deployment of the spacecraft was monitored by means of a TV camera located at the top of the S-IV stage looking up into the canister and center structure. It was completely successful. Only one malfunction was observed; a deployment signal microswitch, redundant in the system, operated momentarily and then failed.

Within the first few orbits, several deviations from anticipated operational characteristics were observed. In the thicker detector materials, where five to eight detectors were grouped to form a single information channel, penetrating impacts occurred in which the panel group was not identified. This malfunction was attributed to a combination of causes; none that could be corrected in flight. The isolation between individual detectors in a group was

insufficient to hold the current level to the impacted capacitor above the threshold level of the panel identification circuitry (current recharge amplifiers) until the current flow could be sensed and processed. Additionally, in the short time available just prior to launch, the sensitivity of the panel identification circuitry had not been changed to a level compatible with the new sensitivity level established for the hit detection electronics. The 0.04-mm-thick detectors were grouped in pairs; their panel identification and pulse verification signals have been generally acceptable.

Pre-launch calibration tests had established an expected detector loss rate, due to shorting, of about 10 percent per year. However, within the first weeks of orbital operation, it was noted that the rate of shorting in the 0.2 and 0.4-mm-thick detectors was appreciably higher than the test loss rate. Since no provision had been made to remove individual shorted detectors from the groups, the rate of sensor area loss was greater, by a factor of 5 to 8, than the rate of shorting of individual detectors. As a consequence, within the first 20 days of orbital operations all of the 0.2-mm-thick detectors were de-activated, and about 40 percent of the 0.4-mm-thick sensor area had been lost. Additionally, some of the shorts that occurred were intermittent in nature, leading to spurious discharges similar to puncture-induced discharges.

Although the causes of detector shorting at a rate appreciably higher than had been anticipated have not been unambiguously established, investigations indicated that better quality control to reduce inclusions in the dielectric and additional electrical burn-out of the detector after fabrication of the panels should help to reduce the failure rate in space. Additionally, the incorporation of a fuse between each detector and its signal line, and circuit modifications to permit switching of the shorted group to an "unlimited" current supply, would allow removal of a shorted detector from a group and retention of the sensor area made up of the good detectors in that group. These modifications were effected in Pegasus II and III.

Analysis of the attitude data revealed that the attitude sensing system was not performing totally within specifications.* Several possible causes of failure were investigated. The conclusions reached were, briefly:

1. Inflight failure of a solar sensor occurred. This failure appears to have been in the "broken wire" class; it could be duplicated in the laboratory, but not repaired in space.

---

* See Chapter VI.

2. A solar sensor was installed in a rotated condition. This was both a design failure and a human error since no keying of the sensor head was provided in the original design, and insufficient caution was exercised during installation and checkout to assure proper orientation of sensors.

3. The threshold levels of some of the earth sensors were improperly set. This was partially a design failure, since the system as finally constructed did not permit highly precise setting and precision matching of the sensitivity levels of opposite sides of a sensor head. It was primarily a human error since no advantage was taken of the latest information on earth radiant energy levels available at the time the sensitivity of the units was adjusted.

4. Some of the earth sensors were receiving reflected energy from the spacecraft. This was a design failure. It was subsequently established that none of the sensors entirely met specifications with respect to the allowed field of view.

In spite of these shortcomings of the attitude system, the attitude data have been usable. The motion of the spacecraft has been readily determined; and spacecraft orientation as a function of time is well established. It probably will not be possible to determine small, short-term deviations in the motion, as had been originally hoped.

All other spacecraft systems have operated normally; however, occasionally throughout the entire orbital operation, easily identified "trash words" have occurred. Such events had been noted during post-assembly testing before launch. They are caused by switching transients reflected through the power subsystem into the word control logic circuitry. Experience indicates that such intermittent malfunctions are easily detected in the data and in no way impair the quality of the data. As the power regulators deteriorate due to normal aging effects, it is anticipated that the frequency of occurrence of "trash words" will increase.

In summary, the meteoroid penetration data collected from the 0.04-mm detectors are quite usable. Those from the 0.2-mm detectors are usable. Those from the 0.4-mm detectors are questionable, but usable with the proper exercise of caution. All other data are usable.

Pegasus II Performance

Based upon the experience gained with Pegasus I, several changes were made in the configuration effective with Pegasus II. The changes of primary importance were those involving the detector electronics:

1. The Hit Amplifier was redesigned to permit adjustment of the threshold level to 4 V without loss of stability in the circuit.

2. The Current Recharge Amplifier was modified to increase its sensitivity to an extent that reliable panel identification and pulse verification were obtained for detector discharges in which the voltage shift, measured at the detector terminals, was as small as 3 V.

3. Isolation between individual detectors in a single group was increased from 1000 ohms to 1 megohm.

4. Fuses were installed between each of the detectors and the signal line; and provision was made to switch the signal line, on command, to an "unlimited" current supply.

With these changes incorporated, sufficient tests were made to verify the functional integrity of the system and to obtain calibration data on the detector electronics subsystem response characteristics.

In addition to these essential circuit changes, a number of minor changes, primarily for ease of assembly and improvement in reliability, were made. No major modification of the attitude subsystem was attempted, since the problem was not recognized and vigorously attacked in time to permit redesign.

Pegasus II was launched without incident on May 25, 1965. Again, deployment was monitored by means of an on-board TV camera. All systems functioned normally.

All primary data systems have continued to function in the expected manner since launch. The meteoroid penetration data are generally "clean" and usable for all three thicknesses of detectors. Rate of loss of sensor area has been close to expected values. Although the rate of occurrence of intermittent shorts is still somewhat higher than anticipated, it is less than in Pegasus I.

The only major subsystem failure occurred in the telemetry system. Beginning about eight days after launch, intermittent failures of both the PAM and PCM channels occurred. Subsequent to some system analysis and commanded switching of the telemetry subsystem components, stable PCM communication was re-established. The PAM channel remains intermittent; however, data transmission occurs with sufficient frequency to permit adequate monitoring of spacecraft performance. The data loss is not sufficiently great to be alarming at this time.

The telemetry failure has been duplicated in the laboratory by the insertion of a resistive network in the clock pulse circuits driving the PAM commutator. It is now assumed that the contact (or, possibly, leakage) resistance in a plug connecting the clock and the commutators is changing in a manner such that the clock pulse amplitude shifts back and forth across the threshold value. During the erection of the spacecraft on the pad, it was exposed, briefly, to a thunderstorm. The spacecraft area that got the wettest contains the failed circuit.

Pegasus III Performance

Pegasus III is essentially identical in its configuration to Pegasus II. However, two changes of importance were made in the spacecraft:

1. The attitude subsystem was reworked. Thresholds were reset to provide better matching of sensitivity of the earth sensor heads. Some of the earth sensors were relocated to assure unobstructed view from the spacecraft. The solar sensors were modified to permit "keyed" installation only.

2. Some of the meteoroid penetration panels were removed from the spacecraft, and in their places "dummy" panels were installed incorporating removable metal "coupons" cut from the detector material, and coupons to which had been affixed samples of thermal control surfaces.

The Pegasus III orbit was changed to a nominal 530-km circular orbit. At the end of about a year of lifetime, the orbit will have decayed to a radius such that rendezvous with a Gemini spacecraft may be feasible, thus making possible the recovery of the removable coupons for laboratory study.

Performance of the Pegasus III has been essentially as anticipated. One of the FM transmitters failed after three months with no resultant data loss. The data are generally usable.

Specific description of the data is contained in portions that follow.

V. METEOROID DATA RECORDED ON PEGASUS FLIGHTS

James B. Dozier*

Introduction

The primary mission of the Pegasus Project is to measure the frequency of meteoroid penetrations through aluminum sheets of various thicknesses. Configuration and operation of the detectors have been described. Several secondary aims involve a more sophisticated and lengthy analysis of the data; they will be discussed in later reports. At the present time, it is felt that the primary mission of Project Pegasus has been accomplished. Penetrating flux figures for the 0.04, 0.2 and 0.4-mm thicknesses of aluminum in the vicinity of the earth can be expressed with reasonable confidence. Continuing data collection will add statistical significance to the measurements already evaluated. The extension of the data analysis to include spatial, temporal, and directional effects, mass distributions, comparison with theories, etc., will require additional data, additional analysis, and additional laboratory work before it can be completed. This chapter is intended to present only the penetration data and the derived flux figures, together with a discussion of how these numbers were determined, and to defer the more detailed scientific analysis until a later time.

Operational procedures and functioning of the satellite systems in flight, were described in Chapter IV from the standpoint of spacecraft operation. In this chapter, several of the events and experiences will again be described, but from the standpoint of data collection and data analysis.

Identification of Punctures

Pegasus I was launched on February 16, 1965. Within a few orbits, it had begun to record and telemeter meteoroid penetration data. Preliminary examination of these early data brought to light several problems not evidenced

---

* Chief, Physics and Astrophysics Branch, Research Projects Laboratory, MSFC.

in the ground testing. These problems were fortunately discovered early enough to be corrected before the subsequent launches of Pegasus II on May 25, 1965, and Pegasus III on July 30, 1965.

The first problem concerned the identification of the detector groups (logic groups). Isolation between capacitors in a logic group and sensitivity of the current recharge amplifiers were not sufficient to generate panel identification and recharge time information for hits occurring in logic groups containing more than two capacitors. Since the three different thicknesses on each wing are serviced by separate hit amplifiers which are identified in the hit word, one could identify the thickness and the wing, but not the logic group of 0.2 or 0.4-mm panels in which the discharge occurred. The detector isolation and current recharge amplifier sensitivity were increased for Pegasus II and III, and all hits in those satellites give complete information.

Another problem was encountered with spurious pulses. Some 0.2 and 0.4-mm panels produce sporadic discharges, presumably after damage from a meteoroid impact. It has been postulated that the Cu-coated mylar in the vicintiy of a jagged hole in the target sheet could, through thermal expansion or contraction, result in a mechanical short. Such a short normally would be quickly burned away by the energy stored in the capacitor. However, the process of intermittent shorting can apparently repeat itself a large number of times, generally one or more times during each thermal cycle. Since each shorting pulse writes a hit word, this situation was fatal to the 0.4-mm experiment on Pegasus I where no panel identification was available. Time did not permit the investigation necessary to completely understand the behavior of such panels, or the determination of whether this problem could be eliminated by a change in sensor construction. However, the ability to identify the logic group for every hit indication, plus the fact that the average hit rate is only about 1 per 100 days on a particular 0.4-mm logic group, makes it obvious that a logic group that registers several hits in a short time must experience intermittent shorting. The procedure in such a case has been to accept the first hit as valid and to ignore the remainder of the hit indications, as well as the total area of the particular logic group, after the time of the first hit. The offending logic group is then disconnected by ground command.

Detector shorting was found to be a more frequent occurrence on Pegasus I than had been indicated from laboratory tests of the detector panels, particularly at higher temperatures. When a short did occur on one of the capacitors on Pegasus I, the entire logic group was disabled. Obviously, several shorts could cause a severe reduction of the instrumented area. It is still not clear whether such shorting was caused by damage resulting from meteoroid impact, or from

inclusions or conductive spots in the mylar. A "burning-in" procedure was used on the panels to be flown on Pegasus II and III which may have eliminated potential trouble spots in the dielectric. The shorting rate observed on Pegasus II and III is substantially lower than on Pegasus I, but the peak temperatures have not been as high. Also, the ratio of shorts to observed penetrations is still somewhat higher than laboratory results would indicate. Pegasus II and III also have a defusing capability for each individual capacitor; this feature allows removal of a shorted panel from a logic group. Thus far, this ability has been used to good advantage, and a number of logic groups have been saved that otherwise would have been lost.

On Pegasus II and III, the transient caused by commanding the fuse relay "ON" fires all the hit amplifiers and writes a spurious hit word with an illegitimate panel identification. The exact reason for this is not yet known, but such an event is easily recognizable. Hits can be commanded into a specific logic group by commanding a panel disconnect, which shorts the detector group to ground, and then a panel reconnect. Such an event is identifiable by the long recharge time, since all capacitors in a logic group must be recharged from ground potential. Such commands are useful for checking the number of capacitors active in a logic group in which fuses may have been blown.

True and False Counts

The cumulative counters respond to every hit amplifier output. They are used primarily to ascertain that all the hit words in the memory have been found. These words are sorted out and classified in the following manner:

1. Command events. Knowledge that a disconnect-connect command was sent to a specified panel at specified time; recharge time corresponds to all active panels being recharged from ground potential.

2. Spurious events. Knowledge that Fuse Relay was commanded "ON" at specified time; generally all hit amplifiers and recharge current amplifiers fire.

3. Intermittent event. Same panel produces more than one hit word in a time which is very short compared to the average interval between two valid hits in a single logic group.

4. Radiation events. Either a hit word on a debiased panel, or a hit word containing no panel identification or no proper recharge current indication.

5. Valid hit resulting in shorted panel. Hit word with the proper form which shows a full-time count in the recharge time register; also continuous current indications in the three recharge current amplifiers that supply that logic group.

6. Normal valid hit. Hit word that fulfills all tests for a normal hit word, i.e., proper panel identification and recharge current indication, corresponding to a single detector panel recharging from a 4 to 40 V-discharge.

In a very few cases the events counted by the cumulative counters exceeded the number of hit words. This has always happened during a time in which a panel showed intermittent shorting. Since the counter is incremented every time the integrator in the hit detector receives a certain voltage-time product during a period of 250 μsec, and since 1.25 seconds are required to write a hit word into memory, it is quite understandable that a rapidly shorting panel can write more events in the cumulative counter than hit words in the memory. In these cases, such counts were disregarded as intermittencies.

Other rare cases have occurred in which too many or too few recharge current amplifiers identify the discharged panel. This is understandable in terms of slight changes in values of various electronic components which may alter the amplifier sensitivities. In such cases, an educated guess can usually be made as to which panel is being recharged.

As has been pointed out in Chapter III, considerable effort was expended in minimizing the anticipated problem of spurious pulses caused by the storage and subsequent discharge of trapped radiation belt electrons in dielectrics. It is now believed that radiation does not affect the data of the meteoroid experiment. In fact, no increase in counting rate with time has been observed in either Pegasus I, II, or III which could be attributed to an accumulated radiation dose, no disproportionate number of hits has occurred in the high-radiation region in the South Atlantic Anomaly,* no debiased panels have indicated hits on Pegasus II, and only one event which may have been a pulse induced by radiation in the insulation of a cable has been observed on Pegasus II. No debiased panels have indicated hits on either Pegasus I or III.

The largest uncertainty seems to be whether or not it is correct to attribute events that result in panel shorting or intermittency to meteoroid penetration, partial penetration, or damage, or whether such events occur spontaneously through prolonged vacuum soak, thermal cycling, and possibly other aspects of exposure to space environment. Laboratory tests to decide such questions are planned, but in any case the number of such events cannot

---

* See Chapter VI.

be more than about 30 percent of the total observations in the 0.2 and 0.4-mm detectors. No shorting or intermittent problems have been encountered in any of the 0.04-mm panels in either Pegasus I, II, or III except for one panel on Pegasus I which may have been inadvertently disconnected and subsequently impacted with no applied voltage.

Pegasus I Results

Pegasus I received 4 hit indications on the 0.4-mm panels in the first 11 days. However, several panels became intermittent at that time, and the lack of panel identification precluded separating valid hits from the intermittent events after that time. Based on 4 events in 1925/m^2 days, a puncture frequency of 0.0021/m^2 day can be computed. However, these data can be used only to establish an order of magnitude.

For some reason, a very high fraction of the penetrations on the 0.2-mm panels resulted in shorts (assuming that shorts result from a meteoroid impact) and since there are only 6 logic groups, the 0.2-mm area very quickly became lost. There were 9 hit indications in 248/m^2 days exposure which resulted in a puncture frequency of 0.036/m^2 day. Again, it should be pointed out that the 0.2 and 0.4-mm hit words did not contain panel identification or recharge time unless a short resulted. Therefore, some of the tests for validity could not be made.

The 0.04-mm panels give panel identification about 70 percent of the time. They are still functioning well. A total of 121 punctures have been recorded in 1020/m^2 days, resulting in a flux of 1.4×10^{-6}/m^2 day. A time history of the cumulative events is shown in Figure 29.

Pegasus II Results

The number of punctures, area-time exposure, and puncture frequency observed by Pegasus I, II, and III (as of Aug. 31) are summarized in Table III. The few punctures observed in the 0.2 and 0.4-mm Pegasus I detectors are in reasonably good agreement with Pegasus II results. The figure of 0.04-mm events gives a somewhat higher puncture rate for Pegasus II than for Pegasus I. The reason for this discrepancy is not yet fully understood.

The time history of cumulative counts on the 0.04-mm panels of Pegasus II is shown in Figure 30. Times of known meteoroid shower activity are indicated

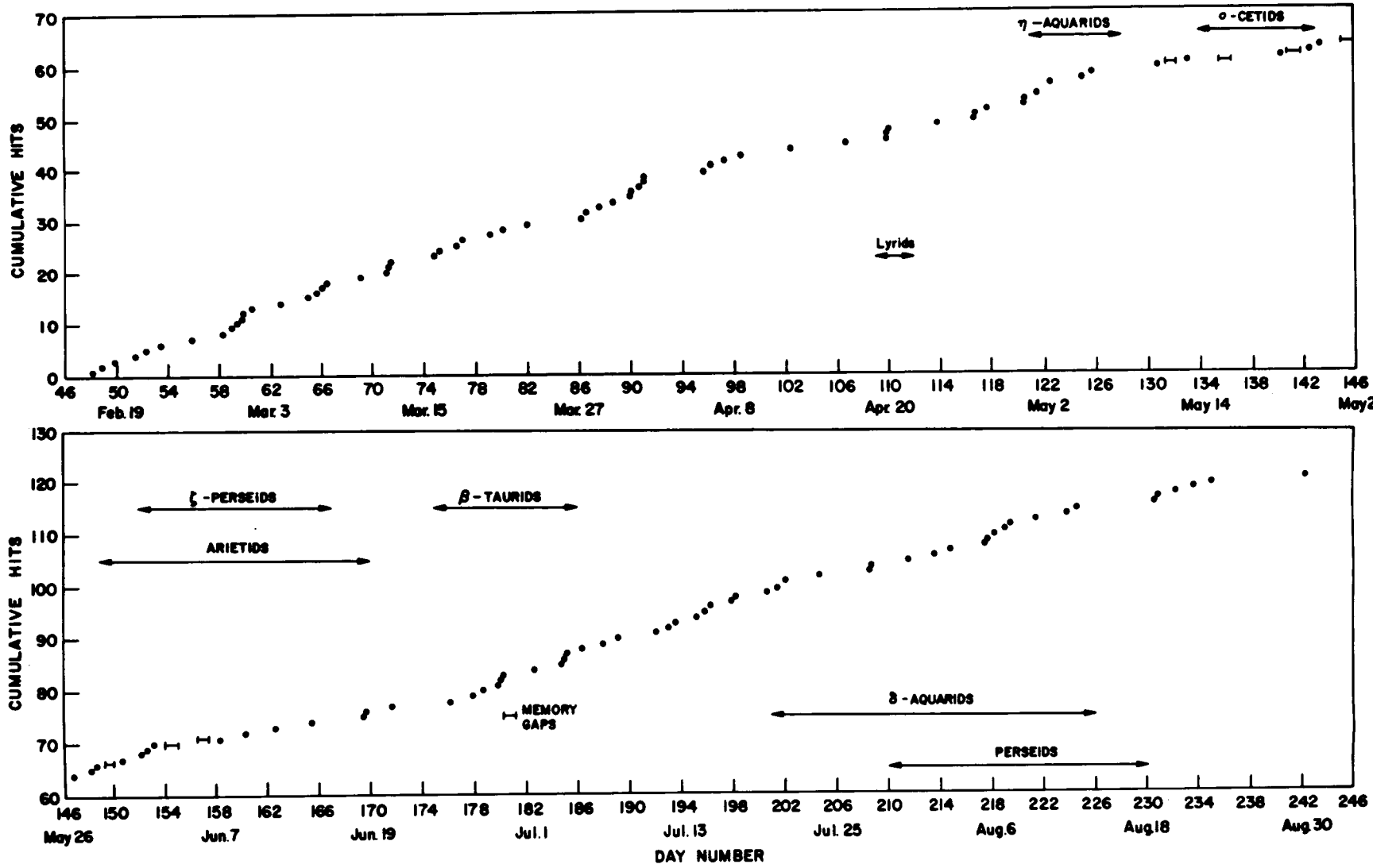

FIGURE 29. TIME HISTORY OF CUMULATIVE HITS ON 0.04-mm PANELS (PEGASUS I)

TABLE III. PEGASUS PENETRATION DATA

(as of Aug. 31, 1965)

	No. Penetrations	Area-Time (m^2 day)	Frequency (No./m^2 sec)	Frequency (No./m^2 day)
PEGASUS I				
0.4 mm	4	1925	2.4×10^{-8}	2.1×10^{-3}
0.2 mm	9	248	4.2×10^{-7}	3.6×10^{-2}
0.04 mm	121	1020	1.4×10^{-6}	1.2×10^{-1}
PEGASUS II				
0.4 mm	58	14387	4.7×10^{-8}	4.1×10^{-3}
0.2 mm	18	1234	1.7×10^{-7}	1.5×10^{-2}
0.04 mm	121	651	2.2×10^{-6}	1.9×10^{-1}
PEGASUS III				
0.4 mm	11	3667	3.5×10^{-8}	3.0×10^{-3}
0.2 mm	4	239	2.0×10^{-7}	1.7×10^{-2}
0.04 mm	23	109	2.4×10^{-6}	2.1×10^{-2}

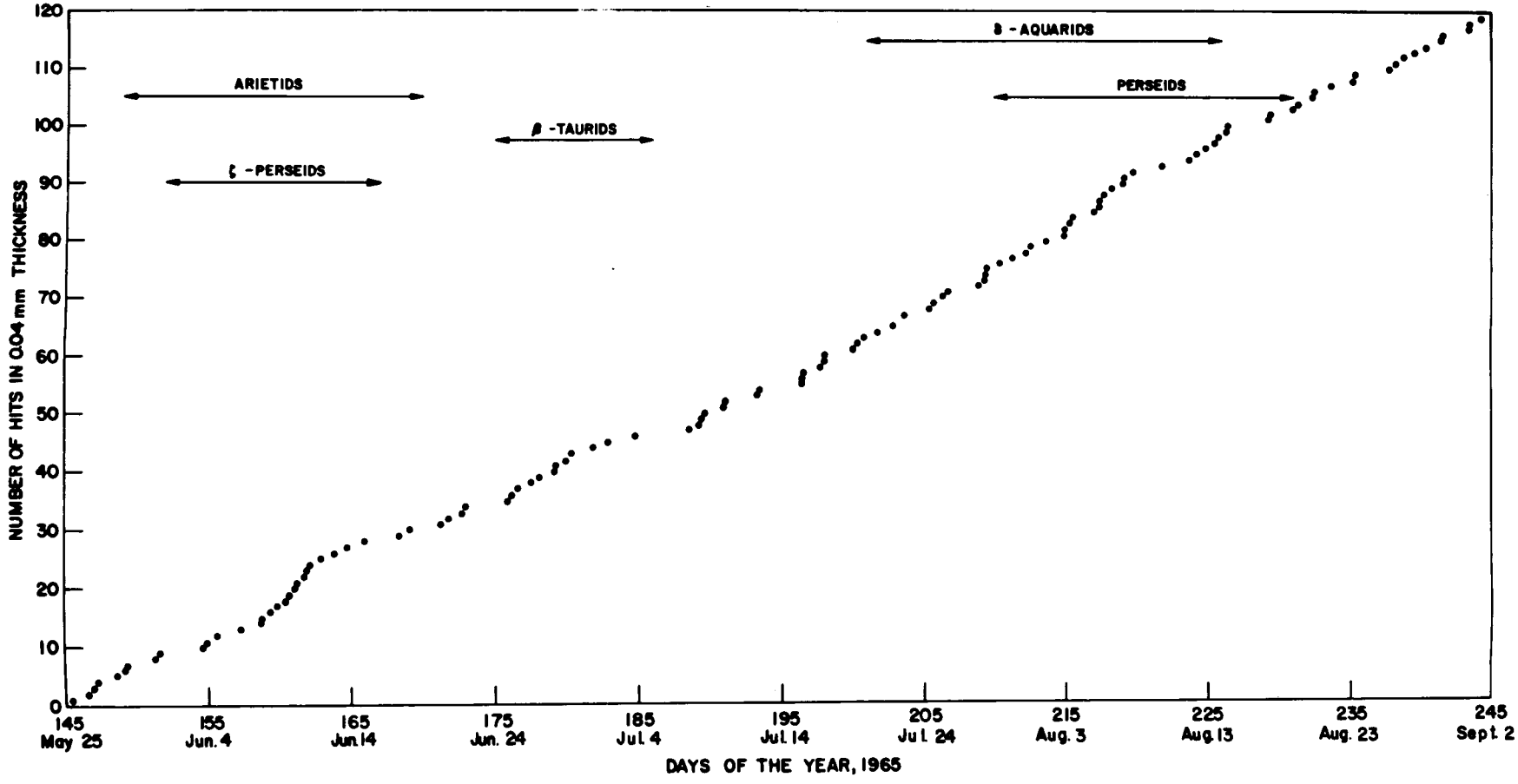

FIGURE 30. TIME HISTORY OF CUMULATIVE HITS ON 0.04-mm PANELS (PEGASUS II)

on these plots. In comparing the results of Pegasus I and II it may be seen that there is no significant increase in counting rate observed by Pegasus I during shower periods. Some increase is observed by Pegasus II during the ζ-Perseids and Arietids shower, although the statistical significance of these data is open to considerable question.

The time histories of the 0.2 and 0.4-mm cumulative counts are shown in Figures 31 and 32, respectively. The sampling rates for these thicknesses are too low to identify any definite shower effects.

Pegasus III Results

The number of penetrations, area-time exposure, and penetration frequency observed by Pegasus III to August 31 are shown in Table III along with similar data from Pegasus I and II. It is still difficult to draw any conclusions from a comparison of Pegasus III with either Pegasus I or Pegasus II since the amount of simultaneous data from the three satellites is still small. An account of satellite orientation, relative shower activity, etc., should be considered in making such a comparison. However, a general agreement among the satellites is readily apparent. A time history of cumulative counts for Pegasus III is given in Figure 33. The gap in the 0.04-mm curve represents a time interval during which no valid penetrations were recorded. At the present time no explanation for this phenomenon can be given.

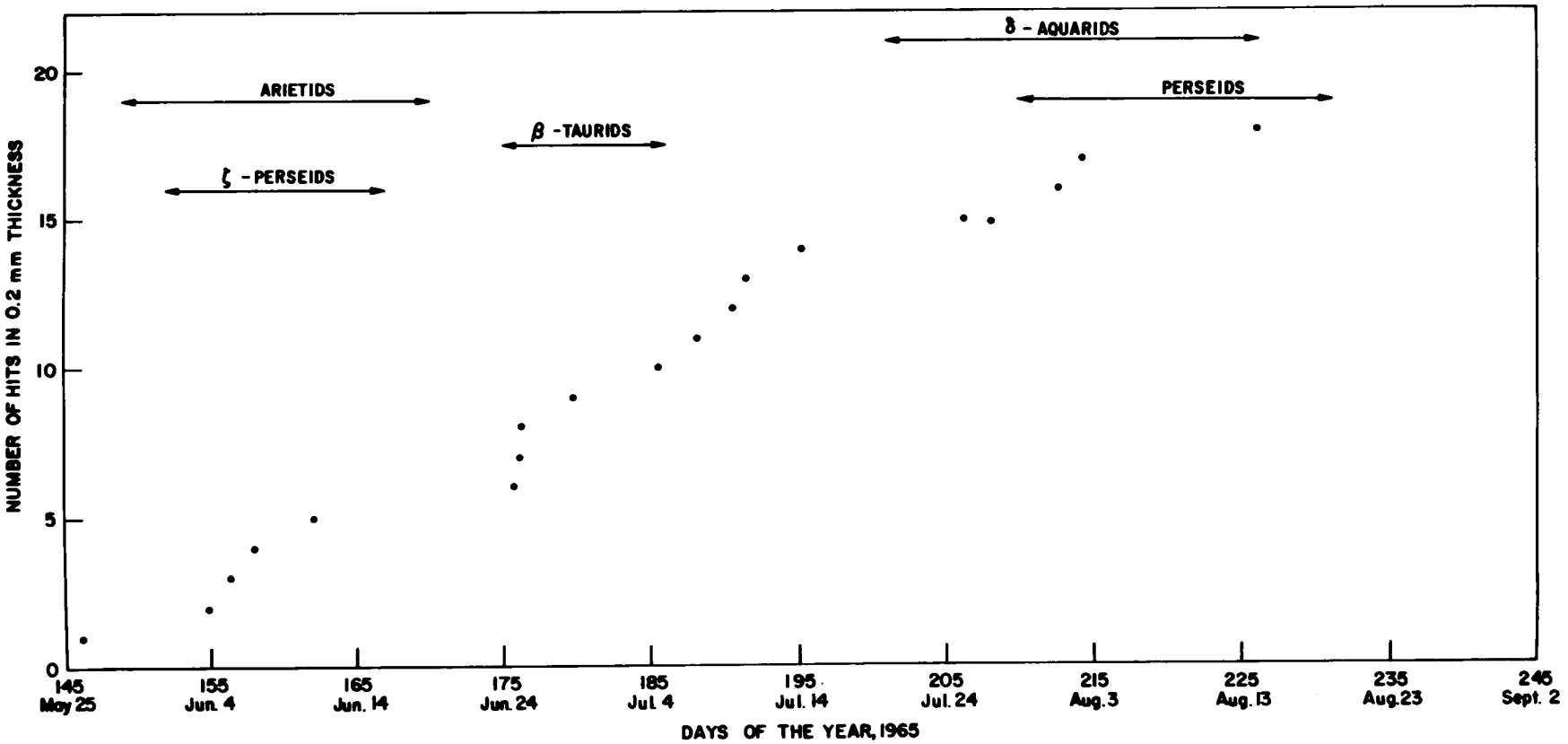

FIGURE 31. TIME HISTORY OF CUMULATIVE HITS FOR 0.2-mm PANELS (PEGASUS II)

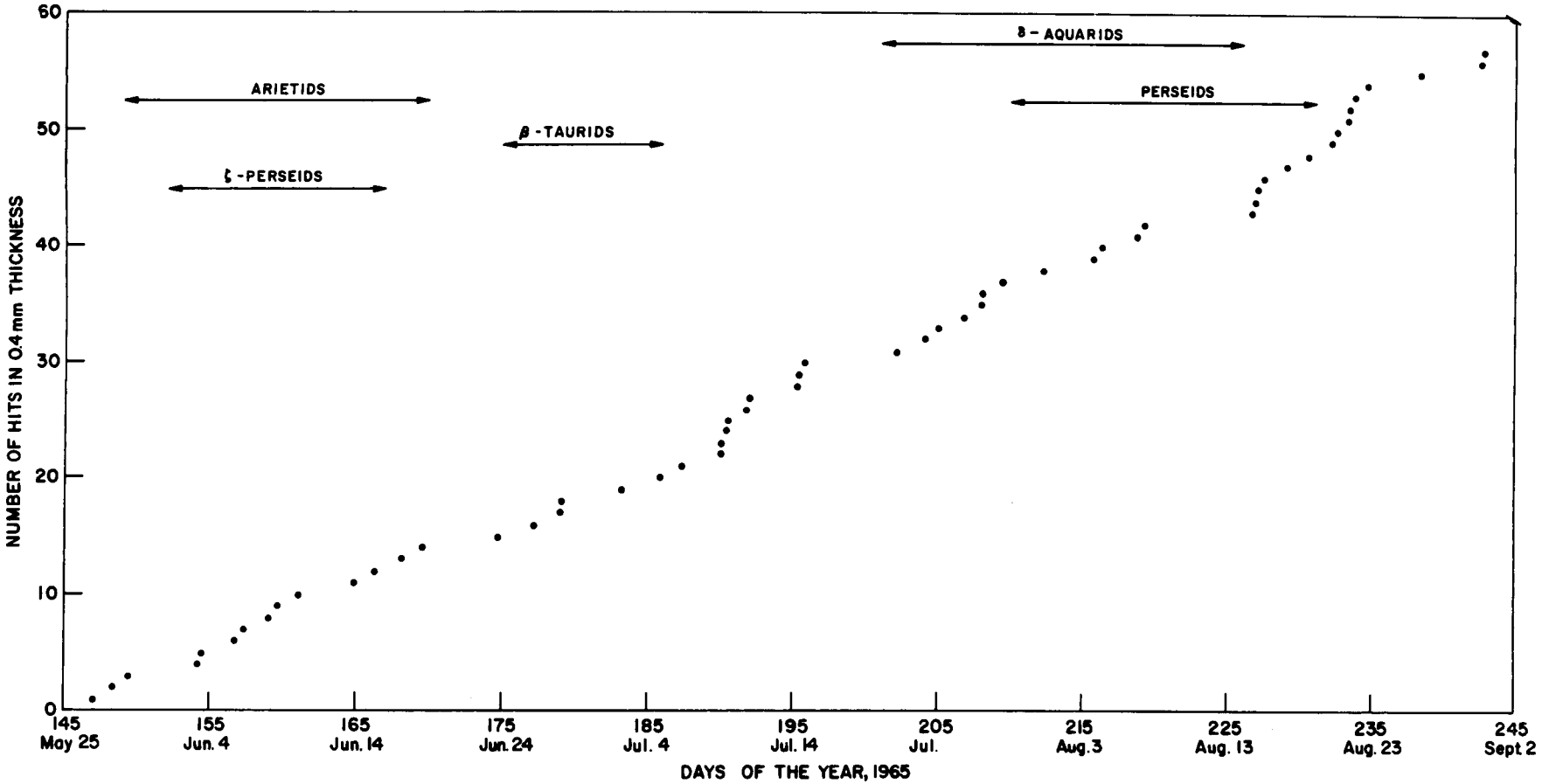

FIGURE 32. TIME HISTORY OF CUMULATIVE HITS FOR 0.4-mm PANELS (PEGASUS II)

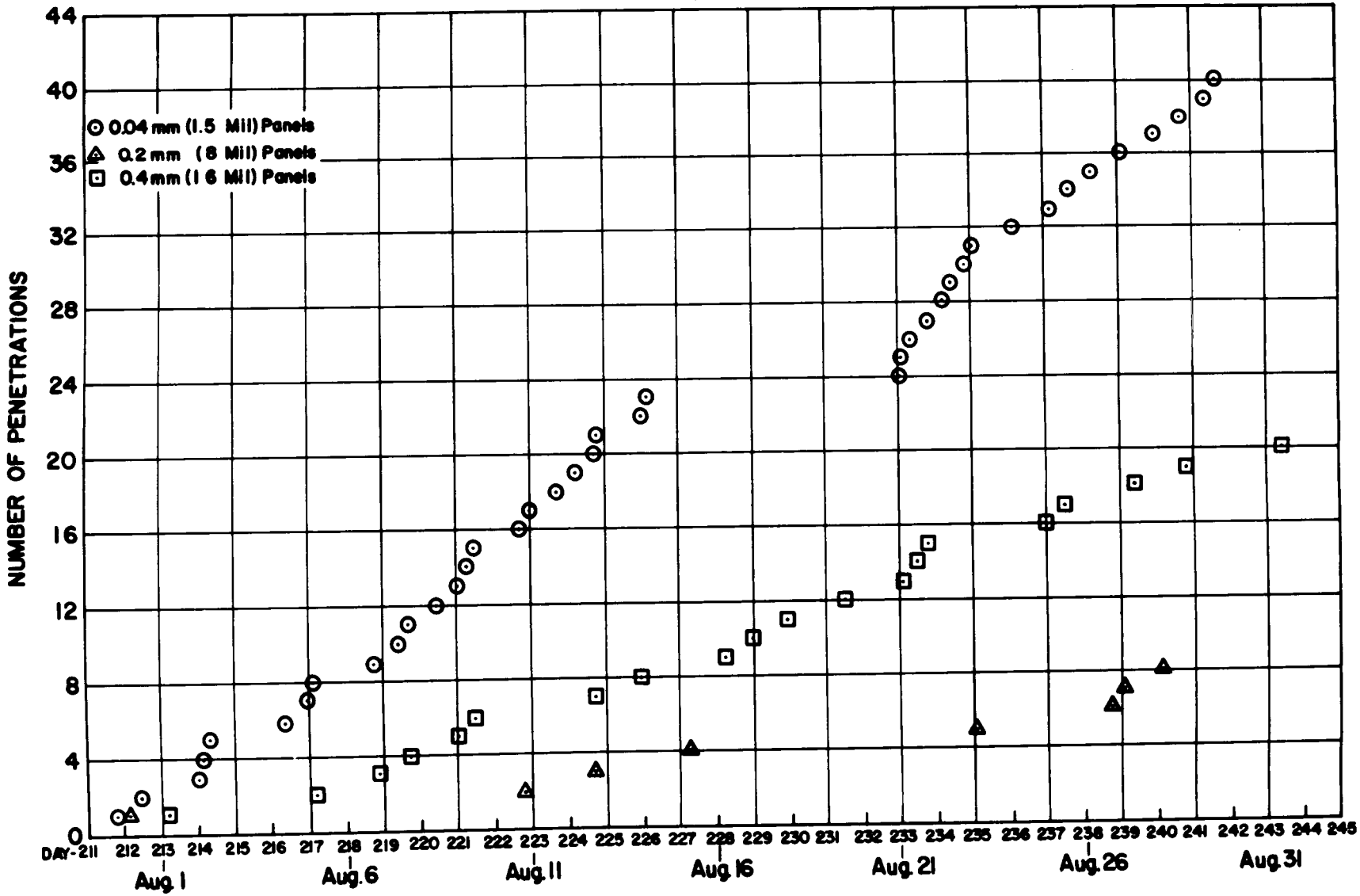

FIGURE 33. TIME HISTORY OF CUMULATIVE HITS FOR ALL THREE PANEL THICKNESSES (PEGASUS III)

VI. SECONDARY MEASUREMENTS BY PEGASUS

Gerhard B. Heller,* Russell D. Shelton,** and James B. Dozier***

Introduction

This chapter will discuss the results from the secondary measurements on Pegasus. In addition to providing valuable data for the complete analysis of the primary meteoroid experiment, these form experiments in their own right.

Temperature Measurements

The temperature measurements on the Pegasus spacecraft consist of two types.**** Nineteen temperature probes are of the pulse amplitude modulated kind, while six are pulse code modulated (digitized). The pulse amplitude modulated (PAM) temperatures are transmitted once each 40 seconds continuously. However, the PAM data are only received for periods of about 15 minutes since the spacecraft is in the field of view of a tracking station for only this short time. Initially, several stations tracked each Pegasus orbit for about two weeks. Thereafter, only one station tracked the satellite during each orbit. The pulse code modulated (PCM) data are stored on board the satellite and rapidly transmitted upon ground command (usually once per day).

Two of the digitized probes are located on the opposite faces of an uncharged meteoroid detector panel. The remaining digitized temperature measurements were taken on special surfaces designed to experimentally study the radiometric properties of the Pegasus thermal control coatings. There are nine temperature probes on the temperature-sensitive components inside the electronic canister, two probes on the radiation detector package, a temperature probe on each of the four solar cell panels, three probes on the Service Module Adapter skin, and a probe on the container of the thermal control coatings experiment (Tab. IV).

---

* Deputy Director, Research Projects Laboratory, MSFC.
** Chief, Nuclear and Plasma Physics Branch, Research Projects Laboratory, MSFC.
*** Chief, Physics and Astrophysics Branch, Research Projects Laboratory, MSFC.
**** See Chapter I.

TABLE IV. TEMPERATURE SENSORS ON PEGASUS

Location	No. of Sensors	Form of Data
Detector Panel	2	Digital (PCM)
Thermal Coating Sensor	4	
Electronic Canister	9	Analog (PAM)
Radiation Sensor	2	
Solar Cell Panels	4	
Service Module Adapter	3	
Container of Coating Sensors	1	
Total	25	

The thermal data from these probes are used to determine the temperature status of components for the evaluation of the spacecraft operation, to evaluate the effectiveness of the thermal design techniques employed to maintain proper temperature control of the temperature-sensitive components, to analyze the effect of the space environment on the thermal design, and to better determine the thermal environment of space. Roger Linton elaborates further on the Pegasus thermal evaluation in "Thermal Design Evaluation of Pegasus," a NASA TN now in publication.

Measured temperatures are shown graphically over both short and long time periods (Figs. 34-37). By superimposing the measurements from several consecutive orbits which are thermodynamically similar, the temperature is obtained continuously for one orbit (Fig. 34). Notice the effects of the earth's shadow on the temperature. Figure 35 shows an example of the data for several months.

All of the temperature-sensitive components have, with the exception of the solar panels, remained well within their design limits (Tab. V). The critical electronic batteries located inside the canister have stayed right in the center of their design ranges on each Pegasus; the louvers and the thermal control coatings have behaved as expected, except for the S-13 paint on the vehicle. The temperature of solar cell panels dropped on four occasions to

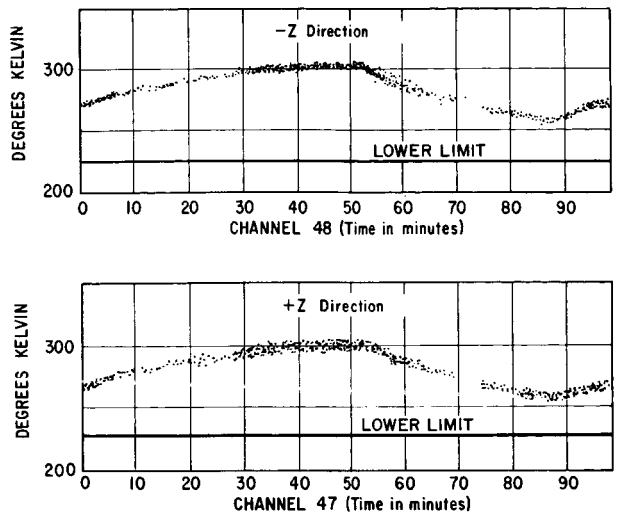

FIGURE 34. COMPOSITE TEMPERATURE GRAPH--FORWARD SOLAR CELL PANELS (FEB. 18, 1965)

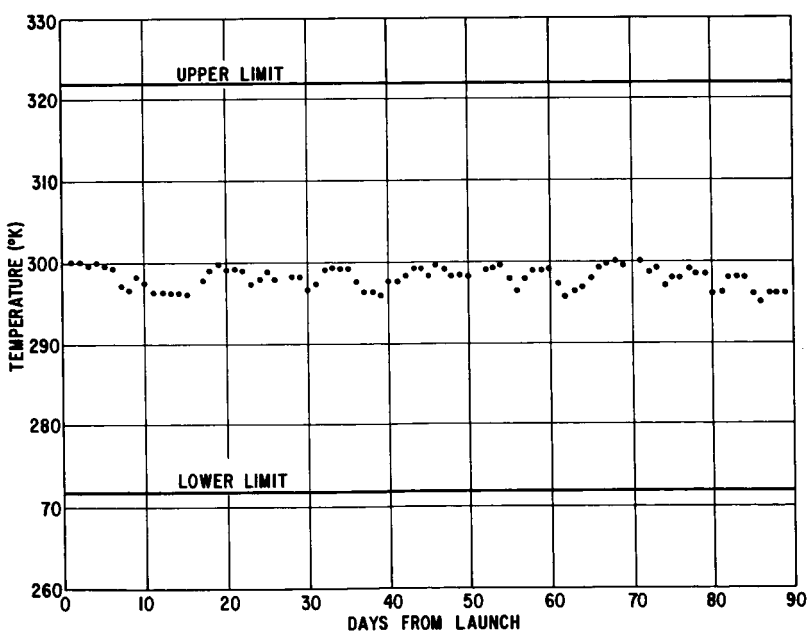

FIGURE 35. BATTERY B INTERNAL AVERAGE TEMPERATURE

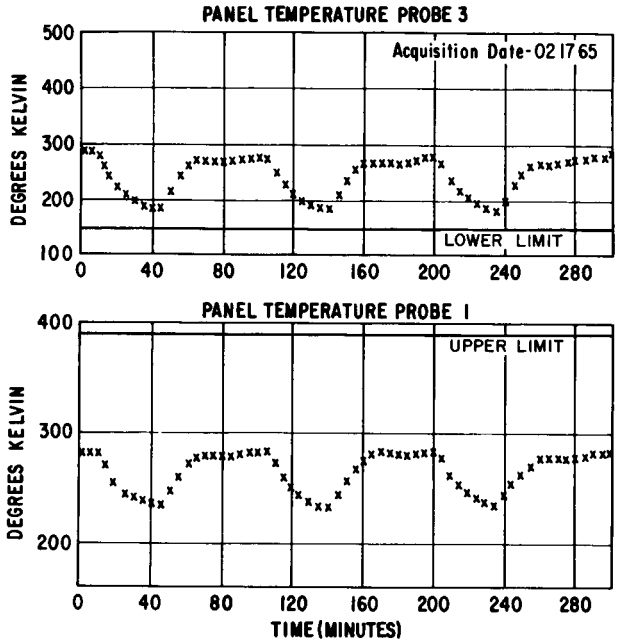

FIGURE 36. TEMPERATURE DATA FROM DETECTOR PANELS IN FLIGHT (FEB. 17, 1965)

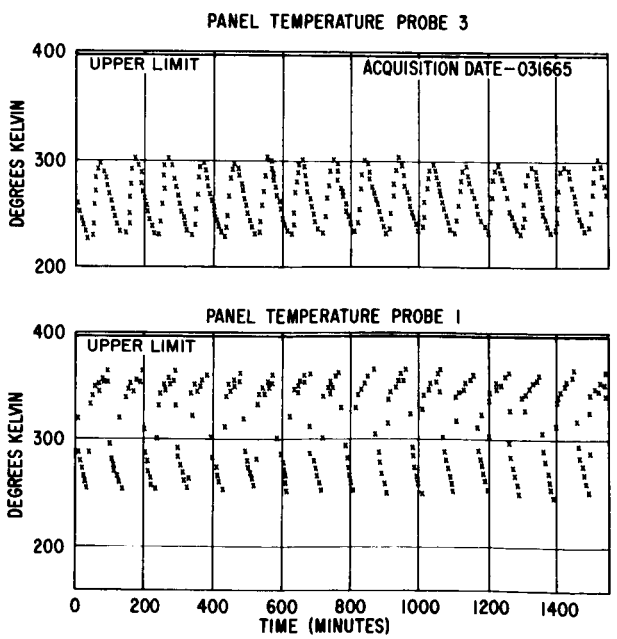

FIGURE 37. TEMPERATURE DATA FROM DETECTOR PANELS IN FLIGHT (MAR. 16, 1965)

210°K; however, this was for comparatively short periods of a few hours and had no adverse effect on the solar-cell performance. The three temperature probes located in the Service Module Adapter show the heat sink to be about 40°K above predicted levels. The louvers are still able to compensate the canister temperature since the original thermal design considered a more severe hot case based on a more eccentric orbit.

TABLE V. RANGE OF PEGASUS TEMPERATURES

Component	Design Range (°K)	Actual Range (°K)
Radiation Detector	222 to 388	230 to 320
Batteries	272 to 322	290 to 314
Other Electrical Components (in the electronics canister)	262 to 332	275 to 330
Solar Panels	194 to 339	210 to 340
Meteoroid Detector Panels	167 to 394	225 to 385

The solar absorptance of the S-13 paint on the heat sink has apparently doubled, while the S-13 reference sensor shows little or no unexpected trends. As the temperatures of the Service Module Adapter (heat sink) have run consistently high since the first orbit, the change in solar absorptance probably occurred during ascent or injection (on-the-pad radiometric measurements were made which show no appreciable changes). The booster retrorocket plume is believed to have contaminated the coating during separation. Further studies are being conducted at MSFC on this problem, since it is of the utmost importance to Apollo and the LM, which are critically dependent upon thermal control coatings. Any unexpected degradation due to rocket plumes would have very adverse effects on these two spacecraft.

Figures 36 and 37 show examples of detector panel temperatures in flight. In the first case, the spacecraft is spinning about its longitudinal axis, in the second case, about the normal to the detector plane. In both cases, the

temperature remained within the specified limits and followed pre-flight predictions of the temperature excursions.

The reference temperature sensors, often called space environmental effect sensors (SEES), are devices flown on Pegasus and other satellites to measure the absorbed radiant heat energy encountered in space [11]. The measurements telemetered from such sensors are used to evaluate thermal control coating stability in space and to evaluate solar, earth infrared, and albedo flux intensities. Each sensor consists of a disc mounted in a case where: (1) the disc has a 2π steradian view of space; (2) the disc is thermally isolated from its case (so that heat fluxes between the disc and case are minimized); and (3) the disc has a small heat capacity (d = 3.15 cm with 0.5-mm-thick aluminum) (Fig. 38). The total absorbed fluxes are deduced from the temperature response of the disc as the satellite orbits the earth. Earth shadow effects and attitude effects are dominant factors in the disc temperature.

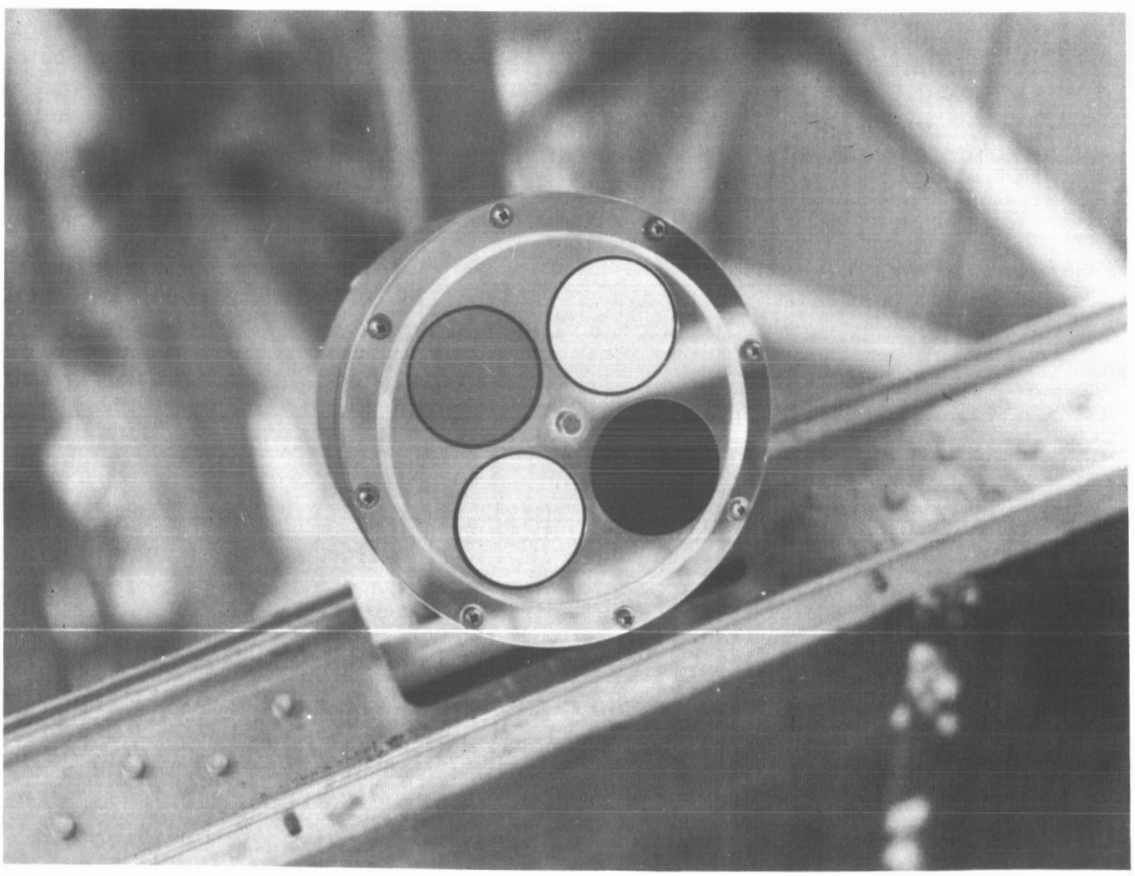

FIGURE 38. REFERENCE TEMPERATURE SENSOR

The Pegasus reference temperature thermal control coatings were the critical coatings used in the Pegasus thermal design, they included a candidate Apollo coating and a stable black coating. Also flown was a coating which was used for nation-wide "round-robin" measurements made by most of the major laboratories across the country, and flown on other satellites. Each Pegasus flight contained a package of four sensors coated with the above mentioned coatings. By necessity, data analysis of these requires completion of attitude data analysis. Figure 39 shows data on the changes of the optical properties of three coatings from Pegasus I; the ratio of solar absorptance to infrared emittance versus equivalent sun time is presented.

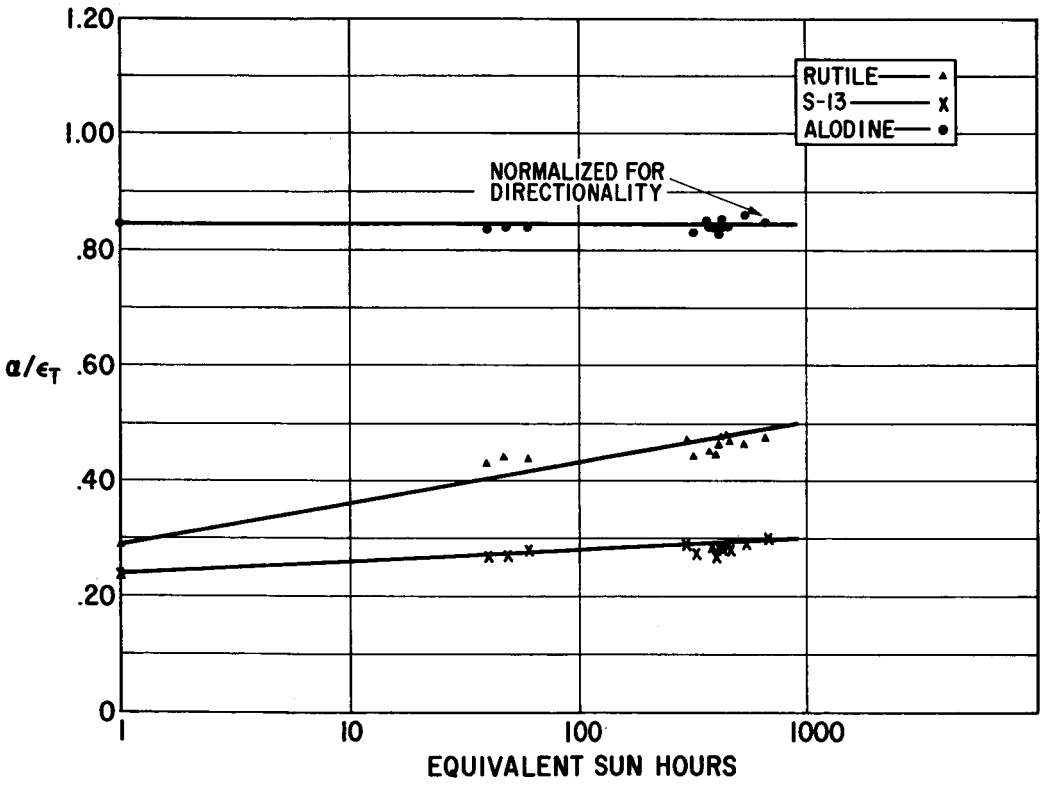

FIGURE 39. ABSORPTANCE-INFRARED EMITTANCE RATIO OF PEGASUS I REFERENCE SENSORS VS EQUIVALENT SUN TIME

Another interesting study being performed with the sensor data concerns the earth's albedo (reflected solar energy). Data from several orbits have been

obtained where the plane of the sensor has remained 180° from the sun; thus the dominant energy input is albedo in the sunlit portion of the orbit. Calculations of the albedo flux are presently being made with a special computer program.

Radiation Measurements

The effect of radiation on the primary meteoroid experiment was a critical unknown prior to launch of the first satellite. It was thought that trapped electrons might be deposited in the dielectrics of the meteoroid detection system in such numbers that spurious electrical discharges could occur. If not effectively discriminated against, these discharges could mask the meteoroid impact data. It was therefore important to know the actual radiation environment experienced by the satellites, and it was decided that an electron sensor would be flown on each Pegasus spacecraft. A secondary justification for the instrument was that the proposed orbits and expected lifetimes of the satellites could provide a much more detailed radiation mapping of the South Atlantic magnetic Anomaly than previously possible.

The electron sensor used on the three Pegasus satellites is shown in Figure 40. It consists of a suitably shielded scintillator with photomultiplier tube and an electronic data processing unit which reduces discrete pulse information to analog voltage outputs for subsequent transmission to the ground. The sensor unit is mounted at the forward end of the satellite's center structure and points in approximately the +Z direction. The scintillator is a 1-cm-radius plastic hemisphere covered by a thin foil as a light shield, and by 0.5-cm-thick tungsten and 1.0-cm-thick aluminum shields through which 24 radial holes are drilled. The holes permit only 1.1 percent of the omnidirectional flux striking the outside of the detector to penetrate into the crystal.

Each of the radiation sensors on Pegasus I and II has two counting channels with energy thresholds set at approximately 0.5 MeV and 2.0 MeV. For Pegasus III the thresholds are approximately 0.1 MeV and 2.0 MeV. The sensors therefore count all incident electrons with energies greater than the two thresholds. The two threshold channels are identified as A and B, respectively. The actual thresholds and the overall system count rate response are known and fairly sensitive functions of the temperatures of the sensor and of the electronics unit. A third counting threshold is used in anti-coincidence to negate signals from particles of $E > 11$ MeV. The effect of the aluminum light shield is to stop protons with $E < 3$ MeV. Consequently, corrections from other information sources may have to be made to the final data for protons with $3 \text{ MeV} < E < 11$ MeV.

Information from the radiation experiment consists of two voltages representing the count rates of particles (with energies greater than the two thresholds), and two voltages from thermistors in the sensor and in the electronics unit. The radiation voltages are telemetered as two parts of a PCM word while the temperature voltages are transmitted as two channels in the PAM signal. Normally, only a few of these temperatures are reduced from the PAM data each day, usually to coincide with the end of a PCM memory dump. The average temperatures of the sensor system are relatively constant during a day, and it has proven adequate to use a single set of temperatures to compute radiation for an entire PCM core dump.

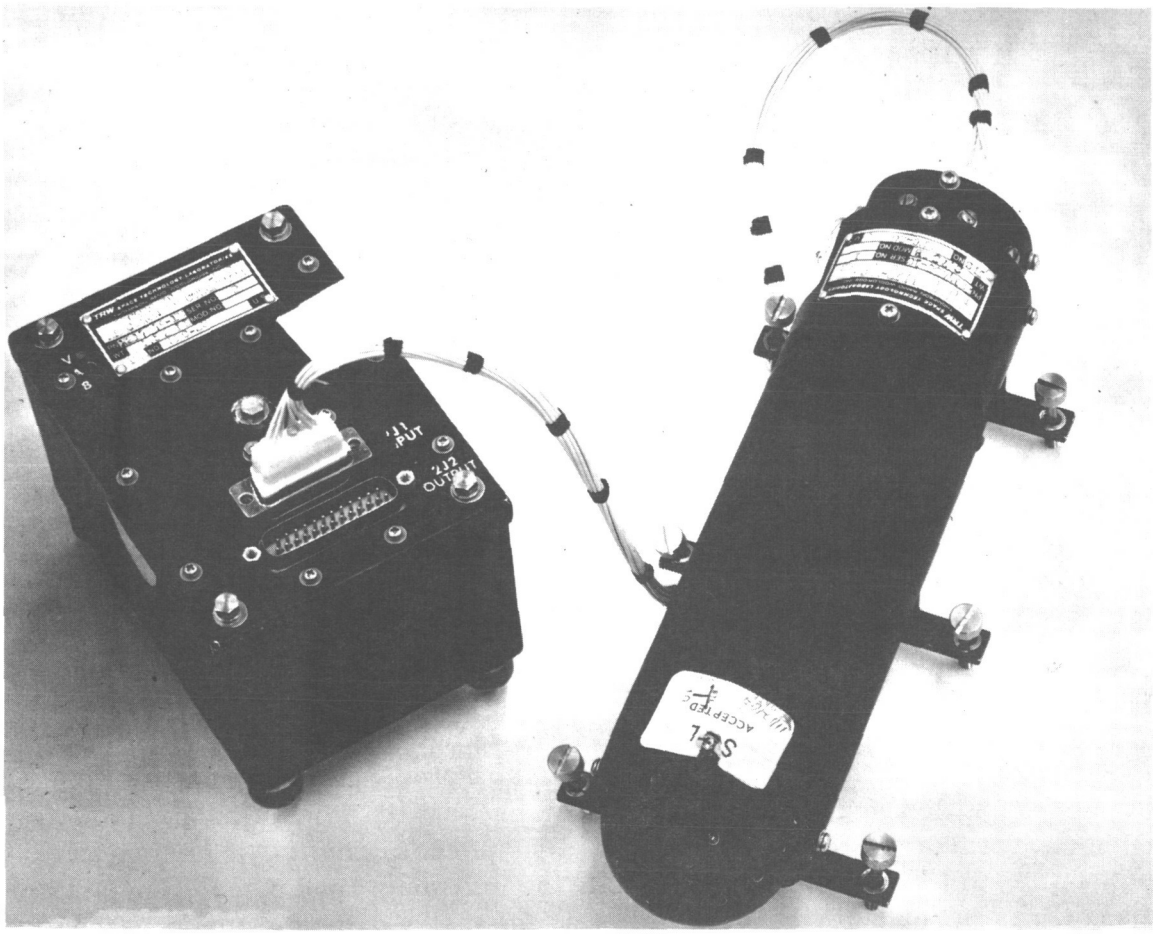

FIGURE 40. ELECTRON SPECTROMETER

For computation purposes sensor calibration data for each flight unit have been put into the form of transformation matrices which are employed in

a Pegasus Radiation Data Program. This program calculates the fluxes of particles for the two thresholds, the difference between them, the logarithms of the two fluxes, and the two count rates. These data are identified with the times at which they were measured, and with the two radiation voltages to which they correspond. In addition, for each memory dump the program calculates the actual thresholds and the sensor and electronics temperatures.

The electronic counting circuit output increases with increasing function of flux for low and medium fluxes. However, above a flux of about 4×10^7 electrons cm^{-2} sec^{-1} for Channel A and about 3×10^7 electrons cm^{-2} sec^{-1} for Channel B the output flattens, then falls off, approaching zero at a true reading of about 10^9 and 4×10^8 electrons cm^{-2} sec^{-1}, respectively. As a result, the voltage outputs can be ambiguous, and the resulting calculated fluxes can be incorrect. Therefore, it becomes necessary to correct the data by hand for this deadtime error. In order to distinguish between the rare flux readings which must be corrected and fluxes which actually did decrease because the satellite moved through a region of less intensity, an intermediate analysis step is taken. Data from the Radiation Data Program are normally sorted to give only points for which Channel A fluxes are greater than 100 electrons cm^{-2} sec^{-1}. Satellite ephemeris and B and L values are then calculated for these remaining higher flux events. Here B is the strength of the magnetic field at the point; L, the magnetic shell parameter, gives the radial distance from the center of the earth to the equatorial intercept of the line of force passing through the point. It is well known that constant trapped flux contours can be plotted as simple curves in B, L space. The B, L coordinate system is then a convenient two-dimensional representation of three-dimensional real space. For the deadtime correction problem, each pass through the anomaly is plotted on a B, L chart, as in Figure 41. When the indicated fluxes are compared with previously published isoflux contours, it is possible to determine those points for which deadtime corrections must be made.

Figures 42 through 44 show a time history from launch to June 4 of the radiation sensor on Pegasus I. The points represent the time of maximum flux during each traverse through the Anomaly; the numbers give the logarithm of the peak flux in Channel A; the x's identify the maximum reading each day. During times indicated by heavy solid lines, telemetry data were faulty. During the two time periods indicated by heavy dashed lines, the sensor was inoperative. The first failure lasted 4 days and the second at least 28 days; both were followed by apparent complete recovery of the unit. No conclusive explanation has yet been given for the failures.

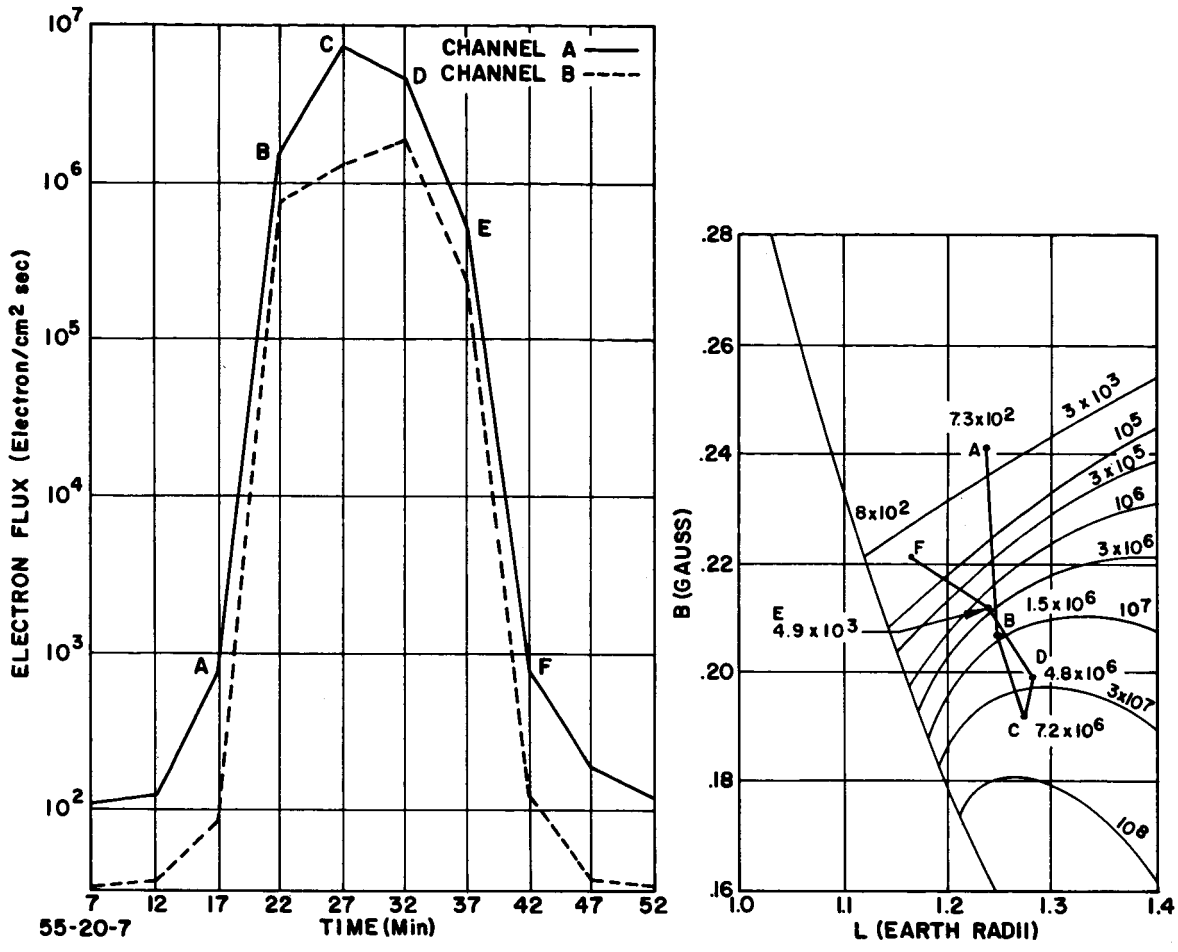

FIGURE 41. PEAK RADIATION PASS FOR FEB. 24, 1965 (PEGASUS I)

The radiation experiment on Pegasus II has operated continuously since launch with results basically consistent with those from Pegasus I. Early data were excellent and not plagued by noise and other problems experienced during the first few weeks of Pegasus I. When the PAM system malfunctioned, the loss of temperature data made it necessary temporarily to suspend radiation data reduction. Later, thermal and body motion analysis led to the conclusion that the radiation unit temperatures were remaining almost constant with a typical variation from a mean value of only about 10° K. It was therefore decided to employ a constant temperature in the Radiation Data Program. If more accurate temperature determinations can be made later, it could prove necessary to recalculate certain periods of data.

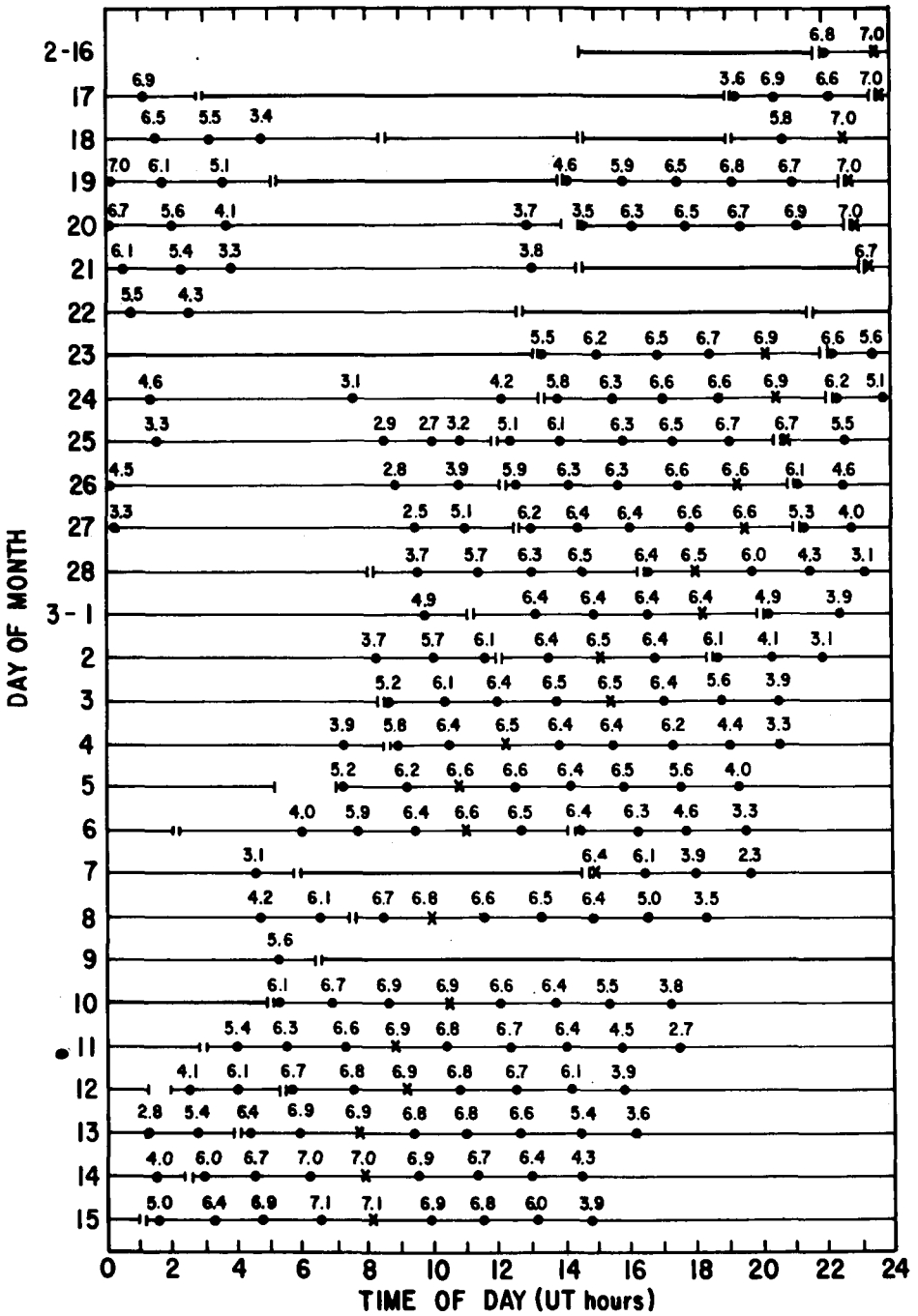

FIGURE 42. DATA COVERAGE AND CHANNEL A MAXIMUM FLUX HISTORY FOR PEGASUS I (FEB. 16 THROUGH MAR. 15, 1965). (Numbers are logarithms of electrons $cm^{-2}sec^{-1}$.)

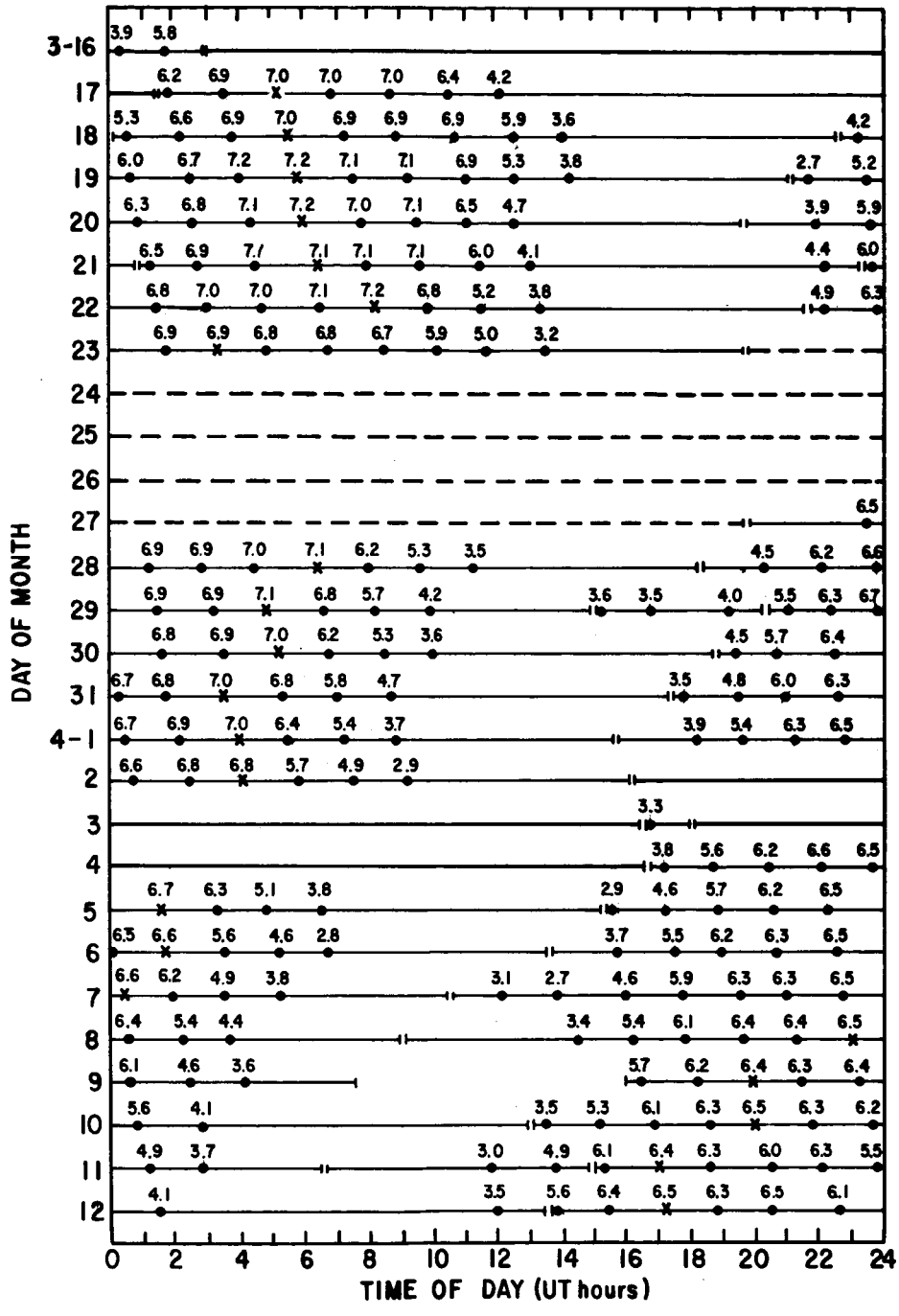

FIGURE 43. DATA COVERAGE AND CHANNEL A MAXIMUM FLUX HISTORY FOR PEGASUS I (MAR. 16 THROUGH APR. 12, 1965). (Numbers are logarithms of electrons cm^{-2} sec^{-1}.)

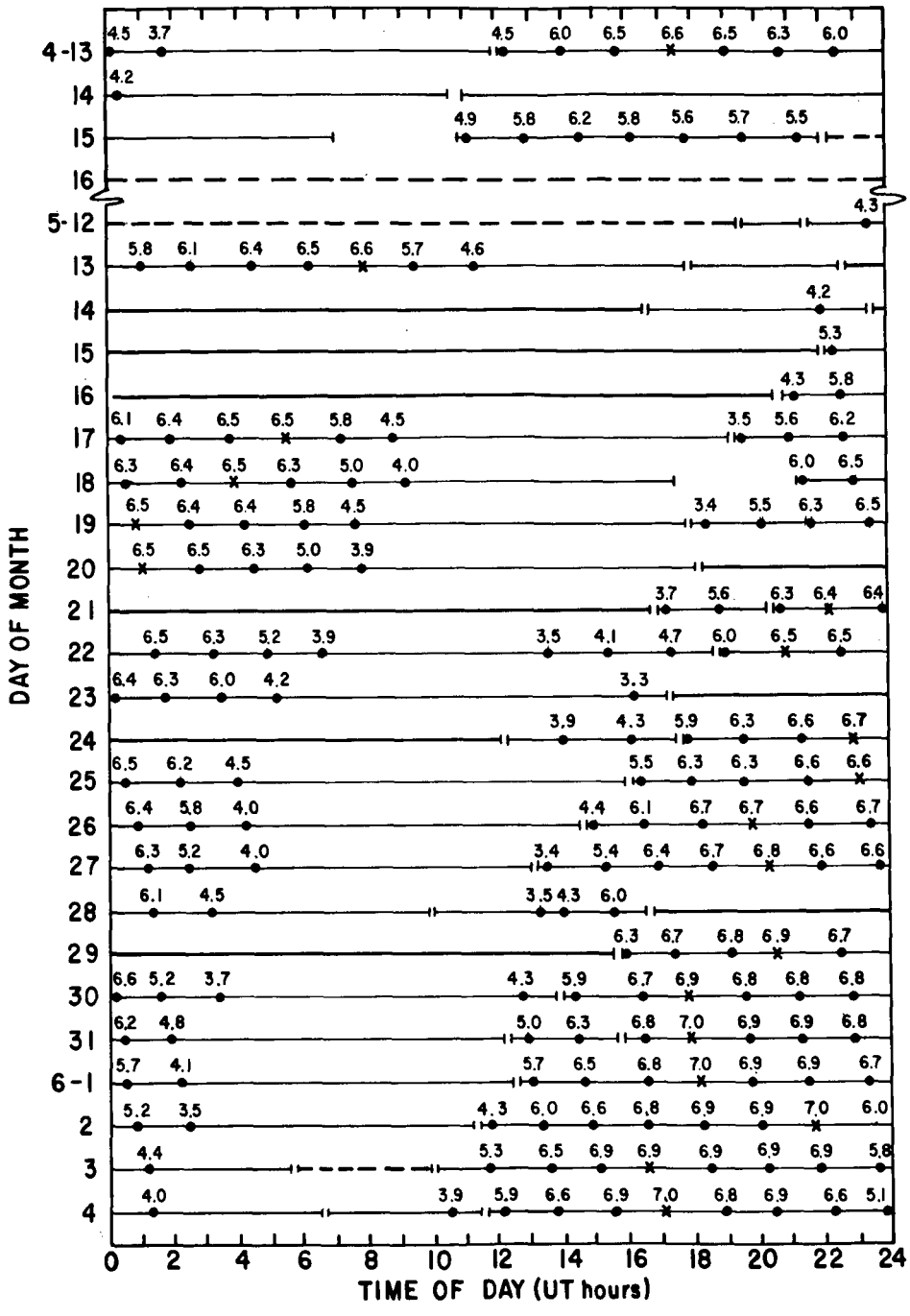

FIGURE 44. DATA COVERAGE AND CHANNEL A MAXIMUM FLUX HISTORY FOR PEGASUS I (APR. 13, 1965 THROUGH JUNE 4, 1965). (Numbers are logarithms of electrons cm^{-2} sec^{-1}.)

The Pegasus III radiation experiment operated well from launch until September 14. The nature of the calibration data for this sensor unit made it necessary to accept large curve fit errors at low flux levels in the Radiation Data Program. Consequently, except at moderate to high flux levels, the data are not as clean as those for the previous two spacecraft. After September 14 measured flux levels in Channel A were consistently about one order of magnitude lower than fluxes observed earlier. A possible explanation for this effect is that a voltage pulse may have occurred during a data system malfunction on that day damaging the amplifier module which was included in the Channel A circuit of this spacecraft to lower the threshold to 0.1 MeV.

The satellites traverse the South Atlantic Anomaly eight to ten times per day in passes lasting from 20 to 35 minutes each. The orbital position and corresponding flux readings are shown for a typical Pegasus I pass in Figure 45. In Figures 42 through 44 each pass for Pegasus I is indicated by a dot marking the time of maximum flux reading; the accompanying numeral is the logarithm of the peak flux (electrons cm^{-2} sec^{-1}) observed in Channel A during the pass. The peak flux each day is further identified by an X. Figure 46 gives a more detailed record of the fluxes in both channels for a 24-hour period on February 24 and 25 for Pegasus I. Figure 41 is an expanded view of the sixth major pass of Figure 46 together with a plot of the corresponding trajectory in B, L space.

For each radiation observation in the Anomaly (flux > 100 electrons cm^{-2} sec^{-1}) satellite ephemeris and B and L coordinates are computed, as noted above. Figure 47 shows a preliminary set of Pegasus I isoflux curves plotted as a function of B and L, together with earlier curves by Hess [12] from other satellite data. The squares are data points and the crosses are a least squares curve fit to the data. The fairly short time period covered (about 60 days of good data) and the narrow flux search range results in relatively few data points. Hess' curves are for data taken roughly two years earlier, and the lower Pegasus fluxes demonstrate an artificial electron belt decay predicted and discussed more recently by Vette [13], Imhoff, W. L., et al. [14], and Imhof and Smith, R. V., [15].

For each day for which complete data coverage exists, integrated flux (electrons cm^{-2} day^{-1}) is computed. In Figure 48 a history of integrated flux is shown for Pegasus I. Occurrence of apogee and perigee in the Anomaly are clearly seen as maxima and minima in the data. These times may also be identified as maxima and minima in the peak flux readings in Figures 42 through 44.

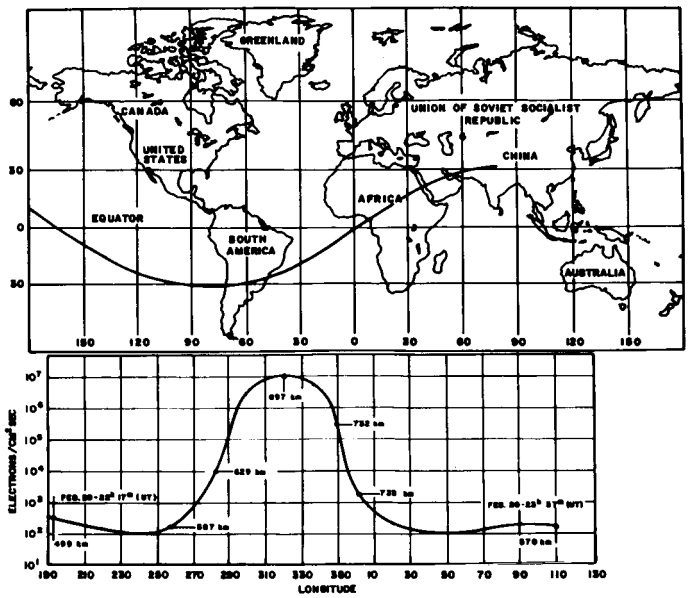

FIGURE 45. ORBIT AND FLUX HISTORY FOR SINGLE PASS THROUGH ANOMALY, PEGASUS I

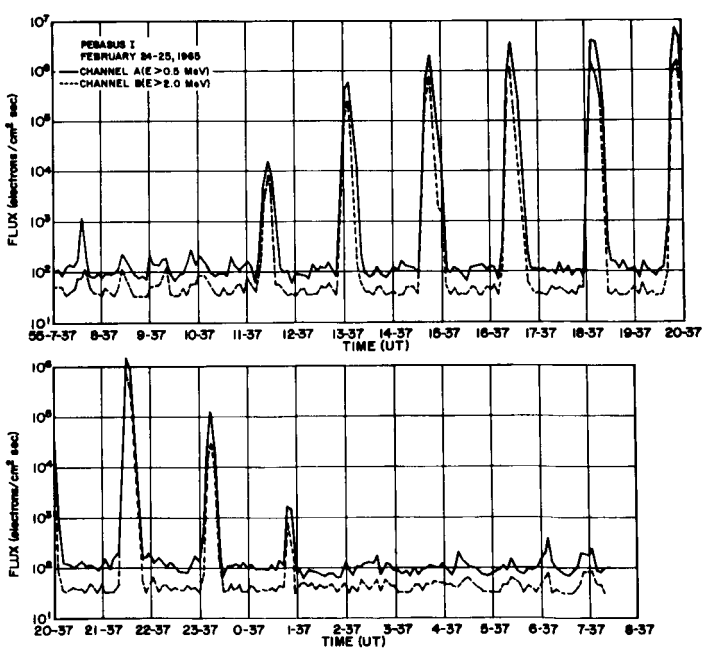

FIGURE 46. FLUX HISTORY FOR 24-HOUR PERIOD, PEGASUS I

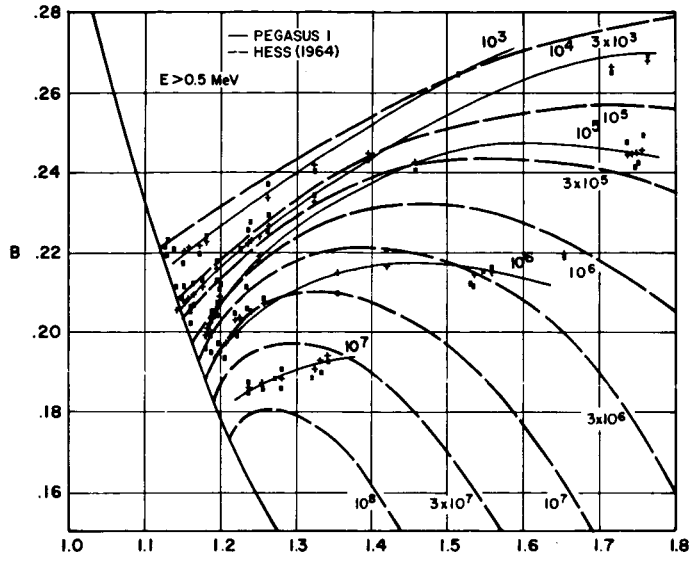

FIGURE 47. ISOFLUX CURVES IN B, L (PEGASUS I)

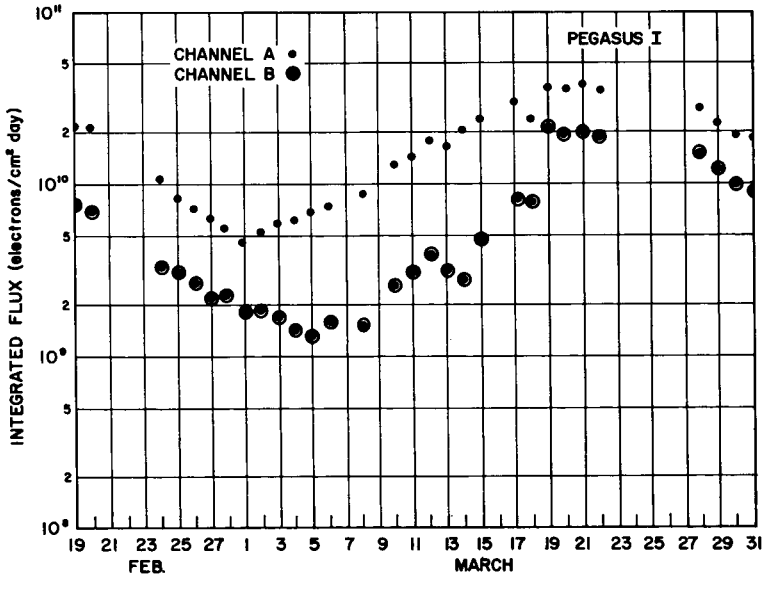

FIGURE 48. INTEGRATED FLUX HISTORY (PEGASUS I)

The Rigid Body Motion of Pegasus

The orientation time history of all three-body axes as shown in Figure 49 is determined by on-board sensors which detect the sun ($\vec{S}'$) and earth ($\vec{R}'$) vectors with respect to the satellite body-fixed axes. The time history of these two vectors are also known from ephemerides with respect to a space-fixed system such as the conventional astronomical system with the vernal equinox and north celestial pole as reference directions, and the celestial equator as the reference plane.

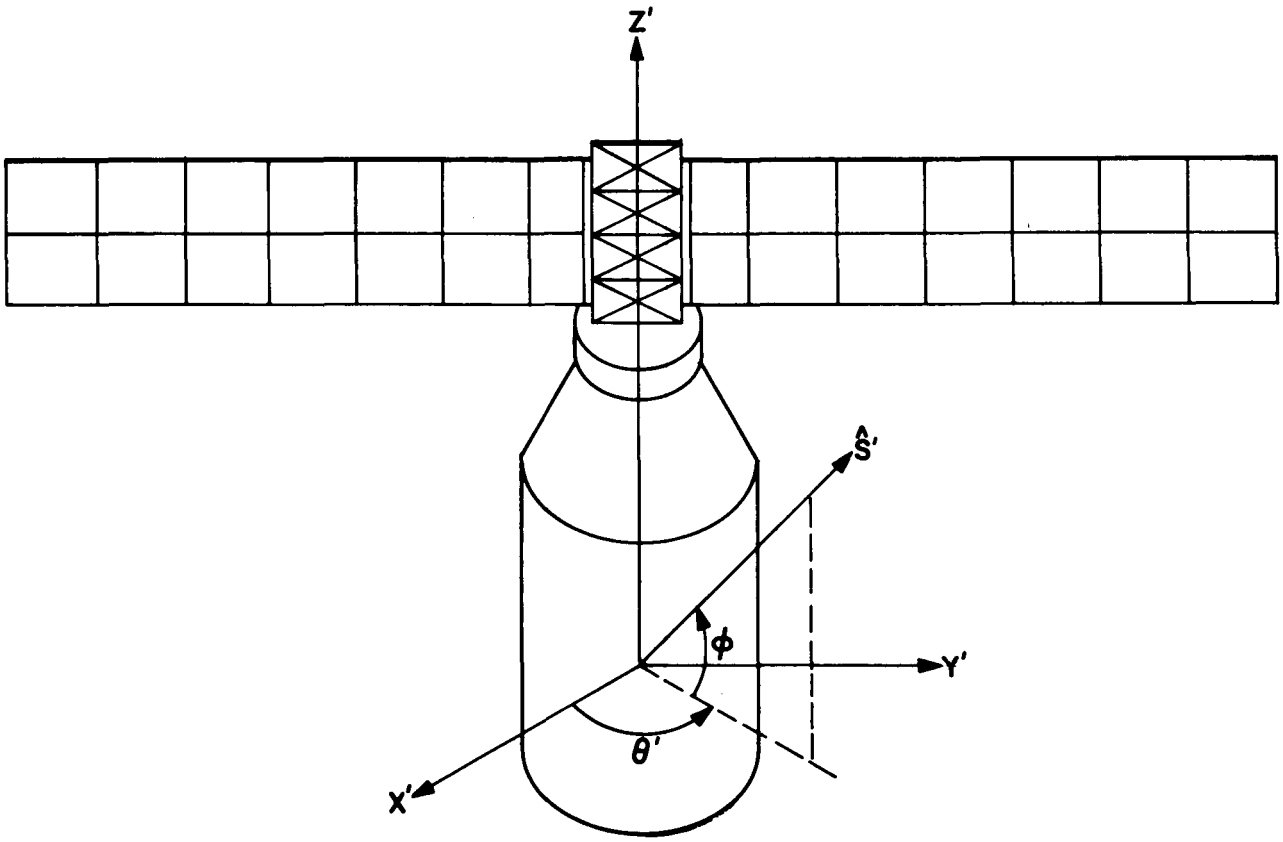

FIGURE 49. SCHEMATIC OF PEGASUS SHOWING COORDINATE SYSTEM

Equipped with these two vectors, known in both the body-fixed and space-fixed reference systems, one can determine the orientation of the body with respect to space or vice versa. Before demonstrating how this is done with the observed data, a brief description of the method of measuring the sun vector $\vec{S}'$ and the earth vector $\vec{R}'$ with respect to the body-fixed coordinate system will be presented.

1. Sun vector $\vec{S}'$ measurements. Figure 50 is a conceptual drawing of half of one of the five sun sensors which are mounted on board the satellite in such a way that the planes of the faces form a pyramid as shown in Figure 51. The other half of the sensor as shown in Figure 50 is identical except that the

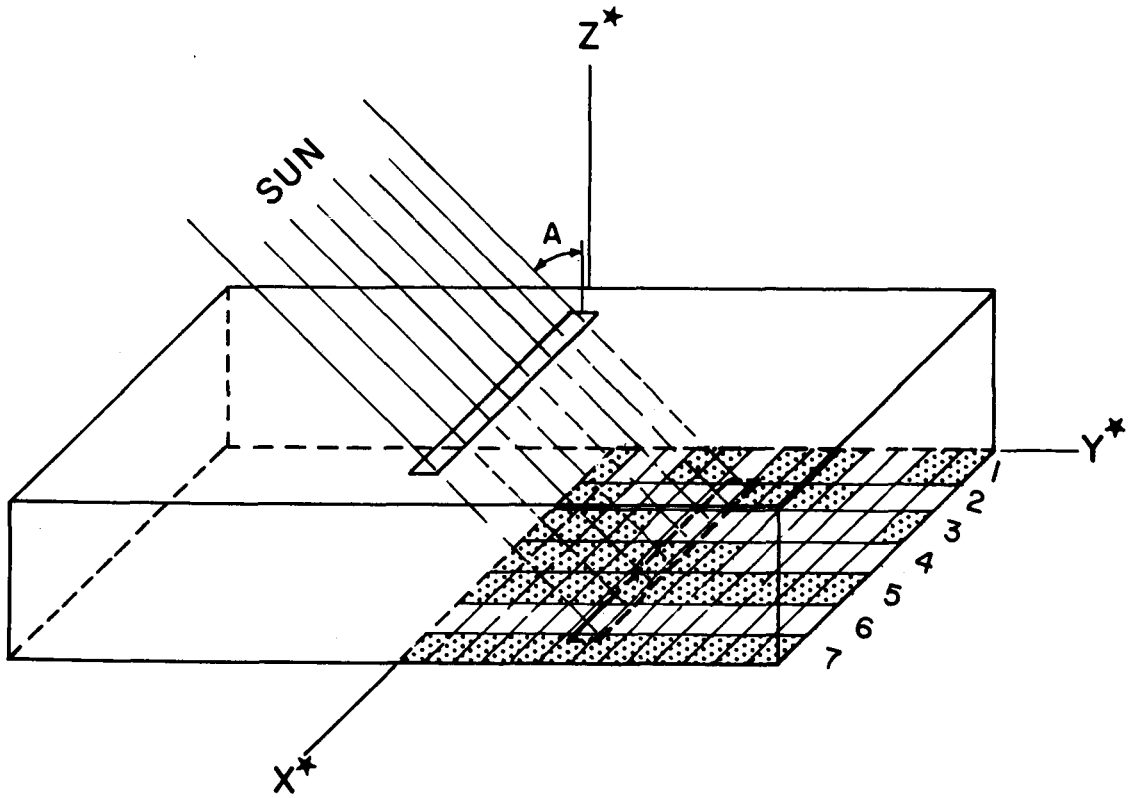

FIGURE 50. ONE SLIT OF SOLAR ASPECT SENSOR

slit which allows the sunlight to fall on the photo-sensitive material is perpendicular to the one shown. The X^*, Y^*, Z^* axes form a coordinate reference system fixed in the sensor. The numbers 1, 2, 3, 4, 5, 6, and 7 indicate the number of binary digits which are generated from each numbered strip. As can be seen, the photo-sensitive material is distributed on each strip in such a way as to cause a current flow in a particular strip only when the sun is at certain angles with respect to the X^*, Z^* plane. Since there are seven strips there are seven yes or no answers (i.e., 7 bit binary word) transmitted every five minutes, normally, for the determination of the angle A which goes from +63.5° to -63.5°. The resolution is approximately 1°. The determination of angle B (Fig. 52) is accomplished in exactly the same manner. There is an

alternate mode of operation called "rapid attitude" mode which reads out the binary words every 2.5 seconds rather than the normal 5-minute interval.

The angles A and B are used to derive the spherical and rectangular components of the unit sun vector $\vec{S}^*$ with respect to the particular sensor coordinates from which the measurements came.

The rectangular components

$$\vec{S}^* = \begin{matrix} (1 + \tan^2 A + \tan^2 B)^{-1/2} \tan B \\ (1 + \tan^2 A + \tan^2 B)^{-1/2} \tan A \\ (1 + \tan^2 A + \tan^2 B)^{-1/2} \end{matrix} \quad (1)$$

are then resolved onto the body-fixed axes through the transformation matrix (M_i) obtained by knowing the orientation of the sensor coordinates with respect to the satellite body-fixed coordinates.

$$\vec{S}' = (M_i)\, \vec{S}^* \quad (2)$$

i = 1, ---, 5 since there are five sun sensors.

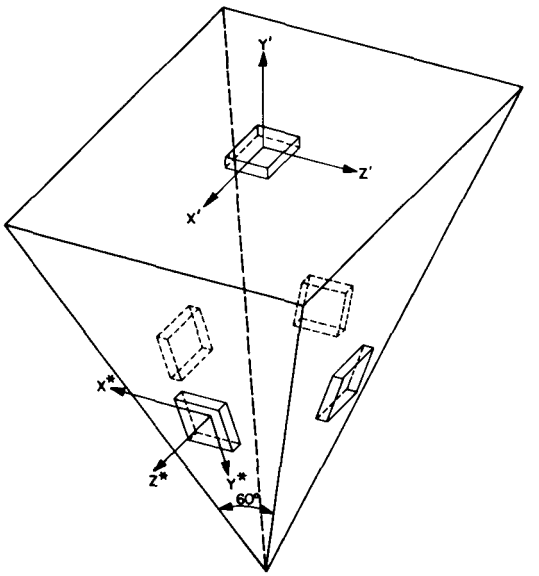

FIGURE 51. SOLAR ASPECT SENSORS

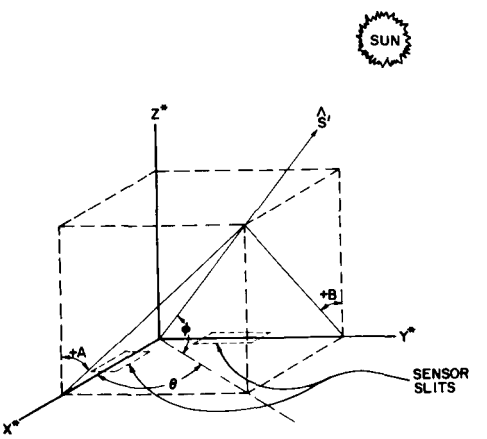

FIGURE 52. SUN VECTOR RESOLVED ON SENSOR AXES

2. Earth vector $\vec{R}'$ measurements. Figure 53 is a conceptual drawing of one of the six narrow fields of view ($\simeq 2°$) infrared earth sensors. These are designed to detect a differential temperature across the thermopile in the center in either direction. The differential is set to correspond as closely as possible with the differential between the earth and space, thus at any time (at normal 5-minute intervals) it is known whether or not the earth is in the narrow field of view of either end of the six sensors. The sensors are

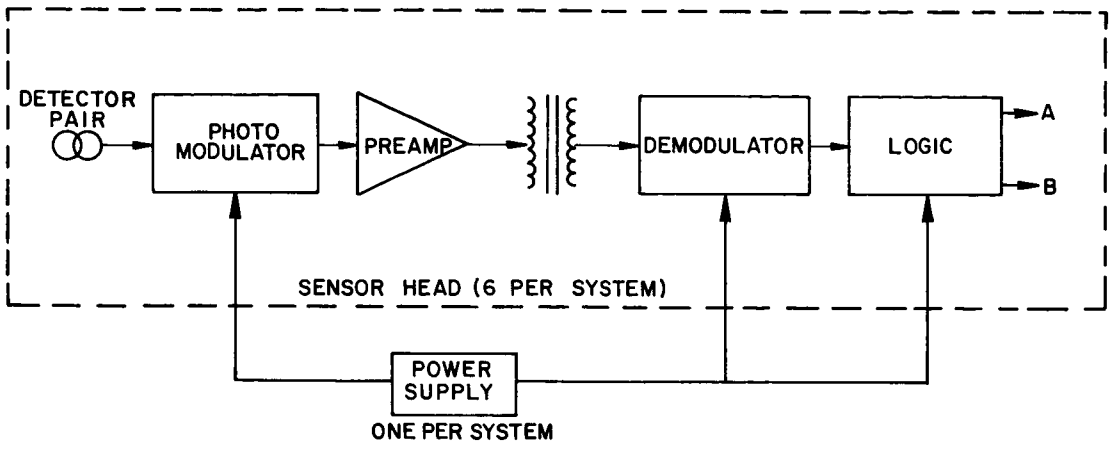

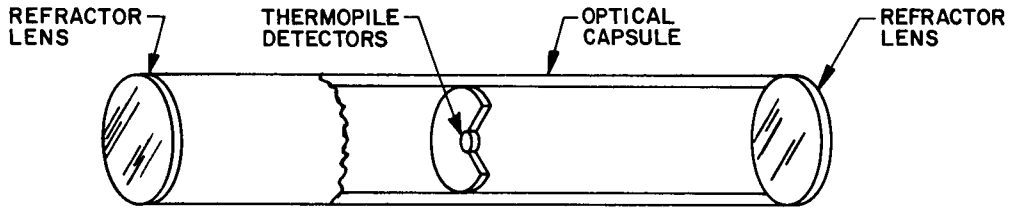

FIGURE 53. PEGASUS EARTH SENSOR

mounted on the satellite in such a way that the directions are normal to the faces of an imaginary dodecahedron centered around the satellite. At each 5-minute readout there are then 12 yes or no answers (i.e., 12 bit binary word) which indicate which of the 12 sensors are "looking" at the earth. For the particular orbits of the Pegasus satellites it is possible for three to six sensors to be looking at the earth simultaneously. Now the earth vector $\vec{R}'$ can be approximated by summing (i.e., averaging) the sensor vector directions which are "ON".

$$\vec{R}' = \sum \vec{A}_i, \tag{3}$$

where $\vec{A}_i$ are the sensor vectors which are "ON."

This approximation can be improved by preserving the angle between $\vec{R}'$ and $\vec{S}'$ as determined by knowing $\vec{R}$ and $\vec{S}$ in space from ephemerides, i.e.,

$$\vec{R}' \cdot \vec{S}' = \vec{R} \cdot \vec{S}. \tag{4}$$

Thus the best value for $\vec{R}'$ is obtained by moving $\vec{R}'$ toward or away from the sun until equation (4) is satisfied. This is normally a very small correction, but it can be as much as 20°.

3. Orientation determination from $\vec{S}$, $\vec{S}'$, $\vec{R}$, and $\vec{R}'$. If $\vec{S}$ and $\vec{S}'$ are resolved onto any other space-fixed coordinate system whatever (call it an intermediate system), the two vectors will be identical. The same is true for $\vec{R}$ and $\vec{R}'$. Thus if a set of orthogonal axes are constructed from $\vec{R}$ and $\vec{S}$ this can be the intermediate system. It is possible, therefore, to transform vectors from space to the intermediate set and vice versa by

$$\vec{G} = (A)\ \vec{G}_I , \tag{5}$$

where the first column of (A) is $\vec{R}$, the second column is $(\vec{R} \times \vec{S}) \times \vec{R}$ normalized, and the third column is $\vec{R} \times \vec{S}$ normalized. G is an arbitrary vector.

If we construct another orthogonal set of axes from $\vec{R}'$ and $\vec{S}'$ and resolve it onto the intermediate set we obtain the same intermediate set as described above. It is also possible, therefore, to transform vectors from the body axes to the intermediate axes and vice versa by

$$\vec{G}' = (B)\ \vec{G}_I , \tag{6}$$

where (B) is made up of $\vec{R}'$ and $\vec{S}'$ in the same way as (A) was made up from $\vec{R}$ and $\vec{S}$. Combining equations (5) and (6), we obtain

$$\vec{G} = (A)\ (B)^{-1}\ \vec{G}' , \tag{7}$$

which gives the total transformation from body-fixed coordinates to space-fixed, and vice versa. The columns in the total transformation $(A)\ (B)^{-1}$ are the direction cosines (i.e., unit vectors) of the three body-fixed axes with respect to space-fixed axes.

4. Spin. Figure 54 shows the build-up in spin (i.e., roll) rate for Pegasus III. This occurred also on Pegasus I and II except that I reached a maximum of 10°/sec, whereas II and III reached a maximum of 6.5°/sec.

This build-up in spin rate was not anticipated before the launching of Pegasus I. It has been attributed to the venting of residual LH_2 and LOX left on board after S-IV engine cut-off. The geometry of the vent values was such that

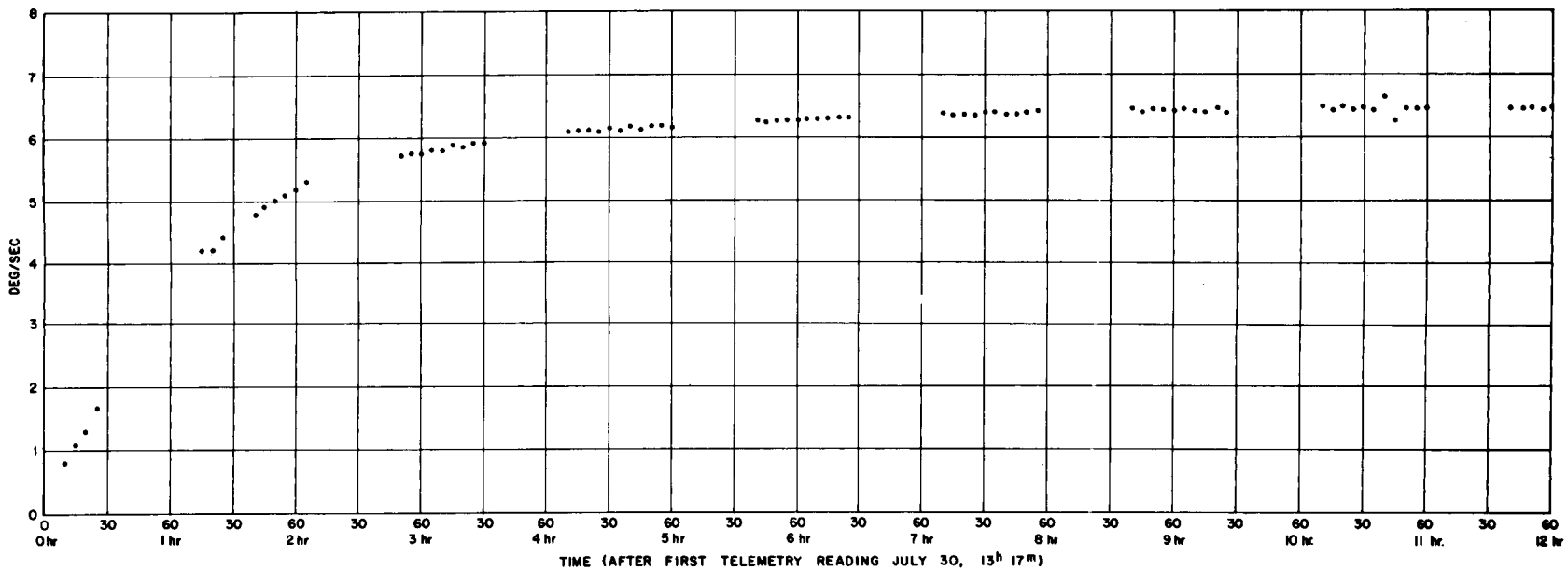

FIGURE 54. BUILD-UP IN SPIN RATE FOR PEGASUS III

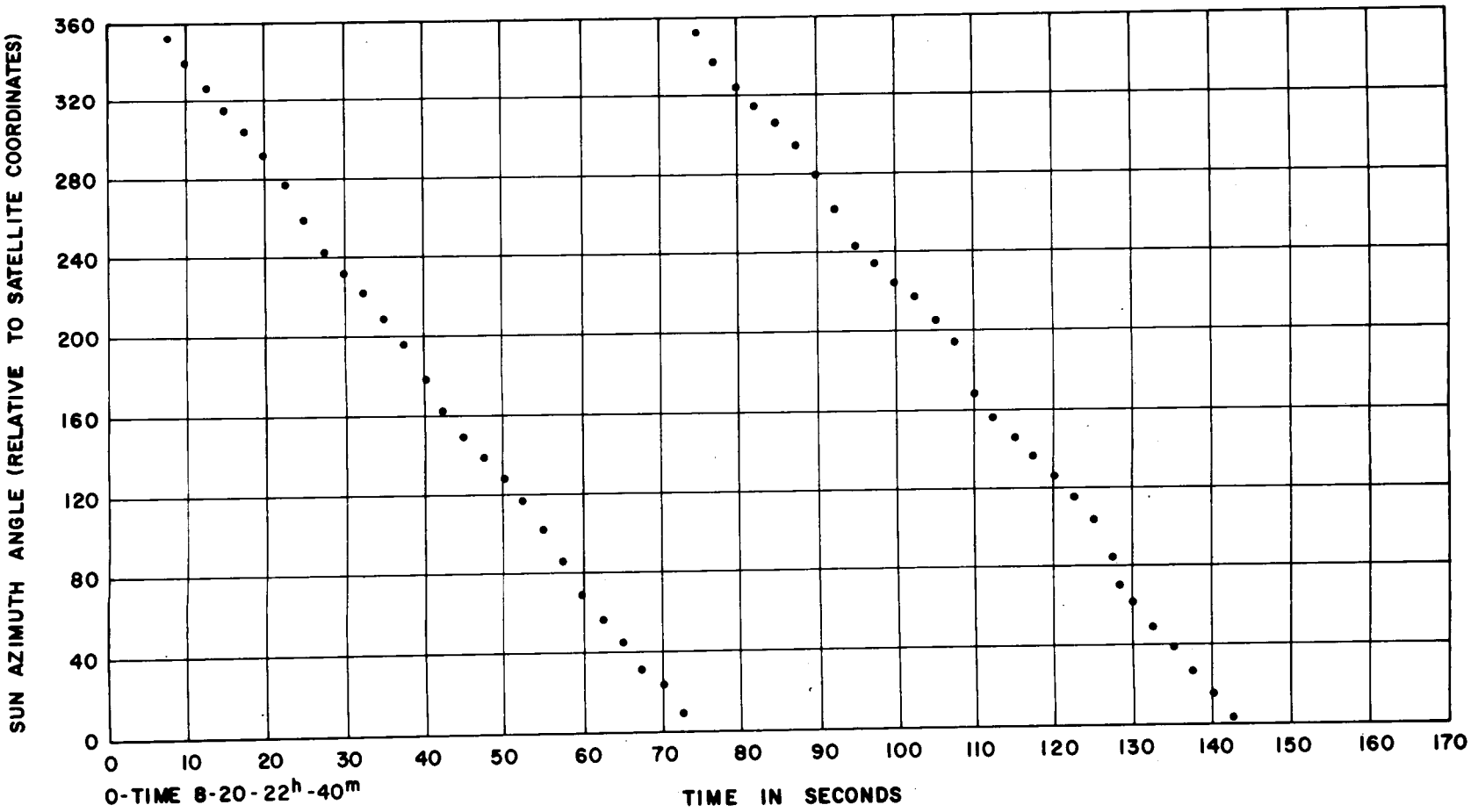

FIGURE 55. SUN AZIMUTH ANGLE IN SATELLITE COORDNIATES (PEGASUS III)

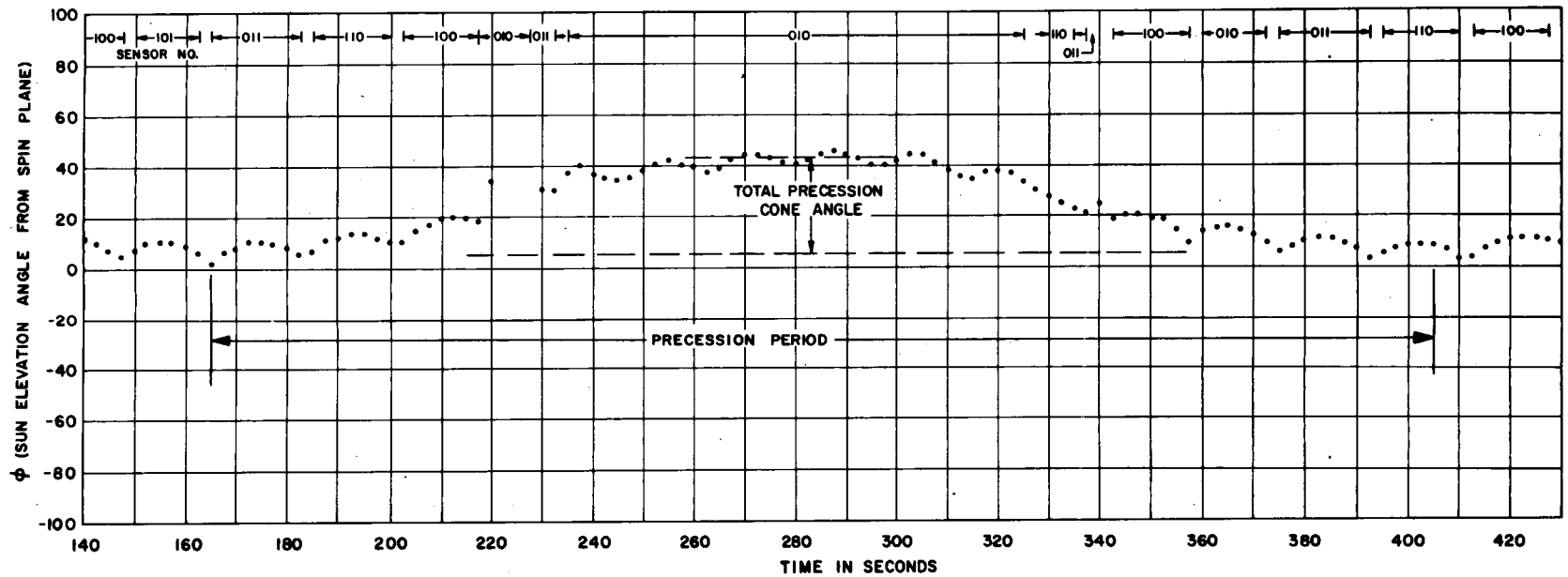

FIGURE 56. SUN ELEVATION ANGLE IN SATELLITE COORDINATES (PEGASUS III)

the gas, after escaping the valves, expanded against the meteoroid detector panels causing a torque around the roll axis. This explanation was strengthened by the accurate prediction of spin on Pegasus II and III after some adjustments were made to the venting system.

Figure 55 and 56, representing Pegasus III, are plots obtained from the rapid attitude mode of the spherical coordinates θ and ϕ of the sun vector with respect to the body-fixed axes (Fig. 49). These figures taken together clearly indicate that the satellite is spinning about the Z' axis at a rate of approximately 5.25° per second. Similar data were obtained from Pegasus I and II. Figures 57, 58, and 59 are the spin rate time histories for I, II, and II, respectively.

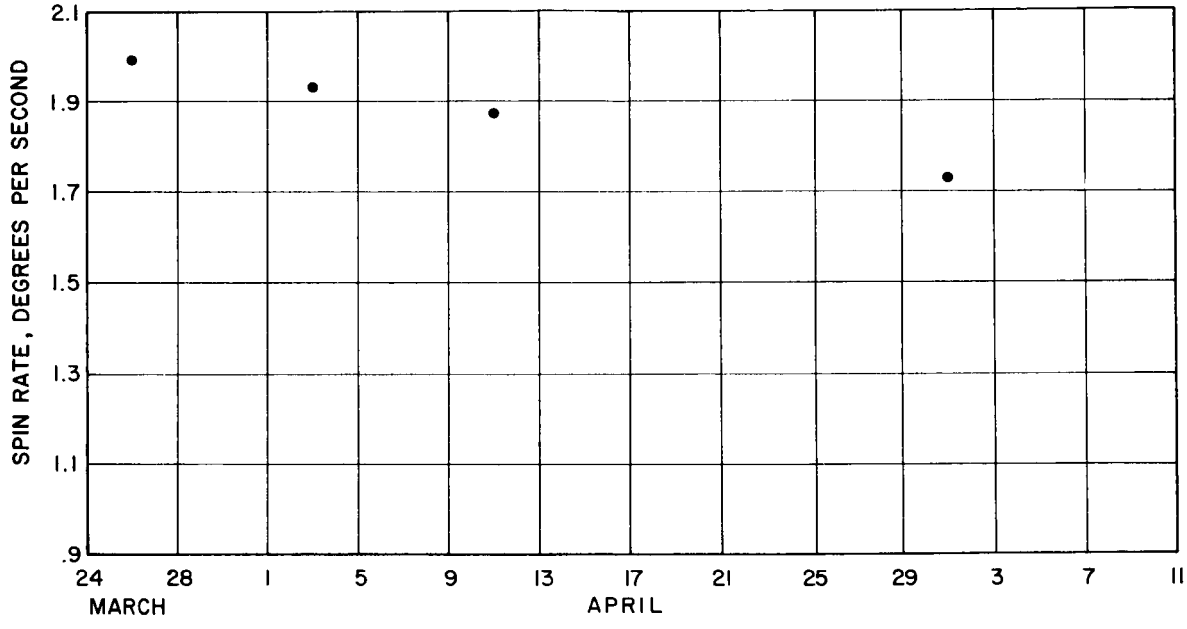

FIGURE 57. PEGASUS I SPIN RATE

The curve for I, however, starts after the spin axis had transferred from the Z' to the X' body axis. The spin rate decay is primarily due to magnetic (eddy current) damping. The time constant k in the expression

$$\omega = \omega_{oe}^{-kt} \tag{8}$$

has been calculated from theory by estimating many of the parameters such as resistivity, permeability, effective current loop, cross sections, magnetic flux, etc. The theoretical value of 0.0043 sec^{-1} for Pegasus I after it reached a flat

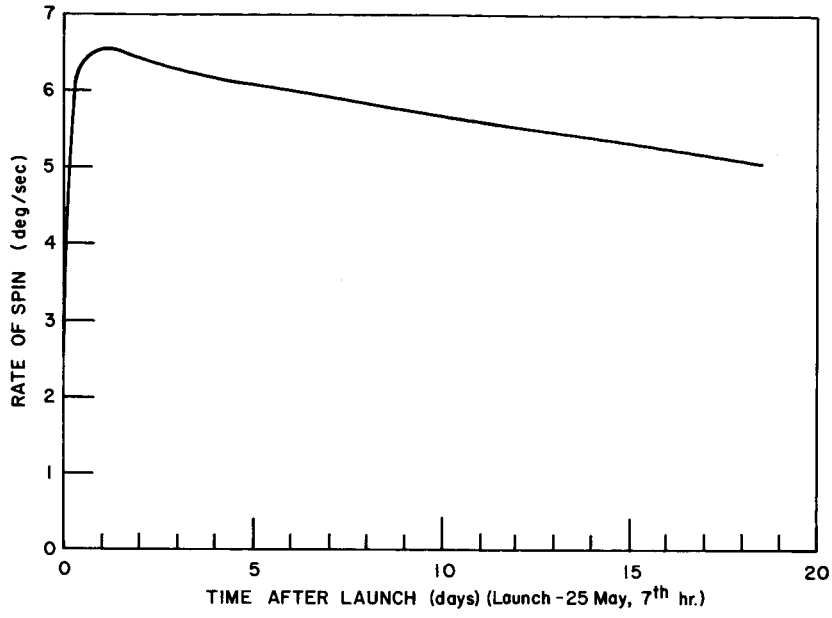

FIGURE 58. PEGASUS II SPIN RATE ABOUT LONGITUDINAL AXIS

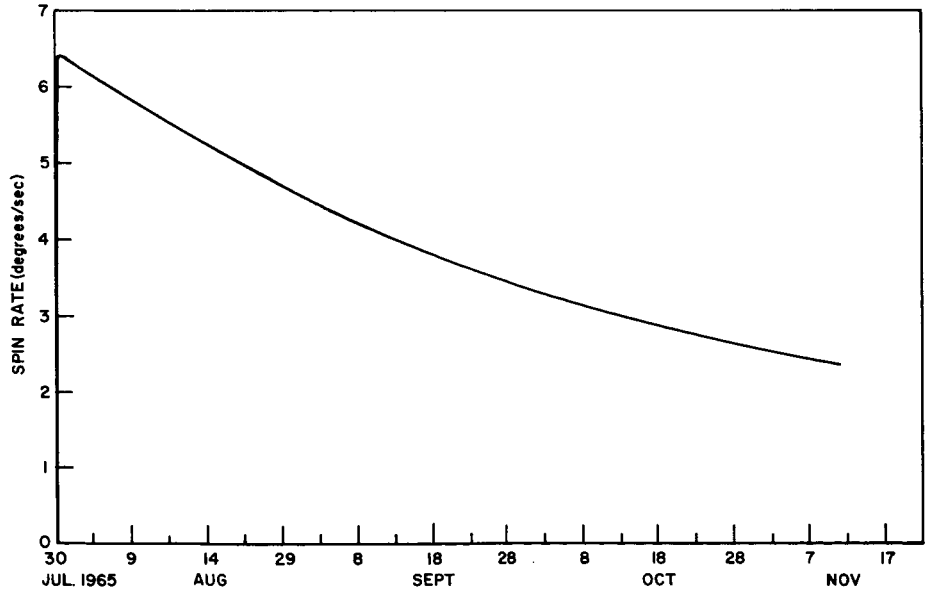

FIGURE 59. PEGASUS III SPIN RATE

spin agreed remarkably well with the actually observed value of 0.0041 sec^{-1}. The theoretical value of 0.025 sec^{-1} for Pegasus II did not agree as well with the actually observed value of 0.0133 sec^{-1}, but a factor of 2 is as close as could be expected considering all the parameters which must be estimated. Also, the agreement is considered adequate proof that the magnetic (eddy current) damping is the predominant cause for the spin decay.

5. Precession. Figure 56 also clearly demonstrates that the satellite spin axis is precessing around its angular momentum vector with a total cone angle of approximately 40° and a period of 4 minutes. This general type of motion has also been observed on Pegasus I and II. Figure 60 is a time history of the total precession cone angle for Pegasus I. As can be seen, this cone angle had completely opened to 180° within the first 14 days. At this time, the spin was around the maximum moment of inertia axis I_1, i.e., the X' axis shown in Figure 49. The rate, however, had decreased to approximately 2°/sec, but the angular momentum $I_1\omega_1 \simeq I_3\omega_3$. I_3 is the moment of inertia around the minimum moment of inertia axis, i.e., the Z' initial roll axis. At the time of this writing, Pegasus II and III have precession cone angles of approximately 20° and 55°, respectively, yet the time since launch has been 119 and 54 days, respectively. This is very difficult to understand since all three satellites had practically the same physical characteristics and similar orbits. The only significant difference was that the initial spin rate for Pegasus I was higher (10°/sec) than that of II and III (6.5°/sec).

For a rigid body the higher spin rate would have had a more stabilizing effect but the reverse has actually been observed. This is one of the problems which has not yet been explained. Perhaps as the data analysis proceeds a satisfactory explanation will evolve. Several mechanisms have been postulated but not yet adequately proven. Among these is a difference in the rigidity of the meteoroid detector panels between Pegasus I, and Pegasus II and III. Another reason which is currently under study is a difference in the aerodynamic drag force direction with respect to the body-fixed axes. In any event the observed fact is that the spin axis of Pegasus I has long since changed from a spin about the minimum moment of inertia axis to the maximum moment of inertia axis while Pegasus II and III continue to spin predominantly about their minimum moment of inertia axes. This type of motion on II and III complicates the meteoroid directional analysis study which was planned. Since the resolution for the time at which a hit occurred is one minute, this means that the detector panel normally associated with the time of hit could be anywhere within a 360° arc with a spin of 6°/sec. Once the spin axis is transferred to the maximum moment of inertia axis, as is now the case for Pegasus I, it moves about very slowly so that the direction of the normal to the detector panel (which is the spin axis) can

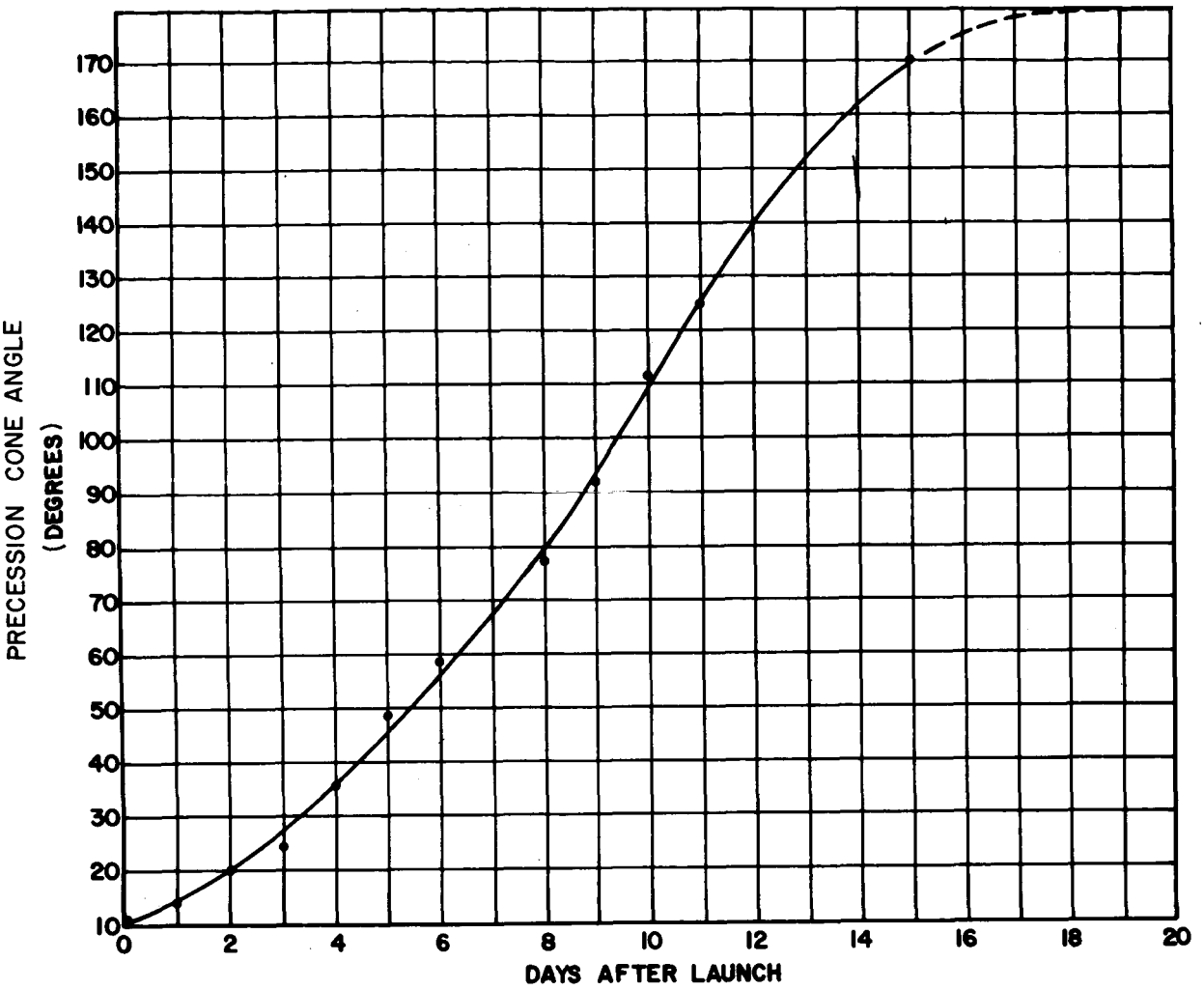

FIGURE 60. TIME HISTORY OF PRECESSION CONE ANGLE ABOUT ANGULAR MOMENTUM VECTOR (OPENING ANGLE - PEGASUS I)

be associated with time of hit. It is believed that Pegasus II and III will eventually reach this configuration so that the directional study can proceed as planned.

6. Nutation. Figure 56 shows a very short periodic variation ($\simeq$ 17 seconds) in addition to the longer period precessional variation. This periodic variation is observed on all three satellites. This was first thought to be due to actual physical nutation of the spin axis or else evidence of "wing flexing," but a careful study of the curves for the associated angles A and B and the resolution of the spherical coordinate ϕ from the measured angles A and B (which have a known uncertainty of a least 1°) showed that the fluctuations are

not physical. They are caused by the nonlinear resolution of ϕ from A and B. The equation for ϕ as a function of A and B is

$$\phi = \text{arc sin}(1 + \tan^2 A + \tan^2 B)^{-\frac{1}{2}}.$$

The change in ϕ due to a change in A and B is

$$\Delta\phi = \frac{\partial \phi}{\partial A} \Delta A + \frac{\partial \phi}{\partial B} \Delta B. \tag{9}$$

Inserting the 1° uncertainty in A and B as ΔA and ΔB and evaluating equation (9) gives an associated change in ϕ up to about 10° depending on the values of A and B. The maximum $\Delta\phi$ occurs when A or B is a maximum or minimum, giving 4 maxima for $\Delta\phi$ per satellite spin period. This is exactly the number of periodic fluctuations per spin period observed on the data. A correlation of Figure 56 with time history curves for angles A and B shows that the minimum points on the ϕ curve coincide exactly with the minimum or maximum points on the A and B curves. There is further evidence that the fluctuations are not physical since they show the spin axis always bobbing in and out toward or away from the sun. This is contrary to rigid body motion theory which describes nutation as bobbing in and out toward or away from the angular momentum vector. Thus the sun sensors would not detect physical nutation if it was nutating perpendicular to the sun direction, but the curve in Figure 56 shows the nutation all the way around the precession cone angle.

7. Angular momentum vector motion. In the preceding discussion, attention was focused on the short-term motion of the various axes, i.e., spin, precession and nutation. The long-term motion over weeks, months, and even years is of interest for practical and scientific reasons.

The motion of the angular momentum vector is one of the most informative studies to make since the time rate of change of this vector reveals information about the external torques acting on the satellite.

Figure 61 is a plot of the motion of the angular momentum vector of Pegasus I during the month of March 1965 after the spin axis was aligned along the principal axis of maximum moment of inertia (i.e., X' axis). It is known that the gravity gradient torque

$$\vec{N'} = \frac{3mk^2}{r^3} \begin{pmatrix} (I_3 - I_2)\ \mu'\nu' \\ (I_1 - I_3)\ \lambda'\nu' \\ (I_2 - I_1)\ \lambda'\mu' \end{pmatrix} \tag{10}$$

is the predominant torque causing the motion of the angular momentum vector h. The I's are the principal moments of inertia, λ', μ' and ν' are the direction cosines of the radius vector R' resolved onto the satellite body-fixed axes, and mk^2 is the gravitational parameter for the earth. Numerical integration studies currently in process have confirmed earlier crude calculations that this torque is predominant.

It can also be learned from perturbation theory that the perturbing effect of the gravitational torque on the magnitude of the angular momentum vector is

$$h = \hat{h} \cdot \vec{N}.$$

$\vec{h} \equiv h\hat{h}$ is a constant of the motion in the force-free theory of rigid body motion. The average value of h over a cycle of Pegasus I is a constant (neglecting the long-term spin decay and the negligible differential over an orbital cycle). If $\vec{h}$ is taken to be a constant, then $\vec{h}' \cdot \vec{N}' = \vec{h} \cdot \vec{N} = 0$. This states that the angular momentum vector and the torque remain perpendicular. One way in which this can happen to a spinning rod is for the longitudinal axis to remain in the orbital plane with the angular momentum vector oscillating about the orbit plane. This type of motion has been observed on Pegasus I. The motion of the momentum vector of Pegasus II and III is much more complicated by the fact that both of these satellites continue to spin about the minimum moment of inertia axis and precess around the angular momentum vector. Analytical work is now in progress to predict the motion of these satellites.

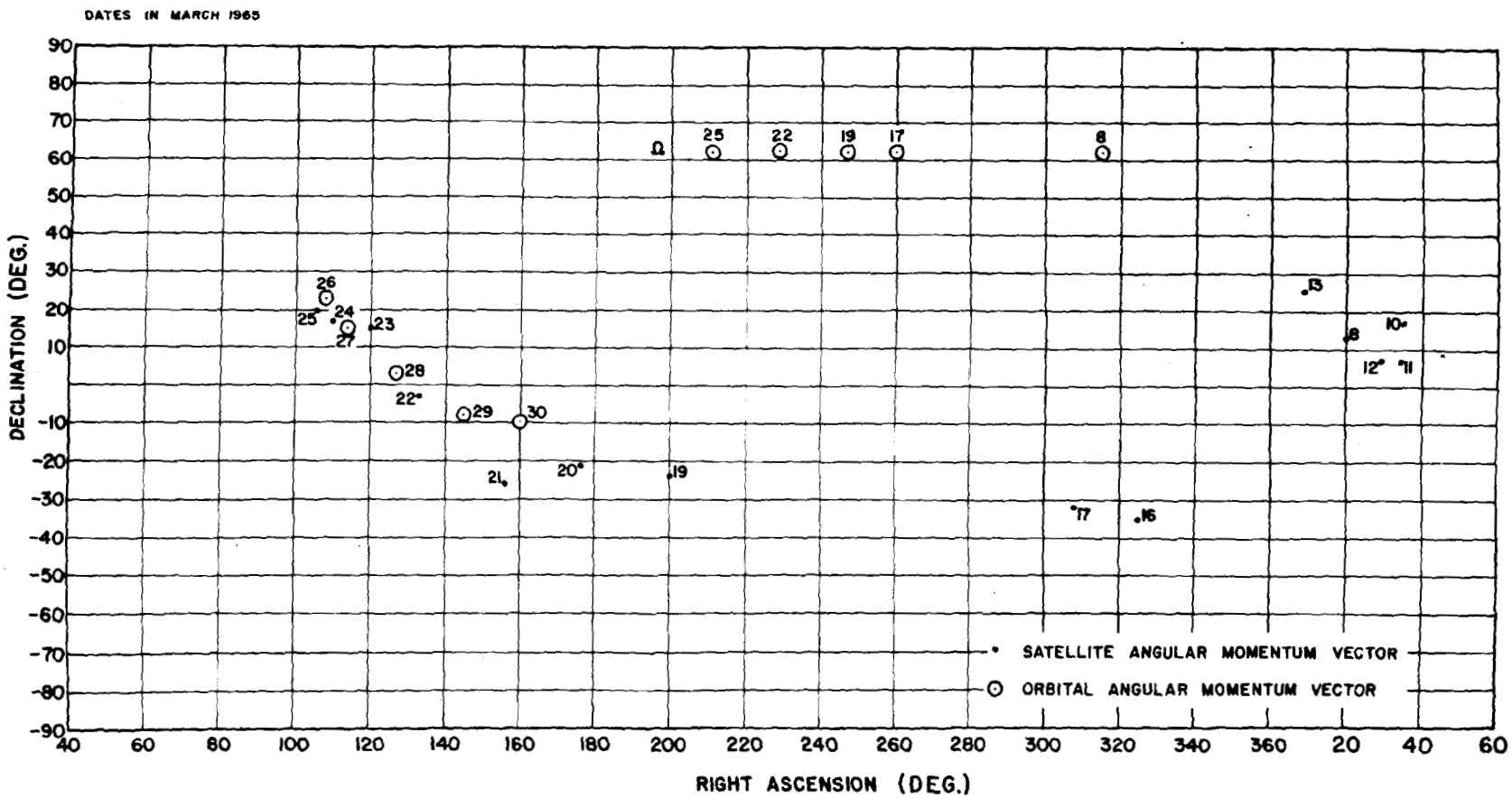

FIGURE 61. MOTION OF PEGASUS I ANGULAR MOMENTUM VECTOR

CONCLUSIONS

The primary mission of Project Pegasus is the collection of meteoroid penetration data in the vicinity of the earth. Limitations imposed by the carrying capability of the Saturn I vehicle restricted the sensitive collecting area to 200 m^2. With this area and an expected lifetime of one year, a statistically meaningful total number of puncturing impacts could only be expected for aluminum target thicknesses below about 0.5 mm. Actually, the number of puncturing impacts through 0.4 mm of aluminum as recorded by Pegasus II and III is about 1.3 per m^2 per year, in rough confirmation of the preflight assumptions.

Project Pegasus accomplished its mission satisfactorily. Puncture data for the three target thicknesses are fairly well established by now. If the spacecraft continue to work properly, it may even be possible to derive some useful information on directivity and systematic fluctuations of meteoroids in the vicinity of the earth.

REFERENCES

1. D'Aiutolo, C. T.: The Micrometeoroid Satellite Explorer XIII (1961 Chi) -- Collected Papers on Design and Performance. NASA TN D-2468, Nov. 1964.

2. Hastings, E. C.: The Explorer XVI Micrometeoroid Satellite. NASA TMX's 824, 899, and 949, Apr. 1963, Sept. 1963, and Mar. 1964, respectively.

3. O'Neal, R. L.: The Explorer XXIII Micrometeoroid Satellite--Description and preliminary Results for the Period Nov. 6, 1964, through Feb. 15, 1965. NASA TM X-1123, Aug. 1965.

4. Naumann, R. J.: Pegasus Satellite Measurements of Meteoroid Penetration (Feb. 16 - July 20, 1965). NASA TM X-1192, Dec. 1965.

5. D'Aiutolo, C. T.; Kinard, W. H.; and Naumann, R. J.: Recent NASA Meteoroid Penetration Results from Satellites. Paper presented at the Symposium on Meteor Orbits and Dust, Smithsonian Astrophysical Observatory, Aug. 9-13, 1965 (to be published in the "Smithsonian Contributions to Astrophysics.").

6. Snoddy, W. C.: Calculations Concerning the Passage of a Satellite Through the Earth's Shadow. MSFC Report MTP-RP-61-1, Feb. 1961.

7. Plamondon, J. A.: Analysis of Movable Louvers for Temperature Control. JPL Report TR 32-555, Pasadena, Calif., Jan. 1964.

8. Pollack, F. G.; Winslow, P. C. Jr.; and Davidson, E. H.: Preliminary Experimental Investigation of a Double Capacitor Coincidence Discharge-Type Micrometeoroid Penetration Sensor. NASA TM X-1037, Nov. 1964.

9. Gernstein, B.; Burdick, A. H.; and Trainor, F. E.: Radiation and Temperature Measurements on Mylar and Other Capacitors. Admiral Corp. Technical Summary Rept., Contract NAS8-5388, Jan. 1964.

REFERENCES (Concluded)

10. Monteith, L. K.: Study on the Electron Irradiation Effects on Capacitor-Type Micrometeoroid Detectors. RTI Report on Contract NAS1-3892, June 1965.

11. Schafer, C. F. and Bannister, T. C.: Pegasus Thermal Control Coatings Experiment, AIAA Paper No. 66-419 presented at the 4th Aerospace Sciences Meeting of AIAA, Los Angeles, Calif., June 27-29, 1966.

12. Hess, W. N.: Letter to Users of E8 Grid. GSFC, Oct. 20, 1964.

13. Vette, J. I.: Models of the Trapped Radiation Environment, Vol. I: Inner Zone Protons and Electrons. NASA SP-3024, 1966.

14. Imhof, W. L., et al.: Analysis and Evaluation of Geomagnetically Trapped Electrons from High Altitude Nuclear Explosions. Lockheed Report, LSMC 3-25-64-1, DASA 1540. July, 1964.

15. Imhof, W. L. and Smith, R. V.: Longitudinal Variations of High Energy Electrons at Low Altitudes. J. Geophys. Res., 70, 569-578, 1965.

"The aeronautical and space activities of the United States shall be conducted so as to contribute . . . to the expansion of human knowledge of phenomena in the atmosphere and space. The Administration shall provide for the widest practicable and appropriate dissemination of information concerning its activities and the results thereof."

—NATIONAL AERONAUTICS AND SPACE ACT OF 1958

NASA SCIENTIFIC AND TECHNICAL PUBLICATIONS

TECHNICAL REPORTS: Scientific and technical information considered important, complete, and a lasting contribution to existing knowledge.

TECHNICAL NOTES: Information less broad in scope but nevertheless of importance as a contribution to existing knowledge.

TECHNICAL MEMORANDUMS: Information receiving limited distribution because of preliminary data, security classification, or other reasons.

CONTRACTOR REPORTS: Technical information generated in connection with a NASA contract or grant and released under NASA auspices.

TECHNICAL TRANSLATIONS: Information published in a foreign language considered to merit NASA distribution in English.

TECHNICAL REPRINTS: Information derived from NASA activities and initially published in the form of journal articles.

SPECIAL PUBLICATIONS: Information derived from or of value to NASA activities but not necessarily reporting the results of individual NASA-programmed scientific efforts. Publications include conference proceedings, monographs, data compilations, handbooks, sourcebooks, and special bibliographies.

Details on the availability of these publications may be obtained from:

SCIENTIFIC AND TECHNICAL INFORMATION DIVISION

NATIONAL AERONAUTICS AND SPACE ADMINISTRATION

Washington, D.C. 20546